Proceedings of the 16th International Conference on Soil Mechanics and Geotechnical Engineering

doi:10.3233/978-1-61499-656-9-123

Challenges of offshore geotechnical engineering

Les défis de la géotechnique offshore

Mark Randolph, Mark Cassidy & Susan Gourvenec
Centre for Offshore Foundation Systems, The University of Western Australia
Carl Erbrich
Advanced Geomechanics

ABSTRACT

Design practice in offshore geotechnical engineering grew out of onshore practice, but the two application areas have tended to diverge over the last 30 years, driven partly by the scale of the foundation elements used offshore, and partly by fundamental differences in construction (or installation) techniques. Groups of many moderate-sized piles are replaced by a few very large diameter piles; excavation of shallow soft sediments is replaced by the use of deep skirts, transferring the effective foundation depth to the level of the skirt tips, or by forcing footings to penetrate several diameters into the seabed; underwater installation has allowed the use of 'suction' (or under-pressure) to aid installation of skirted foundations and caissons. Emphasis in design is focused more on capacity, paying particular attention to the effects of cyclic loading but generally with less concern on deformations compared with onshore design. These differences have led to the development of separate design codes for offshore structures, which are in most cases more prescriptive than onshore codes but are also more sophisticated in key areas. The paper describes design principles for foundation and anchoring systems ranging from shallow footings to piles and caissons, highlighting differences between onshore and offshore practice and also the link (or gap) between research and practice.

RÉSUMÉ

Les méthodes de dimensionnement des ouvrages géotechniques en mer sont nées des méthodes utilisées sur terre, mais les deux domaines d'application ont commencé à diverger il y a maintenant une trentaine d'année, en partie à cause de l'échelle des fondations utilisée en mer, mais également à cause des différentes techniques de construction (ou d'installation) utilisées. Les groupes de plusieurs pieux de diamètre moyen ont ainsi été remplace par quelques pieux de très gros diamètre, l'excavation des couches superficielles des sédiments marins a été remplacée par l'utilisation de fondations avec jupe, transférant le niveau d'encastrement effectif de la fondation au niveau du pied de la jupe. L'installation sous-marine a également permis l'utilisation des techniques de succion, forçant la fondation ou le caisson à pénétrer de plusieurs diamètres dans le sol. Les méthodes dimensionnement des ouvrages en mer mettent plus l'accent sur les problèmes de capacité, avec une attention particulaire pour les effets cycliques, que sur les problèmes de déformations, a l'inverse des méthodes de dimensionnement des ouvrages a terre. Cette différence a conduit à l'élaboration de méthodes de calcul qui dans la plupart des cas sont plus normatives que les méthodes de calcul des ouvrages a terre, mais qui sont aussi parfois plus sophistiquées dans certains domaines clefs. Cet article décrit les principes de dimensionnement des fondations et systèmes d'ancrage, des fondations superficielles aux pieux et caissons, en mettant l'accent sur les différences de pratiques entre les méthodes appliquées aux ouvrages en mer et celle aux ouvrages a terre, ainsi que sur les liens (ou les manques) entre la recherche et la pratique.

1 INTRODUCTION

Offshore geotechnical practice has tended to diverge from onshore practice, both in terms of types of foundation or anchoring systems and in the geotechnical specialists who service the industry. Even in areas such as site investigation, where similar field and laboratory testing techniques are used, strategies, implementation methods and types of test are often very different in the offshore environment. One of the main aims of this paper is therefore to highlight differences in offshore and onshore practice.

The relentless rise in world energy consumption has led to hydrocarbon exploration, and eventually production, in new regions of the world, initially extending onshore fields in Texas and the Middle East into shallow offshore waters, followed by major regional developments in the North Sea, and offshore Australasia and the Far East, South America, India and most recently West Africa. Each new region required adapting design approaches for new soil conditions, for example heavily overconsolidated clays and dense sands in the North Sea; carbonate sediments in Australia, Brazil and India; ultra-high plasticity soft clays in West Africa.

Within each region, there has been an inevitable progression from shallow to deep water, with recent installations in 2000 m of water in the Gulf of Mexico (Newlin, 2003) and deeper fields currently being planned. This progression has also encompassed changing soil types, but more importantly the types of facility have evolved from fixed steel or concrete platforms, to floating facilities. The latter range from tension leg platforms with vertical tethers anchored to piles, to spars and tankers held in position by catenary mooring chains or, more recently, by lightweight 'taut-wire' polyester ropes. Such developments have led to a variety of innovative anchoring systems, each gradually evolving under the different loading regimes imposed.

The rapid increase in water depths, from under 200 m in the 1980s to 2000 m and more now, has necessitated considerable investment in research in order to validate new foundation and anchoring systems. In parallel, design guidelines have been developed by the American Petroleum Institute (API) and the more recent International Standards Organisation (ISO). While these inevitably lag the advances in understanding achieved through research, the industry has strived to keep pace by continuously updating the design codes by means of standing committees of specialists. Regulatory bodies such as the American Bureau of Shipping (ABS), Det Norske Veritas (DNV) and Lloyds, have also played an important role in validating new design approaches supported by research findings and helping to coordinate advances across the industry.

It is not possible within the scope of this paper to cover all aspects of offshore geotechnical design, and the focus here is on

those aspects that differ from conventional onshore design. The paper starts with a brief summary of recent developments in offshore site investigation techniques, before discussing design practice for deep (piled) foundations and shallow foundations. Multi-footing structures, such as mobile drilling platforms resting on temporary foundations, are then considered. Finally, different types of anchoring system are described, and recent developments in design summarised.

2 SITE INVESTIGATION AND LABORATORY TESTING

2.1 *Overview*

The most important consideration in respect of planning offshore site investigation is the very high cost of vessels suitable for carrying out this work, both for mobilisation and in daily rates, which are typically $250,000 to $500,000 per day. Costs for the site investigation itself are over and above those for the vessel. The consequence of the high costs is that site investigations are generally delayed until the project is fully approved, so that much of the early 'concept development' studies have to be undertaken with little or no detailed knowledge of soil conditions. For small projects, only a single site investigation voyage will be undertaken, which necessitates careful planning to ensure that all relevant data are acquired. For larger projects sufficient funding may be available to conduct a preliminary site investigation initially, with a more detailed study undertaken once more definite decisions have been reached regarding the nature of the foundation or anchoring systems to be designed.

As for most onshore projects, offshore site investigation involves a combination of field testing and acquisition of soil samples, followed by a program of laboratory testing. In the field, the two main forms of test are piezoccone penetrometer testing (CPT) and, particularly in the Gulf of Mexico, vane shear tests. In recent years, starting in about 1997, there has been increasing use of alternative forms of penetrometer, in the form of cylindrical (T-bar) and spherical (ball) 'full-flow' penetrometers. These are described in detail later.

A comprehensive review of in situ testing methods for offshore site investigations was given by Lunne (2001), with more recent developments discussed by Randolph (2004). Key aspects of those reviews are summarised here.

2.2 *Field Work*

2.2.1 *Vessel requirements*

The size and type of vessel required for site investigations varies with water depth and with method to be used for in situ testing and sample acquisition. The two approaches for the latter are (a) downhole mode, where testing and sampling are carried out at the bottom of a cased borehole, and (b) seabed mode, where a rig is placed independently on the seabed. Where a seabed rig is used, the vessel need merely be large enough to carry the equipment, which will generally fit within one or two standard 6 m containers, with typical dry weights of around 10 to 15 tonnes. Geophysical survey or supply vessels are sufficient for this mode of testing.

Downhole testing is best carried out from purpose-designed vessels containing a moon pool through which drilling is carried out. An important feature for high quality results is heave compensation to limit the motion of the drill pipe as the vessel responds to swell. Jack-up rigs can be used in water depths of up to 100 m or so, provided one is available in the locality, and they provide a stable platform free of swell-induced motion. Anchored vessels may be used in water depths up to 200 m, beyond which dynamically-positioned vessels are more efficient (Lunne, 2001).

2.2.2 *Downhole systems*

Modern downhole testing systems allow the instrument to fall freely down the drill pipe and latch into the base, after which the device (e.g. cone or vane) can be jacked into the soil hydraulically. Data acquired during the test are saved locally (to be recovered later), and the whole system is then retrieved by a wireline that is lowered within the drill-pipe and latches onto the top end of the instrument. The system of this type operated by the international site investigation company Fugro is referred to as the XP system (Hawkins & Markus, 1998).

Downhole systems allow CPTs, vane tests or sampling to be undertaken, and it is common to alternate, for example between sampling and carrying out a cone or vane test. For CPTs, cone strokes of up to 3 m may be achieved, while vane tests are typically carried out 0.75 m and 1.5 m below the base of the drill string. In soft sediments, disturbance from drilling may extend 0.4 to 0.8 m below the base of the drill string, and that interval would need to be discounted in the interpretation of cone or vane test data, or in recovered samples (Lunne, 2001).

2.2.3 *Seabed systems*

The trend towards deep water hydrocarbon developments, with anchored floating facilities and generally soft seabed sediments, has led to wider use of seabed systems for site investigation. In modern systems, penetration testing is carried out using a continuous push by means of a wheel-drive unit (Fig. 2.1), with the penetrometer rods suspended under tension above the seabed (Peuchen, 2000). The wheel-drives may be fitted with compressible studs around the periphery of each wheel in order to improve grip on the cone rods, minimising slippage.

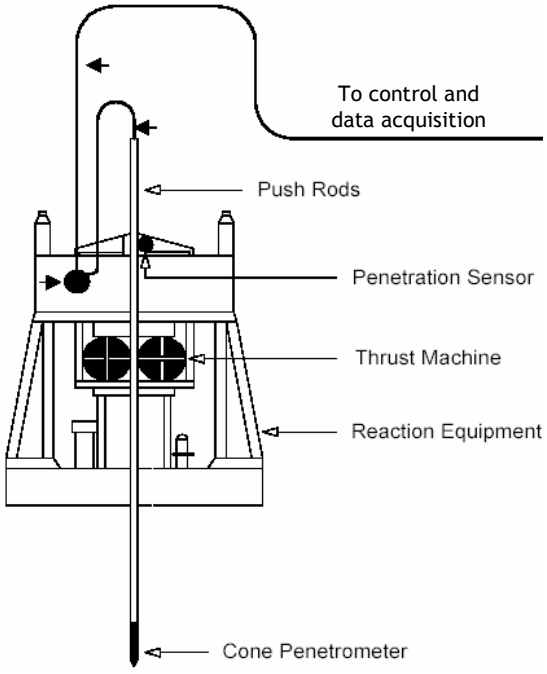

Figure 2.1 Fugro's Seacalf system and wheel-drive

Site investigations based on seabed systems are more limited in depth, compared with downhole systems where sampling and testing may extend to 150 m or more below the seabed. However, they are sufficient for most anchoring systems, which are generally contained within the upper 30 to 40 m. The quality of data from seabed systems is superior to that from downhole systems, as illustrated in Figure 2.2. In addition to generally higher values of net cone resistance, there is much better definition of the seabed strength intercept from the seabed CPT. The shallow peak in shear strength within the top 0.5 to 1 m is a common, and intriguing, feature of many offshore sediments, even where

they are geologically normally consolidated; it can also be very important in the design of pipelines and other subsea facilities.

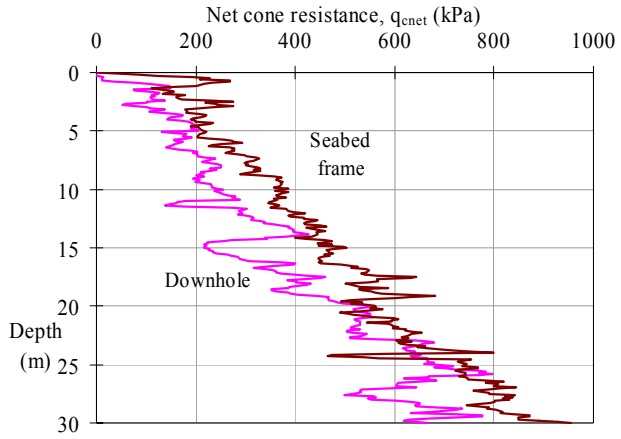

Figure 2.2 Comparison of downhole and seabed frame CPTs

Vane testing can also be carried out from seabed frames, using the wheel-drives to penetrate the vane to the required depth before performing the test. However, seabed frames mostly not cannot take samples deeper than the upper 2 to 3 m, since there is no drilling capability.

An alternative form of seabed system that combines the ability to take samples and perform penetration testing, is the Portable Remotely Operated Drill (PROD) developed by Benthic Geotech (Carter et al., 1999). The capabilities include:

- operating in up to 2000 m water depth;
- rotary drilling and sampling;
- piston sampling, 44 mm diameter and maximum core length of 2.75 m, down to maximum depth of 125 m;
- cone penetrometer device, 36 mm diameter with 2 m pushes to maximum depth of 100 m, using acoustic transmission from the CPT to the drilling module;
- ball penetrometer with 60 mm ball diameter and similar capability to cone penetrometer.

Although the system is still at a relatively early stage of development, it has already shown far-reaching potential for robotic deep-water investigations. Figure 2.3 shows a schematic of the carousel-based system.

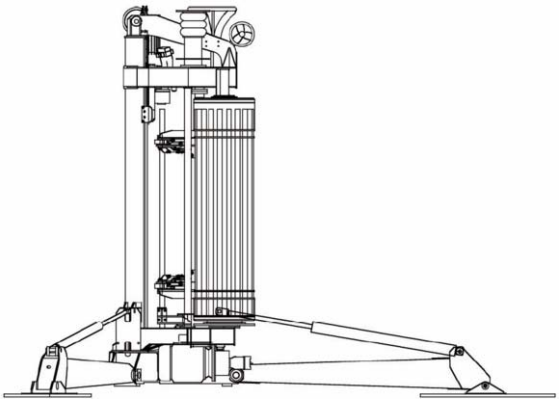

Figure 2.3 Portable Remotely Operated Drill (PROD)

Other forms of remote seabed sampler have been described by Young et al. (2000) (Jumbo Piston Corer or JPC) and Borel et al. (2002) (STACOR sampler). These devices have a steel barrel, with typically a 100 mm diameter PVC liner. They penetrate the seabed under their own weight, and can retrieve samples of up to 20 to 30 m long. Recovery rates in excess of 90 % are achieved through the use of a piston that, in the case of the STACOR, is maintained at seabed level by a pulley system as the corer penetrates (Borel et al., 2002). Strict control of the piston to ensure it remains fixed as the corer penetrates is essential in order to minimise disturbance of the seabed soils ahead of the corer. Disturbance assessed from radiographs appears to be limited to the edges of the core, and strength measurements show similar normalised parameters to those obtained from conventional high quality sampling. For soft sediments, corers penetrating by self-weight have clear advantages in terms of: (a) the speed with which the samples can be obtained without the need for sophisticated drilling vessels; and (b) in the continuous large diameter samples obtained.

2.2.4 *Vane testing*

The vane shear test has been used extensively in offshore site investigations, but in particular in the soft normally consolidated clays in the Gulf of Mexico (Geise et al., 1988; Johnson et al., 1988; Kolk et al., 1988; Quiros & Young, 1988; Young et al., 1988). During that time the equipment has been continuously improved, both in respect of wire-line operations and deployment from seabed frames. In soft clays, the (mostly) standard procedures involve a vane of 65 mm diameter and 130 mm high, with net area ratio of around 9 to 11 % and perimeter ratio of 3 to 4 % (Cerato & Lutenegger, 2004). The strength measured in a vane test is sensitive to the precise testing procedure, in particular the delay between insertion and testing, and the rotation rate (Chandler, 1988). In offshore practice the vane is pushed to the required depth at a rate of 20 mm/s and then left for 5 minutes before being rotated at 0.1 or 0.2 °/s (the onshore standard being 0.1 °/s or 6 °/min).

In onshore practice it is common to apply correction factors to the vane, such as those proposed by Bjerrum (1973) in the range 0.6 (for high plasticity soils) to 1 (for low plasticity soils). Aas et al. (1986) concluded that correlating the correction factor with the strength ratio, s_u/σ'_{v0}, gave better consistency, with the factor reducing from unity for a strength ratio of 0.2, down to 0.6 for a strength ratio of 0.6.

Randolph (2004) showed that the the strain rates imposed on the soil during vane tests are typically 10^4 times greater than a standard laboratory test rate of about 1 %/hour. The increase in torque due to strain rate effects is indicated in Figure 2.4, with μ representing the proportional increase in strength per log cycle of strain rate. For the standard rotation rate of 0.1 °/s, the torque is 40 to 60 % greater than the reference value (i.e. ignoring strain rate effects). In offshore practice, however, vane shear strengths are rarely adjusted, even for strength ratios in excess of 0.4 (Kolk et al., 1988). A partial justification for this is the inevitable disturbance due to insertion of the vane. Cerato and Lutenegger (2004) demonstrated how the degree of disturbance various almost linearly with the thickness of the vane blades. This disturbance compensates, at least partially, for the high strain rates invoked during a vane test.

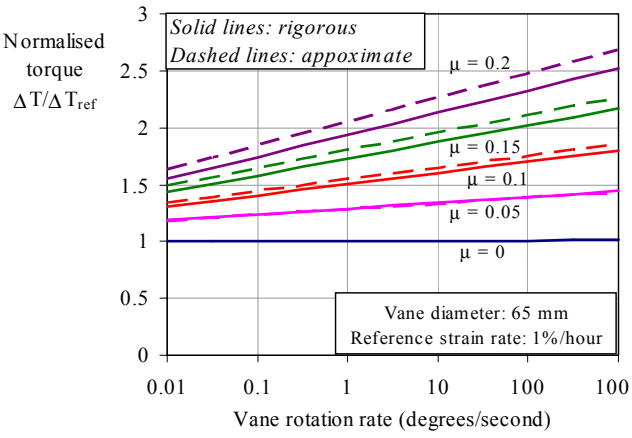

Figure 2.4 Effect of vane rotation rate on torque

2.3 *New Developments in Penetrometer Testing*

Offshore cone penetration testing generally follows the international standard (ISSMGE, 1999), with a 36 mm diameter cone fitted with a 60º tip, pushed into the soil at a rate of 20 mm/s. Almost all offshore cones include pore pressure measurement, with the shoulder, or u_2, position being the most common. Alternative cone diameters are also used, ranging from mini-cones of diameter 11 to 16 mm up to a large, 65 mm, diameter instrument (Lunne, 2001). While the miniature systems are aimed at a minimising weight, and use a coiled rod rather than a suspended length of straight rods, the large diameter cone was developed in order to increase the load on the cone tip for soft sediments. However, in deep water the increased diameter does not change the low ratio of the change in resistance in the upper few metres of soil (typically 200 kPa or less) to the ambient hydrostatic pressure acting on the cone tip (up to 10 or 20 MPa).

In addition to the low signal ratio, corrections to the measured cone resistance due to pore pressure acting on the back face to get the true total cone resistance, q_t, and then subtraction of the overburden stress, σ_{v0}, to obtain a net cone resistance, q_{cnet}, both increase the potential for error in estimating the strength of soft sediments. Once the net cone resistance profile has been established, an appropriate cone factor, N_{kt}, must be chosen in order to estimate the shear strength by means of

$$s_u = \frac{q_t - \sigma_{v0}}{N_{kt}} = \frac{q_{cnet}}{N_{kt}} \qquad (2.1)$$

Lunne et al. (1985, 2001) quote ranges of N_{kt} for North Sea clays in the range 8 to 20, while Quirós & Little (2003) quote N_{kt} values at a single site varying from 17 at shallow depths to 11 at 120 m. Much of this variation is due to variability in sample quality, and also in the type of test used to measure the shear strength, s_u.

It is known (Teh & Houlsby, 1991; Lu et al., 2004) that the cone resistance is affected by the rigidity index, G/s_u (where G is the shear modulus) and also the in situ stress ratio, defined as $\Delta = (\sigma_{v0} - \sigma_{h0})/2s_u$. It is also likely it will correlate better with some tests than others, with N_{kt} showing a closer grouping relative to, perhaps, triaxial compression strengths than those measured in simple shear.

In an attempt to improve the ability to make absolute estimates of shear strength directly from field penetrometer tests, alternative 'full-flow' penetrometers have been introduced over the last few years. The (nominally) plane strain T-bar and axisymmetric ball penetrometers are designed to have a projected area about 10 times the shaft they are attached to, in order to minimise any correction due to the overburden stress. In their simplest form, they can be attached to the normal cone load cell, merely be unscrewing the cone tip and replacing it by the required penetrometer (see Fig. 2.5).

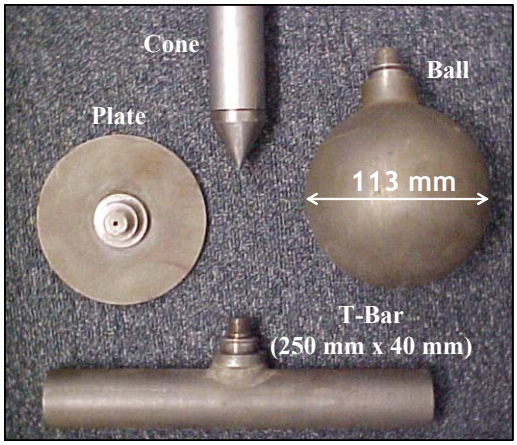

Figure 2.5 Alternative full-flow penetrometers with cone

The T-bar penetrometer (Stewart & Randolph 1991, 1994), was first used offshore in 1997 (Randolph et al., 1998a, Hefer & Neubecker, 1999). The intention was that plasticity solutions for the flow round a cylinder (Randolph & Houlsby, 1984) or sphere (Randolph et al., 2000) would provide the basis for obtaining absolute estimates of shear strength directly from the measured penetration resistance. These solutions are shown in Figure 2.6, together with a range of theoretical cone factors, as a function of the interface friction coefficient.

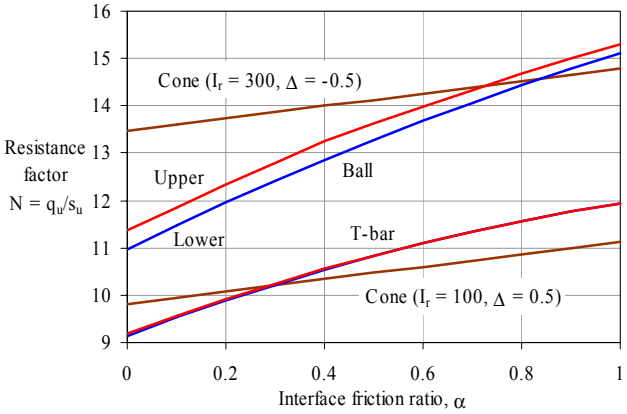

Figure 2.6 Theoretical factors for cone, T-bar and ball

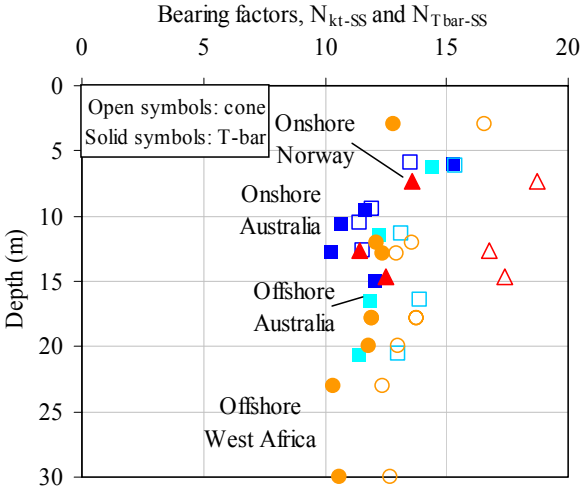

Figure 2.7 Cone (N_{kt}) and T-bar (N_{Tbar}) factors related to simple shear strengths in lightly overconsolidated clays

Early experience with the T-bar tended to support the theoretical factors, with typical values in the range 10 to 12. Note that because of the symmetric nature of the instruments, it is logical to correlate the penetration resistance with the strength measured in simple shear, which is usually close to the average of those in triaxial compression, triaxial extension and simple shear. Randolph (2004) reported T-bar and cone factors from 4 different clay sites, as shown in Figure 2.7, and commented that the average T-bar factor for each site had a much smaller coefficient of variation than the average cone factor, even though the scatter on each individual site was similar for the two instruments. It should be noted that recent experience in carbonate silts has suggested that the T-bar factor might be as low as about 5 in extreme circumstances, at least relative to subsequent simple shear tests, (Erbrich, 2005), although the reasons for this are not fully understood.

Similar consistency with theoretical factors was not found with the ball penetrometer, which tended to show similar penetration resistance to the T-bar, at least in reconstituted soils (Watson et al., 1998), rather than ~25 % higher resistance as suggested from the plasticity solutions. Furthermore full-flow

penetrometer tests in a natural varved clay reported by DeJong et al. (2004) show the ball resistance some 25 % lower than that of the T-bar.

It is clear that the picture is more complicated than implied by solutions based on simple rate independent, perfectly plastic soil models. Analysis shows that average shear strain rates in the plasticity mechanisms are some 6 to 7 orders of magnitude higher for the T-bar than in a standard laboratory test and 4 to 5 orders of magnitude higher for the ball. Partly compensating the effects of high strain rates is the gradual loss in strength due to remoulding of the clay as it passes through the flow field.

Einav & Randolph (2005) analysed cylindrical and spherical penetrometers by combining the strain path method with the kinematic mechanisms derived from optimised upper bound plasticity solutions. Each soil element is followed as it flows through the mechanism, and its shear strength adjusted as a function of the shear strain rate, $\dot{\gamma}$, and the total accumulated plastic shear strain, ξ. The rate dependency is expressed as

$$s_u = s_{u,ref}\left[1+\mu \log\left(\frac{\dot{\gamma}}{\dot{\gamma}_{ref}}\right)\right] \qquad (2.2)$$

where $s_{u,ref}$ is the shear strength at a reference strain rate, $\dot{\gamma}_{ref}$, of 1 %/hour.

Gradual softening of the soil as it passes through the mechanism is modelled by factoring the shear strength by a damage factor, δ, expressed as

$$\delta(\xi) = s_{us}/s_{ui} = \delta_{rem} + (1-\delta_{rem})e^{-3\xi/\xi_{95}} \qquad (2.3)$$

where δ_{rem} represents the fully remoulded damage factor (the inverse of the sensitivity), while ξ_{95} represents the cumulative plastic shear strain to achieve 95 % damage towards the remoulded condition.

They found that the rate dependency led to an increase in penetration resistance expressed as

$$q \approx q_0(1+\rho\mu) \qquad (2.4)$$

where the factor ρ reflects the average strain rate relative to the reference value. Assuming an interface friction ratio of 0.2 and penetration velocities of 20 mm/s for a 40 mm diameter T-bar, or 113 mm diameter ball, the factor was found to be about 6.8 for the T-bar, and 4.7 for the ball, implying average strain rates of just under 10^7 (T-bar) or 10^5 (ball) higher than the reference value.

For typical values of the rate parameter, μ, of around 0.1 (10 % increase in strength per log cycle), this should lead to penetration resistances that are 50 to 70 % greater than the rate independent value, q_0. The fact that experimental values of penetration resistance do not show such enhancement compared to the theoretical solutions shown in Figure 2.6, suggests that softening plays an important compensating role.

2.3.1 *Cyclic penetration tests*

It is standard practice for full-flow penetrometer tests to monitor the T-bar or ball resistance during extraction as well as during penetration. Indeed, this practice is now spreading to include standard cone penetration tests since, after correction for the overburden stress, a net negative extraction resistance is obtained in much the same way as for a T-bar test. Typical ratios of extraction T-bar resistance to penetration resistance are shown in Figure 2.8. Data from the two offshore soft clay sites show a ratio of around 0.6 apart from at shallow depths, while the onshore sites in Australia (Burswood) and Norway (Onsøy) bracket the offshore data. (Note that the periodic reductions in the ratio for the onshore Australia site are due to previous cyclic loading tests, discussed below.)

While a single penetration and extraction cycle leads to significant loss in strength, softening to a fully remoulded state requires 5 to 10 further cycles. Example data from a cyclic test in soft clay are shown in Figure 2.9. The slight eccentricity in the extraction and penetration resistance probably reflects a minor zero offset, due either to temperature effects or slight bending moment acting on the load cell. In interpreting the cyclic strength, the zero may be corrected to give a smooth degradation in absolute resistance, as shown in Figure 2.10, where the resistance in each cycle has been normalised by the initial resistance (plotted as cycle 0.5). Note that, since softening occurs during initial penetration, the final normalised resistance is greater than the true value of δ_{rem} (or inverse of the sensitivity).

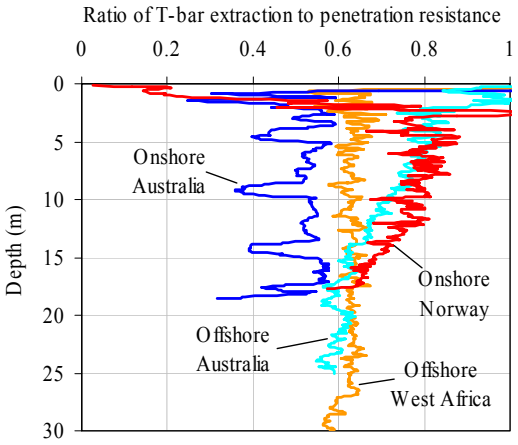

Figure 2.8 Ratio of extraction to penetration resistance for T-bar

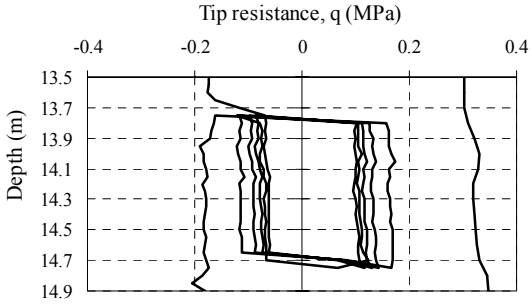

Figure 2.9 Cyclic T-bar test at depth 14.3 m (Chung & Randolph, 2004)

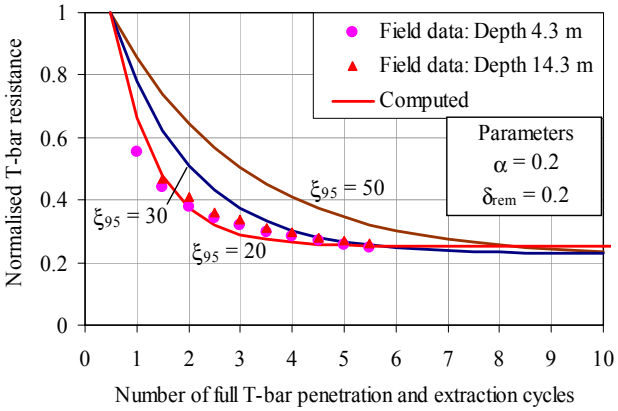

Figure 2.10 Calibration of degradation model from cyclic T-bar tests

The computed curves shown in Figure 2.10 are from the analysis developed by Einav and Randolph (2005), and comparison of these curves with the measured data allow calibration of the parameters δ_{rem} and ξ_{95}, which may then be used to assess the degree of softening that occurs during the original penetration, and hence an appropriate T-bar factor in order to estimate the true peak shear strength.

2.3.2 *Net penetrometer factors*

The effects of high strain rates and partial softening may be combined to provide a revised estimate of the penetrometer factor for T-bar and ball. For the penetrometer sizes indicated in Figure 2.5, and a penetration rate of 20 mm/s, the net factors may be expressed as

$$N_{Tbar} \approx (1+6.7\mu)\left(\delta_{rem} + (1-\delta_{rem})e^{-1.5\xi_{Tbar}/\xi_{95}}\right)N_{Tbar-ideal}$$
$$N_{Ball} \approx (1+4.8\mu)\left(\delta_{rem} + (1-\delta_{rem})e^{-1.5\xi_{Ball}/\xi_{95}}\right)N_{Ball-ideal} \quad (2.5)$$

where ξ_{Tbar} and ξ_{ball} is the average plastic shear strain undergone by soil elements passing through the respective mechanisms. These are approximately 4 (400 %) and 2 for the T-bar and ball. The ideal N factors are those from Figure 2.6, with the interface friction ratio taken as δ_{rem} (for consistency with usual assumptions for objects such as piles penetrating through clay). This result is illustrated in Figure 2.11 for the T-bar.

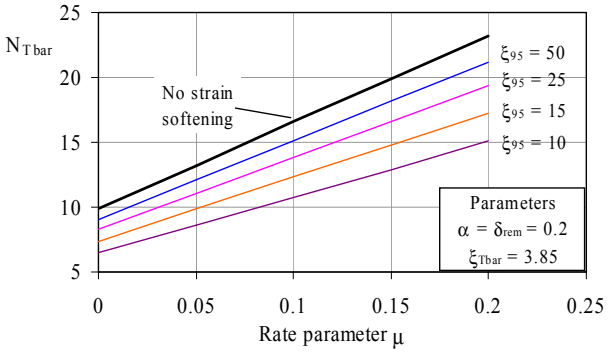

Figure 2.11 Combined effect of strain rate and strain-softening for T-bar (Einav & Randolph, 2005)

It may be seen that for a typical rate parameter of $\mu \sim 0.1$, the T-bar factor varies from 10.7 for rapidly softening soil ($\xi_{95} = 10$) to 15.1 for ductile soil ($\xi_{95} = 50$). The corresponding ranges for the ball are 13.3 to 16.1. For given soil properties, the ball factor still appears to exceed that for the T-bar, although because of a lower rate dependency the difference is less than indicated by the simple plasticity solutions. The range for the T-bar factor compares with average field values for the data in Figure 2.7 in the relatively narrow range 11.9 to 12.5, implying that any variation in the rate parameter, μ, is matched by a corresponding variation in the ductility parameter, ξ_{95}.

The same procedure has been used to evaluate T-bar factors as low as 7.65 for the carbonate sandy silt at the Yolla field, in the Bass Strait, offshore Australia. This arises due to a combination of low viscous rate effect ($\lambda = 0.03$) and very high sensitivity ($\delta_{rem} = 0.05$) found for such soils (Erbrich, 2005). However, a convincing explanation for the observed T-bar factor of about 5, that was reported earlier, remains elusive even with the new understanding provided using the method outlined above.

2.3.3 *Variable rate penetration tests*

The importance of rate effects in determining appropriate factors for interpretation of penetrometer data suggests that it would be advantageous to measure rate effects directly in the field. This may be achieved by varying the rate of penetration over, preferably, two orders of magnitude. A systematic way of doing this has been described by House et al. (2001) and Randolph (2004), and has been referred to as a 'twitch' test. The technique comprises a succession of step decreases in the rate of penetration, with the penetrometer being advanced a fixed distance (for example 2 diameters) each time.

In clays, as the penetrometer velocity is reduced from initially undrained conditions the penetration resistance initially decreases due to reduced viscous effects, and then starts to increase again as partial consolidation (and local strengthening of the clay) becomes significant (Roy et al., 1982). This is shown in Figure 2.12 for cone tests conducted in soft clay at Burswood, in Western Australia. The penetration rate is halved sequentially, from an initial rate of 20 mm/s, and the resistance decreases initially before starting to increase again for penetration rates below about 0.2 mm/s. The onset of partial consolidation at that point is demonstrated by the B_q value, which remains approximately constant initially (independent of rate) but then starts to drop rapidly once the penetration rate falls to 0.2 mm/s and below.

For undrained conditions, the rate dependency may be assessed by plotting the resistance, normalised by its value at the standard penetration rate of 20 mm/s, as shown in Figure 2.13. The various penetrometers show an average rate effect of 13 % per log cycle, with the T-bar giving the maximum effect (16 %) and the cone least (10 %).

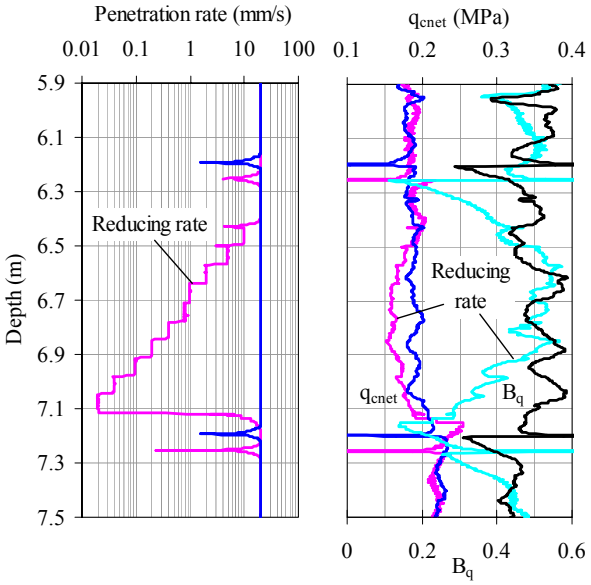

Figure 2.12 Results from standard and 'twitch' cone tests in Burswood clay (Randolph, 2004)

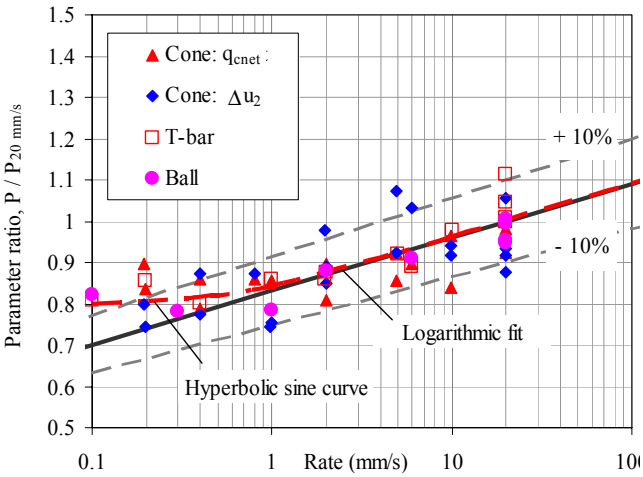

Figure 2.13 Effect of penetration rate for undrained conditions

As partial consolidation occurs the penetration resistance will increase gradually towards a fully drained value. Typically, this has been found to develop over about 2 to 3 orders of magnitude of the penetration rate. Figure 2.14 illustrates this (a) for the excess pore pressure ratio, B_q, from a cone test, and (b) for the T-bar resistance in a similar 'twitch' test. The data have been fitted by backbone curves of the general form

$$\frac{q}{q_{ref}} = \left(a + \frac{b}{1+cV^d}\right)\left\{1 + \frac{\mu}{\ell n(10)}\sinh^{-1}\left(V/V_o\right)\right\} \qquad (2.6)$$

where the first part of the expression models the transition from undrained to drained conditions as a function of the normalised penetration rate, V, while the second part reflects the viscous enhancement of resistance at high penetration rates.

The normalised velocity in Equation (2.6) is expressed (non-dimensionally) as

$$V = \frac{vd}{c_v}\,\frac{s_{u-cyc}}{s_{u-mono}} \qquad (2.7)$$

where v and d are the velocity and diameter of the penetrometer, and c_v is the coefficient of consolidation for the soil. As may be seen, partial consolidation starts for V ~ 30 to 100, with B_q starting to decrease slightly before the resistance starts to increase (the latter being delayed by viscous effects).

As described by House et al. (2001), variable rate penetration tests with a step-wise reduction in rate may be used to assess the velocity at which the penetration resistance starts to increase (or the B_q value from a piezocone test starts to decrease), and hence deduce a value of consolidation coefficient for the soil with reference to these transition values of V (= vd/c_v). They also point out that, even targeting a final normalised velocity of V ~ 2 to 4, the total time for such a test is comparable to the time for 50 % dissipation in a conventional piezocone dissipation test. The potential to terminate the test at V ~ 10 (less than the range of transition values above) would lead to a considerable reduction in test time needed to establish c_v values.

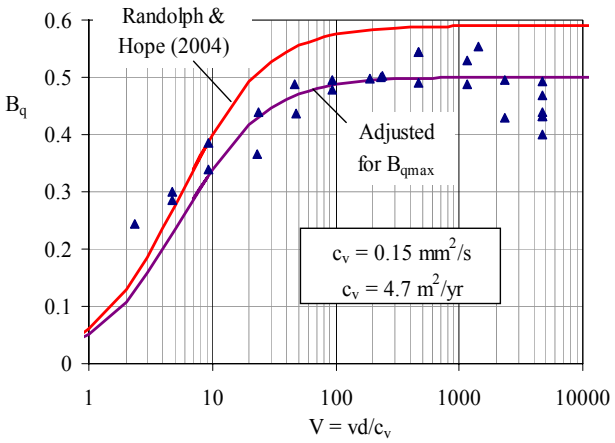

(a) Excess pore pressure ratio from 'twitch' cone tests

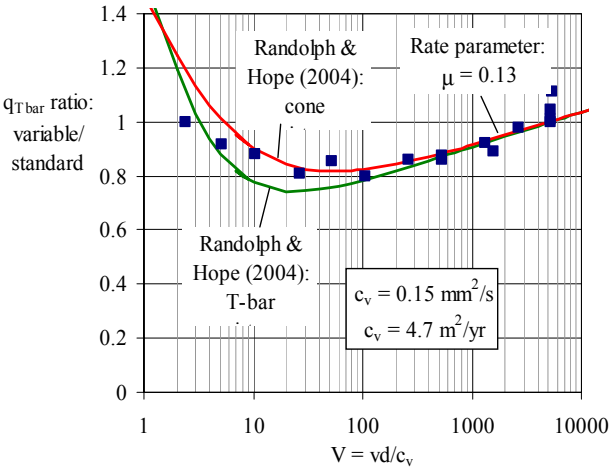

(b) Penetration resistance from 'twitch' T-bar tests

Figure 2.14 Normalised response from variable rate penetrometer tests (field data from Burswood; Randolph, 2004)

2.4 *Laboratory Testing*

After the field work phase is complete, a laboratory testing program is invariably undertaken to determine soil parameters for engineering design purposes. Depending on the application under consideration, the laboratory testing may comprise no more than simple classification tests, similar to those performed for most onshore projects, or it may extend into advanced specialised testing to model features that are only encountered in offshore applications. The subject of laboratory testing is extensive, and hence only a brief review is presented here.

In every laboratory testing program, classification testing is an important feature. Standard tests that should be undertaken in every case include; moisture content, dry density, particle specific gravity, particle size distribution, Atterberg limits and carbonate content. More specialised classification testing that is also commonly performed includes X-ray diffraction for assessing particle mineralogy, and electron microscopy to enable detailed geological classification. The latter tests are most commonly undertaken where carbonate sediments are encountered. Rudimentary strength tests such as torvanes, mini vanes or pocket penetrometers are also carried out routinely on 'end logged' samples. These are often undertaken during the offshore site investigation phase when the initial sample logging is performed, usually on just the ends of samples in order to preserve the main part intact. In cemented carbonate soils, simple tools such as the pin probe (Fahey & Jewell, 1988) have been developed and are often used to aid in classifying the degree of cementation during the logging process. Fall cone tests are also commonly performed on intact and remoulded soil to assess the sensitivity of fine grained soils.

For many traditional piled jackets, the only other tests that are routinely undertaken are simple unconsolidated undrained (UU) triaxial tests on 'cohesive' samples (generally clay). In most cases, these relatively crude tests will underestimate the true undrained strength of a soil sample. However, these tests underpin the calibration of the current API pile design method in clay. Hence, since these tests are also relatively cheap, they remain very popular.

For cemented soils, the 'equivalent' of a UU test is the unconfined compression strength test (UCS). These tests are very commonly used where such soils are encountered, but there is often a large degree of scatter in the results due to both natural variability and the difficulty of recovering samples without damaging the cementation to a greater or lesser degree. Correlation of the results to cone resistance is the most reliable method of addressing this variability.

Where foundation systems other than piled jackets in 'traditional soils' are being considered, more sophisticated testing is generally required. It is important that the tested samples should be of the best quality and hence it has often been useful to X-ray samples before testing, since this can reveal severe sampling disturbance. Systems have also been developed to classify the quality of recovered samples in fine grained soils based on reconsolidation strains (Lunne et al. 1997b).

For the design of large shallow foundations, a comprehensive program of static and cyclic strength testing is required. These include monotonic and cyclic triaxial (compression and extension) and simple shear tests. The cyclic tests need to be performed with cyclic to average shear stress ratios that reflect the conditions appropriate for the foundation under consideration, but it is common to simplify the testing regime to 'pure 1-way' and 'pure 2-way' cyclic loading. Combined with the monotonic strength data, it is generally then possible to interpolate appropriate cyclic strengths for any given bias of cyclic loading.

It is now becoming increasingly common to focus the cyclic testing on simple shear tests, since each test requires much less material and hence a whole suite of tests can be performed over a limited depth range on almost uniform material. Similar cyclic testing programs are also usually performed for the design of

large suction caisson systems. Over the years, an enormous quantity of data has been compiled by the offshore industry and it is now common to minimise new test programmes by performing a limited number of tests and comparing these results to standard databases, such as that compiled for Drammen Clay. Andersen (2004) presents a summary of the Drammen Clay results as well as results for several other clay soils. An example summary of cyclic simple shear test results is shown in Figure 2.15, giving combinations of average (τ_a) and cyclic (τ_c) shear stress, normalised by the monotonic shear strength in simple shear, s_u^{DSS}, required to cause failure in 10 cycles

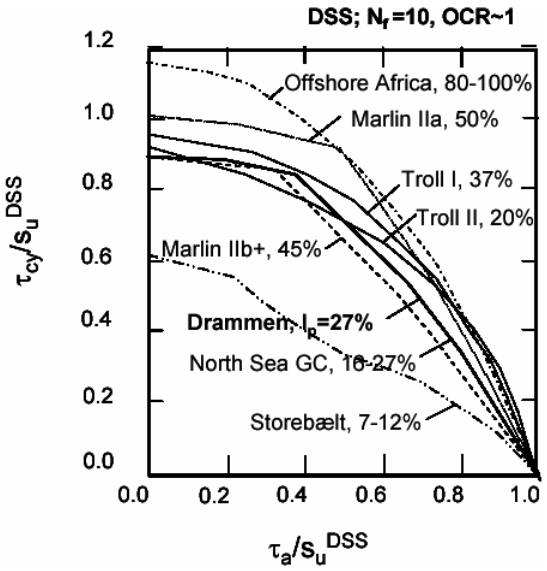

Figure 2.15 Normalised shear stresses that give failure after 10 cycles in simples shear for various clays (Andersen, 2004)

In Australia, Advanced Geomechanics have compiled an extensive database of cyclic simple shear strength test results for over 20 different uncemented carbonate soil types and locations. From this database, upper and lower bounds can be established, and the results from any new sites can be quickly evaluated relative to the existing data. Typical results from this database, obtained for 20 cycles of pure 2-way loading, are presented on Figure 2.16.

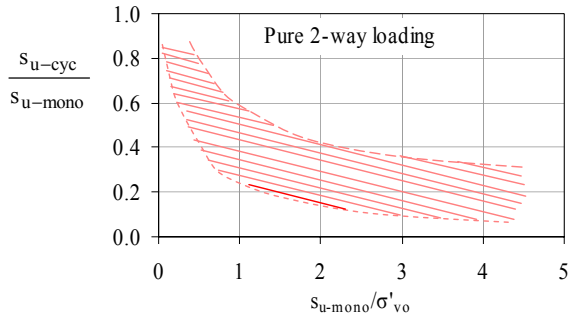

Figure 2.16 Cyclic strength database for uncemented carbonate soils.

For uncemented silica sands, onshore practice where cyclic loads needs to be considered (mainly seismic applications) has generally moved to cone-based correlations for assessing the cyclic strength, due to the difficulty of recovering and testing undisturbed samples. This difficulty is no less important for offshore applications, but to date design of important structures has relied on site specific cyclic testing of (usually) reconstituted samples, and has therefore probably included some inherent conservatism. Procedures such as cyclic drained pre-shearing of the samples have been developed to try to minimise the effects of reconstitution and sample bedding problems.

Although foundation deformations are generally less important for offshore structures than onshore, the small strain stiffness is often an important design parameter (e.g. for seismic analyses, assessment of natural period for the structure and pile design in brittle materials). Resonant column, bender element or internal strain measurements during triaxial tests are generally used for this assessment. In soft offshore soils, which are a common occurrence, consolidation settlements are often large. Standard oedometer tests or more sophisticated Rowe cell tests and isotropically consolidated triaxial tests are generally used to assess the relevant design parameters. These tests also provide an estimate of the coefficient of consolidation, although, in faster draining soils, the stiffness assessed from these tests needs to be combined with results from separate permeability tests in order to obtain an accurate estimate of the coefficient of consolidation.

The development of new design methods for driven piles has increased the use of interface shear box or ring shear tests to assess appropriate interface friction angles (Jardine et al. 1992) For drilled and grouted piles in carbonate soils, specialised tests such as CNS shear box tests are recommended, which are similar to a standard interface direct shear test but include a 'constant normal stiffness' spring that controls the normal stress applied to the sample as it is sheared (monotonic or cyclic loading). The spring stiffness is chosen to be representative of the soil in the far-field surrounding a pile.

From this short and partial summary it may be seen that laboratory testing for offshore applications covers the full range from the most basic testing to the most advanced. Due to the scale of most offshore projects, many very sophisticated testing procedures have been developed to address aspects of soil behaviour that are sometimes encountered, but rarely considered in the same detail, during onshore projects.

3 PILE FOUNDATIONS

3.1 *Applications*

Steel lattice (or 'jacket') structures are still the most common form of fixed offshore platform, with the design evolving gradually from their first use for the shallow offshore fields in the Gulf of Mexico, and are now used in water depths of up to 400 m. The platforms are fixed to the seabed by piles inserted through sleeves attached to the jacket, with the piles eventually grouted to the sleeves after installation.

In the simplest configuration, a small platform may have one pile per corner, inserted inside the main tubular column of the jacket. For large platforms, additional 'skirt' piles may be added along the sides of the rectangular base, or multiple piles installed through sleeves at the platform corners. An example of the latter is shown in Figure 3.1, for the North Rankin A platform on the North-West Shelf of Australia, which sits in 125 m of water. That platform has 8 piles per corner, and an adjacent flare support structure has 2 piles per corner. Note that the under-reamed bell foundations, and the stabilising guys and box-anchors, were added during remedial work to supplement the very low shaft capacity of the driven piles, as documented in the conference proceedings, Jewell & Khorshid (1988).

Piles for conventional platforms are designed to resist the deadweight of the structure, together with significant environmental loading, which is much greater relative to the gravity loading than for most onshore structures. This has necessitated greater sophistication in the assessment of cyclic loading, with piles often being subjected to both tensile and compressive loading, and also the treatment of the lateral pile response. Piles are also used as anchors to moor floating facilities, with loading primarily horizontal, or for specific support such as the 45º lattice struts installed in the Bass Strait of Australia to stiffen the first generation platforms (Wiltsie et al., 1988).

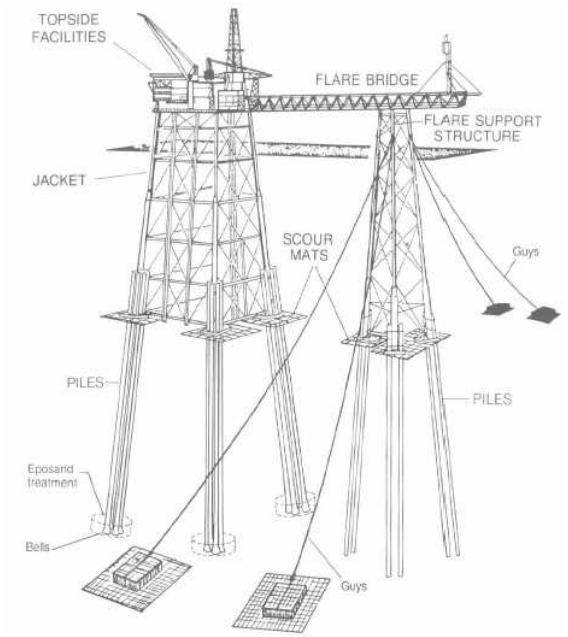

Figure 3.1 Example jacket structures – the North Rankin A platform

A particular type of floating platform, known as a tension-leg platform (TLP), uses vertical tethers attached, either via a seabed template or directly, to piles that are loaded permanently in tension. The first platform of this type was the Hutton platform, installed in 1984 in 150 m water depth in the North Sea (Tetlow et al 1983). Recent applications in water depths of around 1,000 m include the Mars and Ursa platforms in the Gulf of Mexico (Garside et al., 1997; Digre et al., 1999). The strain-softening response of a tension pile, with upward movement gradually reducing the embedment and hence capacity, poses a particular challenge in design.

3.2 *Construction methods*

3.2.1 *Driven piles*

The majority of piles used offshore are steel pipes, driven open-ended into the seafloor. Pile sizes range from a standard conductor, 0.76 m diameter, up to over 2.5 m. In exceptional cases, such as used recently for offshore wind turbines, piles of 5.1 m diameter have been driven successfully. The wall thickness of the pile will generally vary along the length, with thicker walls used near the pile head where bending moments are maximum. Through the body of the pile, typical diameter to wall thickness ratios (d/t) are ~40 (range 30 to 50), giving a net steel area, termed the area ratio, ρ, of 10 % of the overall pile cross-section.

Although driving shoes have been used in some cases, they are increasingly rare. External driving shoes have been shown to compromise the pile shaft capacity. Internal shoes are occasionally specified in order to relieve internal friction where piles need to be driven through dense sand layers. However, their effectiveness is open to question, and can lead to uncertainty in the ability of the pile to respond in a plugged manner under static loading.

With onshore piling, final pile penetrations are usually determined empirically according to the driving performance, with the capacity verified by dynamic testing. By contrast, offshore driven piles are driven to a specified penetration, calculated from pile design algorithms. This approach is necessary, partly because of the relatively high costs of adjusting pile lengths during installation (either by cutting to remove excess length, or by welding additional sections), but mainly because the upper profile of the pile will have been fabricated to end at a particular elevation. Fabrication details will include variations in wall thickness to accommodate operational bending moments, and also external weld beads over the upper few diameters of the pile to ensure sufficient bond strength when the pile is grouted into the external sleeve attached to the jacket structure.

In the early days of offshore developments, piles were driven using diesel and steam hammers, with 'followers' being used to extend the actual piles up to the sea surface. However, underwater hydraulic hammers were developed in the 1980s, capable of following the pile down inside the jacket sleeves. Modern offshore hydraulic hammers range in energy up to 3000 kJ, with rams of 180 tonnes falling through an equivalent of 1.7 m, and are designed to operate in water depths of at least 2000 m.

The most common construction problems for driven piles are associated with incorrect choice of design penetration, either with insufficient capacity (as indicated by driving performance or dynamic monitoring) at the end of driving, or due to premature refusal. The former problem can be addressed by welding on an additional section to the pile (complete with whatever weld beads are needed) and driving the pile further. The latter may involve drilling out the internal soil plug in order to eliminate damping from the soil column (which can absorb a significant proportion of the driving energy) and relieving the internal friction (or thus the net end-bearing resistance). To be effective in the latter, the soil plug needs to be removed down to within a diameter of the pile tip, balancing this against the danger of upheaval failure of the remaining soil plug.

A more catastrophic failure, with collapse of the pile at tip level, can occur; this has been documented on at least two occasions, but may have gone undetected on a number of others. For the Goodwyn gas platform on the North-West Shelf of Australia, thin-walled primary piles (d/t = 60) were driven to a depth of 120 m, below which grouted insert piles were to be installed. However, 16 out of the 20 piles were found to have deformed in a peanut shape over the lower 20 to 40 m, in some cases becoming completely flattened, preventing passage of the drilling auger (Barbour & Erbrich 1994). Although the driving through the variably cemented calcareous sediments was relatively easy, collapse was attributed to contributing factors including the method of stabbing the piles (which may have led to some structural damage at the pile tips), the presence of a hard layer 2 to 4 m thick at a depth of 75 m, and the high d/t ratio. It was shown that any slight imperfection in the roundness of the pile, particularly if due to a localised distortion, can propagate as the pile is driven; sufficiently strong soil can act as a die leading to progressively greater distortion of the tip as it advances.

A more recent collapse occurred at the Valhall Water Injection Platform in the North Sea (Alm et al., 2004). In that case 5 out of 8 piles (2.44 m diameter with d/t ~ 40) met premature refusal when driven through extremely dense sands (cone resistance exceeding 60 MPa). Attempts to drill out the soil plug revealed significant distortion of the piles near their tips, which may have been triggered by the tip detail of an external taper of the pile wall in conjunction with the very dense sands.

Both the above examples led to very costly remedial actions; reforming (expanding) the collapsed piles in the case of the Goodwyn platform (with remedial costs of ~A$300 m), and attaching additional 'piggyback' piles for the Valhall platform. They emphasise our still limited understanding of soil-structure interaction at the pile tip during pile installation, although novel approaches (Barbour & Erbrich, 1995) have allowed significant advances in analysis of the problem.

3.2.2 *Grouted piles*

The offshore equivalent of a bored pile (or drilled shaft) is referred to as a drilled and grouted pile, and comprises a steel tubular section grouted into a pre-drilled hole. Drilled and grouted piles are generally more expensive to install than driven piles, owing to the long construction period required, which may amount to several weeks. However, they are sometimes preferred in situations where a drilling barge with the necessary pile-handling capability is already on location. In that case,

drilled and grouted piles obviate the need to mobilise specialist offshore pile driving hammers.

Drilled and grouted piles have also been preferred in calcareous sediments, and potentially other crushable material, where the shaft friction obtained with driven piles can be extremely low. When the piles were driven at the North Rankin A platform on the North-West Shelf of Australia, some piles penetrated over 100 m penetration in just a few blows, with deduced shaft friction of just a few kPa (Dolwin et al., 1988). The low shaft friction is associated with very low radial effective stresses around the pile, a situation remedied by drilled and grouted pile construction, where the original horizontal effective stresses in the ground can be restored by appropriate grouting design.

Figure 3.2 shows the stages in construction of a drilled and grouted pile. In order to avoid collapse of loose uncemented material near the seabed, it is often necessary to drive a primary pile first. In the case of the Goodwyn platform referred to earlier, the primary pile extended 120 m, until cemented calcarenites were encountered. Generally, the primary pile would be rather shorter, and may be avoided entirely where fine-grained (low permeability) soils or cemented cap-rock occur near seabed level.

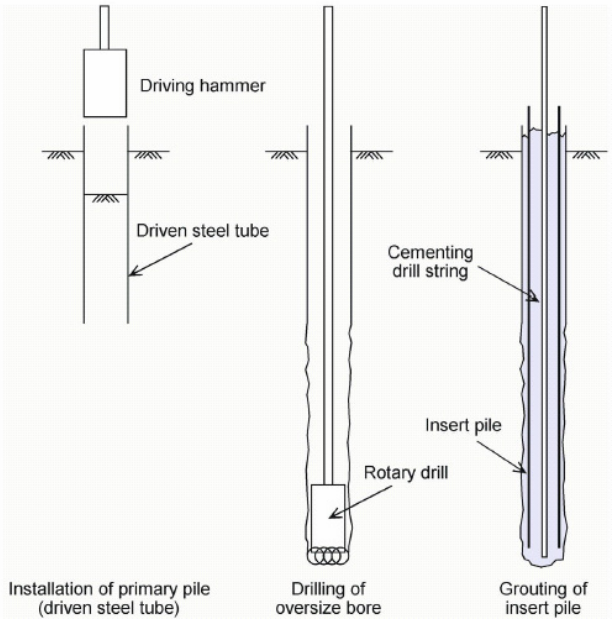

Figure 3.2 Stages in installation of an offshore drilled and grouted pile

As an alternative to a primary pile, mud is sometimes used to stabilise a drilled hole. This is most common where the piles can be constructed using direct circulation well drilling technology (and the construction is performed by well drillers), which limits the pile diameter to no more than about 900 mm. In the offshore environment continuous drilling with mud is difficult due to the volumes of mud required, and hence it is usual to drill the hole using water as the drill fluid, but with regular mud 'sweeps' to clean the cuttings. When the drilling is complete, the hole is usually displaced with mud to enhance the hole stability. Importantly, it should be appreciated that this approach does not preclude the development of hole instability during drilling, leading to the potential for an irregular shaped hole, which may or may not maintain stability when the hole is eventually displaced with mud; significant problems can arise in the subsequent grouting operation if hole stability is not maintained after the final mud cleaning 'sweep' is performed.

This leads directly to another significant difficulty with this approach: ensuring that the mud is properly displaced from the hole when the grout is injected. In offshore pile foundation construction an important landmark was a case history from the Bass Strait, offshore Australia (Angemeer et al., 1973). In this case the use of bentonite drilling mud in weakly cemented calcareous sand led to a 90% reduction in the skin friction that could be mobilised compared to that obtained in seawater. However, if good construction practices are followed, such as ensuring that the mud is continually circulated in the hole, ensuring that all debris is properly flushed from the hole, incorporating a pile centralising system and applying systems to ensure that the grout is able to properly displace the mud from the hole (such as those proposed for oil well construction by Pelipenko & Frigaard, 2005) then there is a reasonable prospect that a good grout job can be obtained.

Nevertheless, it should be appreciated that while the oil well construction industry has developed sophisticated tools for designing appropriate cementing (grouting) systems for their wells, pile construction is a much more demanding application. For example, in a typical well the required axial capacity may be only one tenth of the theoretical capacity or less, as compared to an offshore pile, where a much smaller factor of safety of about 2 is generally applied in design. For all these reasons the offshore construction industry has developed a justifiably healthy skepticism about using mud for offshore pile construction, particularly when well drillers inexperienced in pile construction are also used to install the piles.

Other critical issues in the construction of drilled and grouted piles include the potential for hydraulic fracture of the liquid grout into the formation, and appropriate monitoring systems to ensure grout returns at mudline. Hydraulic fracture can be a critical issue in weak uncemented formations. Conditions for hydraulic fracture in clay have been addressed by Andersen et al. (1994) and in sands by Schotman & Hospers (1992). It should be noted that grout returns may initially be reported at mudline even when hydraulic fracture occurs, but the grout may slowly subside over time before it sets. Hence some means of tagging the top of the grout (and adding extra grout if necessary) after it has set is essential if there is any risk of hydraulic fracture. Multi-stage grouting systems or lightweight grout mixes can be adopted to minimise the risk of hydraulic fracture.

The schematic in Figure 3.2 shows the grout filling both the inside of the steel tubular pile and the outer annulus. This leads to a very large volume of grout, and thus high temperatures generated during hydration of the grout. Problems caused by the high temperature, including the effects of subsequent shrinking of the pile along its length as it cools, may be alleviated by filling the inside of the pile with precast concrete blocks or other (non-structural) material. Alternatively, closed ended piles may be adopted, weighted to avoid flotation in the liquid grout.

In an attempt to reduce the risks and costs associated with drilled and grouted pile construction, an alternative approach was proposed by Rickman & Barthelemy (1988), where driven piles are subsequently pressure-grouted using pre-installed grouting conduits and T-valves fitted into the pile shaft. This construction approach appears to combine the potentially high shaft capacity of drilled and grouted piles with substantially reduced construction costs. However, although the technique was demonstrated to work well in onshore tests (Fahey et al., 1992), a critical flaw remains in the lack of quality control to ensure that the pressure-grouting leads to adequate coverage of the pile shaft, rather than hydraulic fracturing into the formation.

3.3 *Axial capacity*

In spite of significant advances in understanding the mechanisms that determine the eventual shaft friction and end-bearing capacity of different types of pile, design methods still rely heavily on empirical correlations. The most challenging aspect of offshore pile design is therefore the need to extrapolate design parameters from an experimental database that is largely limited to piles of less than 1 m in diameter, the majority of which are solid or closed ended piles, often installed by jacking. This compares to modern offshore piles with diameters often in

excess of 2 m, with relatively low displacement ratios and invariably installed by dynamic driving.

Increasingly, the cone (or, in clays, alternative full-flow penetrometer) resistance is used as the primary measure of the soil strength from which pile design parameters may then be deduced; unlike in onshore design, standard penetration test data are thankfully avoided! For sands, design parameters can be expressed directly in terms of the cone resistance, while for fine-grained sediments parameters are based either on the undrained shear strength or the in situ vertical effective stress together with an overconsolidation (or yield stress) ratio.

3.3.1 *Current offshore guidelines*

The current API and (draft) ISO (2004) design guidelines adopt a conventional design approach for end-bearing, with the limiting bearing pressure expressed as

$$q_{bu} = N_q \sigma'_{vo} \leq q_{bu\text{-}max} \tag{3.1}$$

The value of N_q is taken to vary from 12 to 50 according to the grain size and relative density of the material. Limiting values of end-bearing pressure are also specified. A summary of the different categories of sand and silt and recommended pile design parameters, as in the current draft ISO document (ISO, 2004), is given in Table 3.1.

The corresponding design approach for shaft friction is expressed as

$$\tau_s = K\sigma'_{vo} \tan\delta \leq \tau_{s\text{-}max} \tag{3.2}$$

with the interface friction angle, δ, and limiting values of τ_s varying with soil type and density (see Table 3.1). The stress ratio, K, is recommended as 0.7 to 0.8 for open-ended piles loaded in compression and 0.5 to 0.7 for piles loaded in tension, with the lower end applying to loose deposits and the upper end for dense conditions (ISO, 2004).

Table 3.1. Pile design parameters in draft ISO (2004)

Soil type	Soil density	D_r (%)	δ (°)	$\tau_{s\text{-}max}$ (kPa)	N_q	$q_{bu\text{-}max}$ (MPa)
Sand	Loose	15-35	20	65	12	3
	Medium	35-65	25	80	20	5
	Dense	65-85	30	95	40	10
	Very dense	85-100	35	115	50	12
Silty sand	Loose, Med	15-65	20	65	12	3
Clayey sand	Dense	65-85	25	80	20	5
	Very dense	85-100	30	95	40	10
Sandy silt	Loose	15-35	15	45	8	2
	Med. dense	35-85	20	65	12	3
	Very dense	85-100	25	80	20	5

Although the design approach of Equations (3.1) and (3.2), and the parameters in Table 3.1, are the most up to date in terms of industry design codes, it is widely accepted among offshore geotechnical engineers that design methods for axial pile capacity in sands are in urgent need of revision, and indeed this feeling has inspired major initiatives in terms of high quality load tests (Al-Shafei et al., 1994; Zuidberg & Vergobbi, 1996) and a recent API project to synthesise the results of those and other load tests into a new design method (Fugro, 2004). The discussion below reviews these developments.

3.3.2 *End-bearing resistance*

The cone penetrometer may be viewed as a model pile, and hence provides a logical basis for estimating the end-bearing resistance of prototype piles. In practice, the (average) unit end-bearing pressure assumed in pile design is generally taken as some fraction of the cone resistance (Bustamente & Gianeselli, 1982). The reduction factor has been interpreted as a scale effect, although a more rational explanation lies in (a) the displacement required to mobilise the full cone resistance and (b) the influence of partial embedment into the bearing layer. Since piles are often used to transfer load into strong soil at depth, a penetration of only a couple of diameters into a strong layer is common. A penetration of 5 to 10 diameters is required for the 'full' strength of a hard layer to be mobilised and the overlying soft layer no longer 'felt' by the CPT or pile tip. Therefore, these shallowly-embedded piles cannot mobilise the local CPT resistance.

Under static loading, open-ended piles will generally act as fully plugged, even though they will drive in an unplugged manner. The difference in behaviour is due to the high inertial forces under dynamic conditions, which help to ensure mobility of the soil plug up the pile, and the reverse silo effect during static loading, which leads to very high internal shaft friction (Randolph et al., 1991).

In slow-draining soils such as clays, a substantial proportion of the steady-state (large displacement) end-bearing capacity is mobilised with moderate movements. Lu et al. (2004) show that, although the steady-state cone resistance is not reached until a displacement of 4 cone diameters, 62 % of that value is mobilised within a displacement of 10 % of the diameter, and 70 % within 20 % of the diameter. For the case of an open-ended pile, a design end-bearing capacity of 62 to 70 % of the cone resistance seems reasonable, supporting the conventional figure of $9s_u$ (cone factor of 13 to 15). That figure is probably conservative for closed ended piles, where greater residual base load will be developed during installation.

For rapidly draining soils, the hyperbolic base response suggested by Fleming (1992) for cast-in-situ piles gives only 15 to 20 % of the steady-state (or plunging) capacity mobilised at a displacement of 10 % of the pile diameter. Design values of end-bearing resistance, as a proportion of q_c, will therefore be much lower than for clays, and will be affected to a greater extent by the magnitude of any residual base loads locked in after installation (Randolph, 2003).

Data from pile tests give an apparent diameter effect for piles in sand, and this led to the design approach proposed by Jardine & Chow (1996), referred to in the offshore industry as the MTD approach (after the initials of the Marine Technology Directorate that supported the research), expressed as:

$$\frac{q_{bu}}{q_c} = 0.5 - 0.25\log\left(\frac{d}{d_{cone}}\right) \geq \rho \tag{3.3}$$

for piles of diameter less than $0.02(D_r - 30)$ m, where D_r is the relative density of the sand. This relationship gives a decreasing end-bearing capacity as the pile diameter, d, increases relative to the diameter of the cone, d_{cone}. The lower limit, ρ, is the area ratio of the pile, and applies for all larger piles; it corresponds to mobilising the cone resistance around the steel annulus of the pile, ignoring any resistance mobilised by the soil plug. No particular logic is offered for the basis of the diameter effect implicit in this relationship.

The MTD approach leads to very conservative end-bearing capacity for typical offshore piles (d > 2 m, $\rho \sim 0.1$). Lehane & Randolph (2002) described an approach for estimating the *minimum* design end-bearing capacity for open-ended piles, as shown in Figure 3.3. The approach took account of compression within the soil plug as well as below the base of the pile, and assumed no densification of the soil plug or residual base loads due to pile installation. With minor allowance for such densification, a minimum design ratio for q_{bu}/q_c of 0.2 was suggested by Randolph (2003).

The recent report to the American Petroleum Institute (API) (Fugro, 2004), has proposed end-bearing capacity for driven open-ended piles of

$$\frac{q_{bu}}{q_c} = 8.5\frac{DR^{0.25}}{\sqrt{q_c / p_a}} \tag{3.4}$$

where p_a is atmospheric pressure (100 kPa) and DR is the displacement ratio of the pile. Conservatively, assuming fully unplugged installation, the displacement ratio should be taken as

equal to the area ratio, ρ, implying an incremental filling ratio, IFR (Brucy et al., 1991), of unity. Note that for a typical area ratio of 0.1, the end-bearing capacity would be approximately 32 % of that for a closed-ended pile. For q_c in the range 10 to 50 MPa, the normalised end-bearing capacity for a typical open-ended pile halves, from 0.48 to 0.21. The physical basis for this reduction is closely linked to the reducing stiffness ratio, G/q_c, which is generally taken to decrease proportionally with the square root of q_c (Lo Presti et al., 1991).

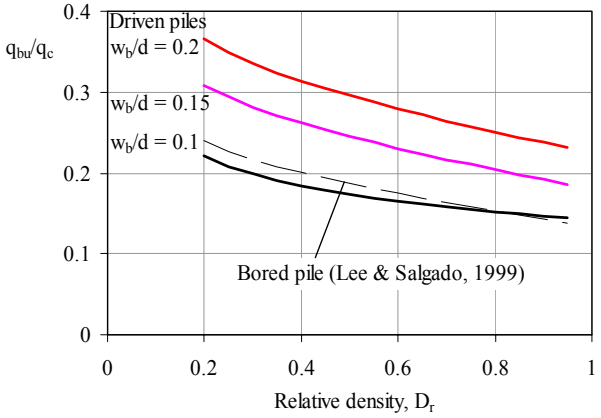

Figure 3.3 Minimum end-bearing resistance for open-ended piles (Lehane & Randolph, 2002).

It should be noted that the proposed approach of Equation (3.4) gives rise to end-bearing capacities for piles in dense sand that exceed the upper limits given in Table 3.1. However, that is consistent with conclusions from Hossain & Briaud (1993), who found that the base resistance was underpredicted by a factor of 2 using the API criteria in dense sands.

In fine-grained soils, the end-bearing capacity is rarely a significant contribution, and is usually treated in the conventional way by means of a bearing capacity factor, N_c, of 9. The resulting limiting pressure is normally assumed to act across the gross area of the pile, since the pile will plug under static loading conditions.

3.3.3 *Shaft resistance in sand*

Research over the last 15 years has revealed major shortcomings in this approach, since it is not consistent with the physical processes that occur around a driven pile. For one thing, the interface friction angle has been found to be most strongly affected by the ratio of grain size to pile roughness and therefore increases with decreasing grain size, rather than the reverse trend indicated in Table 3.1 (Uesugi & Kishida, 1986; Jardine et al., 1992). There is also no evidence to suggest that δ should vary with the in situ density of the sand, owing to the major changes that occur during installation, and the likelihood that critical state conditions are developed along the pile-soil interface.

A more fundamental issue concerns the distribution of limiting shaft friction with depth. Adoption of a constant K value with depth in Equation (3.2), together with a limiting value for τ_s is not consistent with data from field tests; even the original work of Vesic (1970) shows evidence of what is often referred to as friction fatigue (Heerema, 1980), and a more quantitative picture was provided from the Imperial College instrumented model pile tests (Lehane et al., 1993; Chow, 1996).

Figure 3.4 shows profiles of shaft friction recorded by the 3 instrument clusters in a 6 m by 100 mm diameter pile jacked into sand. For comparison, the cone resistance profile is also shown (scaled down by a factor of 100). The leading instrument cluster (4 diameters from the pile tip) shows a shaft friction profile that follows the cone profile closely; the two subsequent instrument clusters show progressively reduced values of friction for any given depth. The implication is that a maximum value of K occurs close to the pile tip, where the shaft friction is 0.5 to 1 % of the cone resistance (similar to that measured on a cone friction sleeve). The value of K then reduces with distance, h, from the pile tip.

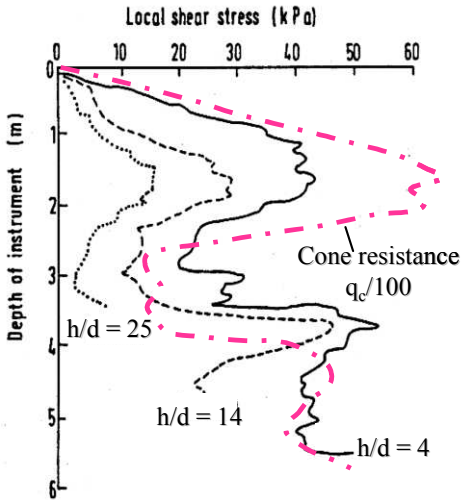

Figure 3.4 Measured profiles of shaft friction on a pile jacked into sand (Lehane et al., 1993)

This form of degradation has been adopted by Randolph et al. (1994) and in the MTD method of Jardine & Chow (1996), building on Lehane & Jardine (1994). The latter method expresses the shaft friction for open-ended piles as

$$\tau_s = \left(\frac{q_c}{45} \left(\frac{\sigma'_{vo}}{p_a} \right)^{0.13} \left(\frac{d_{eq}}{h} \right)^{0.38} + \Delta\sigma'_{rd} \right) \tan\delta_{cv} \qquad (3.5)$$

where d_{eq} is the diameter of a solid pile of equivalent steel area to the open-ended pile (so that $d_{eq} = \rho^{0.5} d$), $\Delta\sigma'_{rd}$ is a stress change due to dilation effects, generally negligible for prototype pile sizes and δ_{cv} is the interface friction angle corresponding to constant volume or steady state shearing.

Friction fatigue is accounted for in the above expression by the power law expression in d_{eq}/h, and the expression is to be applied only for $h \geq 4d$ (below which τ_s is taken as constant). Recent work (White & Lehane, 2005; White, 2005) has shown that friction fatigue (as its name implies) is dictated more by the number of loading cycles applied to the pile during installation, rather than the distance, h. Thus a continuously jacked cone, with multiple friction sleeves, showed essentially identical friction on each successive sleeve (DeJong & Frost, 2002). By contrast, the Imperial College pile is jacked in stages (typically 0.2 m strokes) so would undergo around 30 loading cycles during installation to a depth of 6 m, giving rise to moderate friction fatigue; a typical prototype pile might be subjected to several thousand blows during installation, resulting in much greater friction fatigue.

The mechanism of friction fatigue is illustrated in Figure 3.5. Incremental densification of soil adjacent to the pile, aided by crushing and migration of the fines away from the interface, leads to relaxation of the radial stress according to cylindrical cavity theory (White & Bolton, 2004).

Example data taken from centrifuge model testing of a pile subjected to 2-way cyclic axial load tests are shown in Figure 3.6, and illustrate the gradual reduction in stress level. Variations in stationary horizontal stresses during 2-way cyclic load tests (including any cycles applied to the pile during installation) are shown in Figure 3.7. That figure includes (as crosses) normalised values obtained during 'pseudo-dynamic' installation, where the model pile was installed by a form of cyclic jacking that involved reversal of displacement direction, as described by White & Lehane (2005).

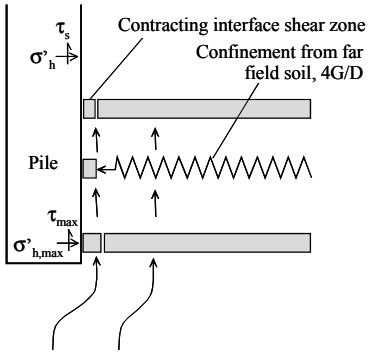

Figure 3.5 Schematic for friction fatigue (White & Bolton, 2004)

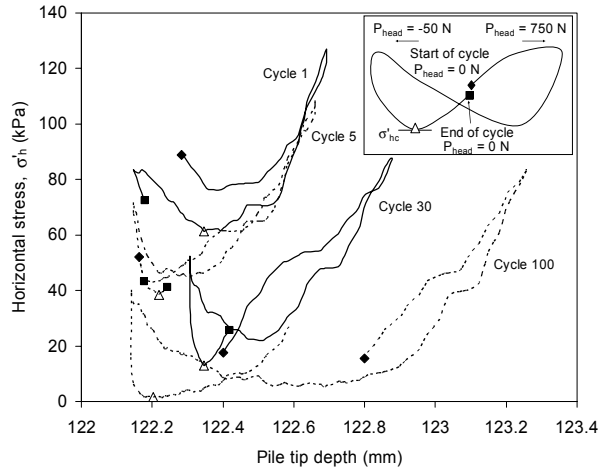

Figure 3.6 Degradation of horizontal stress during 2-way cyclic load tests (White & Lehane, 2005)

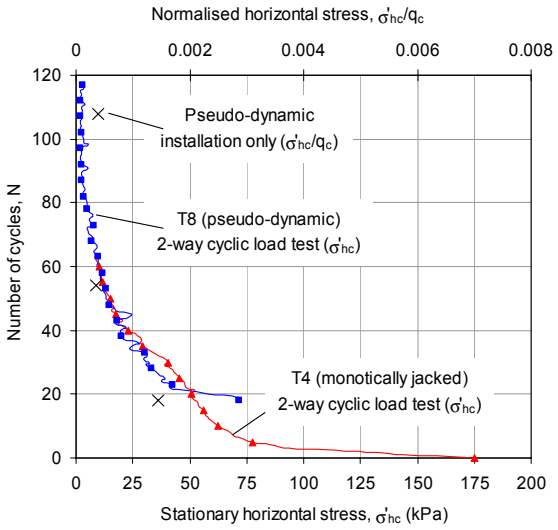

Figure 3.7 Degradation of stationary horizontal stress at h/B = 1 with 2-way cycling (White & Lehane, 2005)

White (2005) assembled field data from a number of different pile load tests in soils ranging from carbonate silts and sands (North Rankin) to dense (Dunkirk) and very dense (Euripides) silica sand. He found that normalising the average shaft friction by the average cone sleeve friction, $f_{s,av}$ (considered to represent the maximum shaft friction near the tip of a pile) gave a consistent pattern when plotted against the number of blows or jacking cycles used to install the pile (see Fig. 3.8). He also tried to link the decay exponent, c (the power law factor for h/d) with the number of blows, as indicated in the figure, although noting that the link was quite sensitive to the assumed distribution of maximum pile friction (or sleeve friction) with depth and the minimum value of h/d for which the power law was applied.

A logical conclusion that might be drawn from the above work is that the fewer blows used to install a pile, the higher will be the shaft capacity. In particular, the application of a large number of blows during the final diameter or so of penetration may prove counterproductive, with as much loss in capacity due to friction fatigue as gained by further penetration. From a design point of view, it is difficult to predict beforehand the number of blows required to install a pile, and hence the pattern of friction fatigue. Design approaches in terms of the normalised distance, h/d, are therefore necessary, such as in the MTD approach of Jardine & Chow (1996).

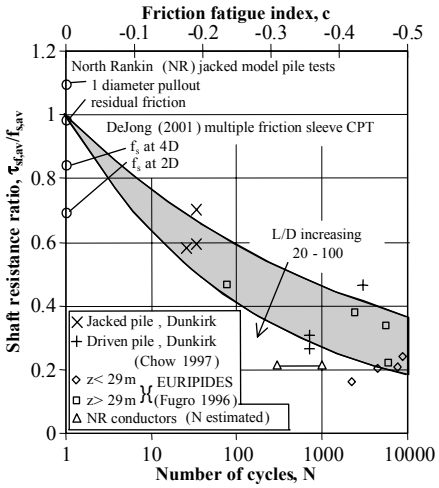

Figure 3.8 Variation of mean normalised shaft friction with number of installation cycles (White, 2005)

A slightly modified form of the MTD design approach was suggested by Fugro (2004) in their report to API, with the shaft friction calculated as

$$\frac{\tau_s}{q_c} = 0.025\left(\frac{\sigma'_{vo}}{p_a}\right)^{0.15}\left(\frac{d_{eq}}{h}\right)^{0.85} \quad \text{for } h/d_{eq} \geq 2 \qquad (3.6)$$

This equation subsumes implicitly allowance for the interface friction angle, on the basis that this shows little variation for practical pile surfaces (especially once abrasion of the surface during installation is allowed for). A notable feature is the much higher exponent for h/d_{eq} compared with the value of 0.38 in the MTD approach, implying much greater friction fatigue.

As discussed by White (2005), the main ingredients in any new design approach for driven piles in sand are:

1. to express the maximum shaft friction, τ_{max}, at, say, a distance of 1 diameter from the pile tip in terms of the local cone resistance, q_c, with appropriate allowance for the area ratio (or anticipated displacement ratio) of the pile;
2. to express the friction fatigue in terms of a power law, or other decay function of normalised distance, h/d, from the pile tip.

For a solid pile, the cone sleeve friction provides a guide to the maximum friction near the pile tip, although in practice the sleeve friction is known to be particularly sensitive to the condition of the cone equipment (Lunne et al., 1997a), and thus a somewhat unreliable measurement on which to base pile design.

For an open-ended pile, lower maximum friction is expected, since the radial stress changes imposed during pile installation will be reduced (Paik et al., 2003). Ideally, the incremental filling ratio (of soil plug movement to pile penetration) should be used to gauge the effective area ratio of the pile, but this is also

not known prior to installation. Thus the actual area ratio, ρ, of the pile must be the basis for design.

Combining these various effects leads to an expression for the shaft friction of the form:

$$\frac{\tau_s}{q_c} = A\rho^b \left(\frac{q_c}{\sigma'_{vo}}\right)^n \left(\frac{d_{eq}}{h}\right)^c \quad \text{for } h/d \geq (h/d)_{min} \tag{3.7}$$

where the coefficient, A, accounts for the interface friction ratio, tanδ, or alternatively (White, 2005), the above expression can be recast to give σ'_r/q_c at the pile surface, which is then multiplied by tanδ.

The tensile capacity of piles in sand is lower than the shaft capacity measured in compression. Two factors were identified by De Nicola & Randolph (1993) that contributed to lower tensile shaft friction, the first being a reduction in effective stress levels adjacent to the pile compared with loading in compression (even for a rigid pile), and the second being the Poisson's ratio reduction in diameter (and consequential reduction in radial effective stress). These two effects were quantified for piles fully embedded in sand, by the expression

$$\frac{(Q_s)_{tens}}{(Q_s)_{comp}} \approx \left(1 - 0.2\log_{10}\left(\frac{100}{L/d}\right)\right)\left(1 - 8\eta + 25\eta^2\right)$$
$$\eta = \nu_p \frac{L}{d}\frac{G_{ave}}{E_p}\tan\delta \tag{3.8}$$

where Q_s is the shaft capacity and G_{ave}, E_p and ν_p are respectively the average soil shear modulus, Young's modulus of an equivalent solid pile and Poisson's ratio for the pile. Figure 3.9 shows the resulting variation in reduction factor with pile aspect ratio, L/d; for a typical modulus ratio of $E_p/G_{ave} = 400$, the shaft capacity ratio is ~0.8 for a range of L/d, and generally remains within the range 0.7 to 0.85 for other values of E_p/G_{ave}.

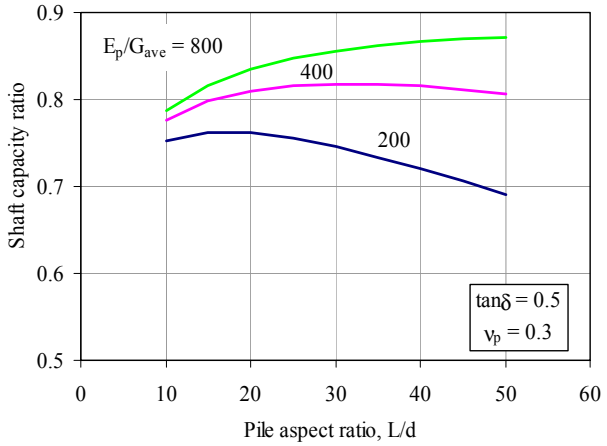

Figure 3.9 Calculated ratio of shaft capacity in tension and compression

Although other effects, such as local stress changes due to dilation, will influence the shaft capacity ratio, the expression in Equation (3.8) provides a reasonable design basis for assessing the reduced shaft capacity for loading in tension, compared with that for loading in compression.

3.3.4 *Shaft friction in clay*

Onshore design practice for displacement piles in clays and silts was originally couched in terms of a friction ratio, α, giving the shaft friction as a proportion of the local undrained shear strength, s_u. The value of α was found empirically to be around unity for soft soil with shear strength less than 25 kPa, reducing to 0.5 or less once the strength exceeded 75 kPa (Tomlinson, 1957). However, pile load tests conducted for offshore developments showed that it was not the shear strength of the clay that mattered in determining the value of α so much as the degree of overconsolidation. This led in turn first to the lambda method (Vijayvergiya & Focht, 1972), where the shaft friction was expressed as

$$\alpha = \frac{\tau_s}{s_u} = \lambda\left(2 + \frac{\sigma'_{vo}}{s_u}\right) \tag{3.9}$$

with λ decreasing with increasing pile length from a maximum of 0.5 for very short piles, and then to the current API (1993) and draft ISO guidelines, based on the expression suggested by Randolph & Murphy (1985), of

$$\alpha = \frac{\tau_s}{s_u} = 0.5 \cdot \text{Max}\left[\left(\frac{\sigma'_{vo}}{s_u}\right)^{0.5}, \left(\frac{\sigma'_{vo}}{s_u}\right)^{0.25}\right] \tag{3.10}$$

A variation of the above relationship was suggested by Kolk & van der Velde (1996) to take account of the length (or slenderness ratio, L/d) of the pile, expressed as

$$\alpha = \frac{\tau_s}{s_u} = 0.55\left(\frac{\sigma'_{vo}}{s_u}\right)^{0.3}\left(\frac{40}{L/d}\right)^{0.2} \tag{3.11}$$

Randolph (2003) discussed different mechanisms for the apparent length effect for piles in clay, including progressive failure of long piles under static loading, due to strain-softening load transfer between pile and soil, and damage caused by pile installation. The latter mechanism is similar in principle to the concept of friction fatigue for piles in sand, and has been incorporated into the MTD approach. The relationship for shaft friction at any distance h from the pile tip is expressed in the form of Equation (3.2), with the stress ratio, K, given by

$$K = \left[1.7 + 0.011R - 0.61\text{Log}(S_t)\right]R^{0.42}\left(\frac{d_{eq}}{h}\right)^{0.2} \quad \text{for } h/d_{eq} \geq 4 \tag{3.12}$$

where R is the yield stress ratio (or apparent overconsolidation ratio, allowing for aging and structure of the natural clay) and S_t is the sensitivity.

This expression gives shaft friction for a typical open-ended pile, with area ratio of 0.1 and thus $d_{eq} \sim 0.32d$, that reduces gradually from being equal to that for a closed-ended pile near the pile tip, to a value of about 80 % of the closed-ended equivalent for larger h values. The logic for the h/d effect for piles in clay is less clear cut than for piles in sand, assuming that installation occurs in a fully undrained manner (Randolph, 2003). If it exists, however, it would seem more appropriate to separate the adjustment for open-ended piles into two parts: firstly that associated with reduced 'cavity expansion' (governed by the area ratio of the pile); and secondly any degradation along the pile.

For thin-walled caissons, cylindrical cavity expansion appears to offer a reasonable approach for estimating stress changes during installation and subsequent consolidation (Randolph, 2003). Comparison with centrifuge model tests on suction caissons, where the radial stresses acting on the outer surface of the caisson were measured directly, has shown very good agreement (Chen & Randolph, 2005).

Quantification of the effect of reduced cavity expansion, due to the thin-walled nature of the pile, is particularly important when assessing the time-scale of consolidation (or 'set-up' as it is often termed), but also when considering the shaft friction mobilised on the skirt walls of suction caissons, where the diameter to wall thickness, d/t, may be as high as 200 (area ratio of 0.02). The rate of dissipation of excess pore pressures around open-ended piles is controlled by the volume of steel forced into the soil, and hence dissipation curves for piles with different d/t ratios are very similar when plotted as a function of $T_{eq} = c_h t/d_{eq}^2$, where c_h is the consolidation coefficient for horizontal drainage, as shown in Figure 3.10 (Whittle, 1992; Randolph

2003). Essentially the time scale for consolidation can be scaled directly from piezocone dissipation tests, factoring the latter by $(d_{eq}/d_{cone})^2$.

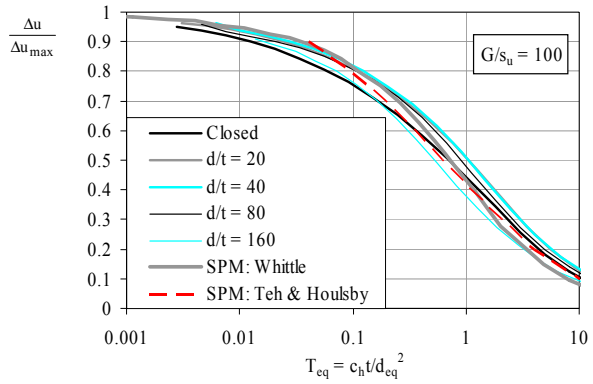

Figure 3.10 Pore pressure dissipation at pile shaft (Randolph, 2003)

Typical values of consolidation coefficient lie in the range 3 to 30 m^2/yr, and even for the upper end of this range significant consolidation times occur for typical driven piles and suction caissons, as indicated in Table 3.2. There is little difference between the two types of foundation, owing to the much thinner wall of the larger diameter suction caisson. It is clear, however, that the full shaft capacity for either will take a significant period (in excess of 1 or even 2 years) to develop. This needs to be taken into consideration in the design process, checking that the foundation can survive an appropriate design storm during the first months of operation.

Table 3.2 Typical consolidation times for offshore foundations

Foundation type	Driven pile	Suction caisson
Diameter (m)	2	5
Wall thickness, (mm)	50	30
Equiv. diameter (m)	0.63	0.79
Assumed c_h (m^2/yr)	30	30
t_{20} ; t_{50} ; t_{90} (days)	5 ; 50 ; 500	7 ; 70 ; 700

3.3.5 *Axial capacity in carbonate sediments*

As may be seen from Figure 3.8, the magnitude of shaft friction, relative to cone sleeve friction, and the pattern of friction fatigue appear consistent between both carbonate and silica sands, although the absolute magnitudes of friction are much lower for the former. Typical values of average shaft friction for the 120 m long driven piles at North Rankin range from as high as 40 kPa (after allowing the piles to 'set up' for a period following installation) to less than 10 kPa, with a very rapid loss in shaft friction during re-drive tests (Dolwin et al., 1988). Alternative techniques such as drilled and grouted construction, or driving closed-ended piles (DeMello et al., 1989), are therefore used in carbonate sediments in order to increase pile capacity.

For drilled and grouted pile construction, it is tempting to estimate shaft friction using the simple friction approach of Equation (3.2), with the horizontal stress $K\sigma'_{vo}$ replaced by the grouting pressure. However, Hyden et al. (1988) showed that dilation plays a significant role in increasing the shaft friction, and more recent design approaches are based on correlations with the cone resistance. Abbs (1992) suggested taking the shaft friction as 2 % of the cone resistance, which provides a robust lower bound to field measurements, but becomes increasingly conservative in lightly cemented sediments, where the cone resistance reduces below 10 MPa.

An alternative approach was suggested by Joer & Randolph (1994), with the peak shaft friction, τ_p, expressed as

$$\frac{\tau_p}{q_c} \approx 0.02 + 0.2e^{-0.04q_c/p_a} \qquad (3.13)$$

Bounds to experimental data from laboratory tests on grouted driven piles are shown in Figure 3.11, with the coefficients replaced by 0.05 and 0.3 (upper) and 0.01 and 0.13 (lower). The average relationship of Equation (3.13) was also shown to provide a good fit to field data from drilled and grouted piles and grouted driven piles, with the latter construction technique giving slightly higher values of shaft friction (Randolph et al., 1996).

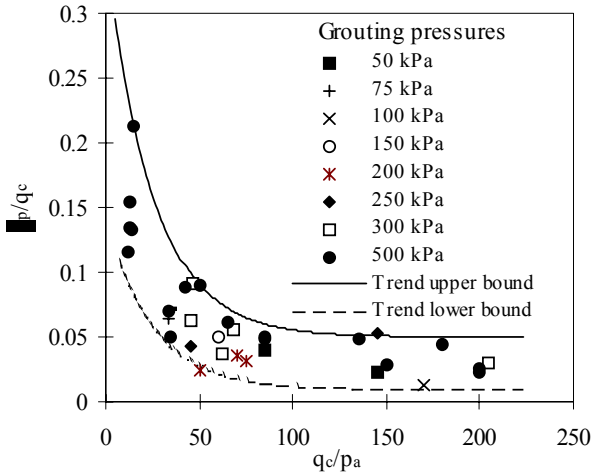

Figure 3.11 Correlation of shaft friction with cone resistance for grouted driven piles (Joer & Randolph, 1994)

3.3.6 *Modelling effects of cyclic loading*

The load-displacement response of offshore piles is generally evaluated using load transfer approaches, with the pile divided into elements along its length, and interaction with the soil modelled as independent non-linear springs. Axial and lateral responses are usually assumed to be independent, although new approaches have recently been developed to explore interaction effects (Levy et al., 2005).

For both modes of loading, the API (1993) and ISO (2004) guidelines suggest default forms for the load transfer curves. Under axial loading in clay soils, the shape up to peak is very similar to an inverted parabola, with the peak shaft friction reached after a displacement of 1 % of the pile diameter; beyond the peak, linear strain-softening may be allowed for, with (in clay soils) a residual shaft friction of 70 to 90 % of the peak reached after a further displacement of the same magnitude as that to mobilise the original peak. In sandy soils, the pre-peak is assumed linear with the peak mobilised (somewhat incongruously) at a displacement of 2.5 mm, independent of the pile diameter. For piles in excess of 2 m in diameter, the assumed load transfer stiffness implies very large ratios of shear modulus to shaft friction (~1500 or more).

The effects of cyclic loading are rarely evaluated explicitly for conventional situations, such as piles supporting jacket structures in normal clays and sands, since negative effects from cyclic degradation are balanced by increase in shaft friction due to increased strain rates during storm loading. However, for more critical designs such as tension piles (where the response is inevitably strain-softening) or for piles in carbonate soils (where the shaft friction can reduce significantly under cyclic loading), explicit assessment of the effects of cyclic loading is undertaken. The mechanisms of degradation under cyclic loading are still only partly understood, but the effects – even those occurring during installation, as discussed earlier - are receiving increasing emphasis in design.

Poulos (1988) has described the construction of cyclic stability diagrams, categorising pile response into threes zones (Fig. 3.12): a stable zone, typically where the cyclic load amplitude is less than about 30 % of the compression capacity, Q_{comp}; a metastable zone where the pile survives the cyclic loading, but

suffers some degradation; and an unstable zone where the pile is brought to failure. For piles that are compressible, relative to the stiffness of the surrounding soil, the stable zone will reduce in size, due to the concentration of (cyclic) load transfer near the head of the pile and consequential degradation in that region.

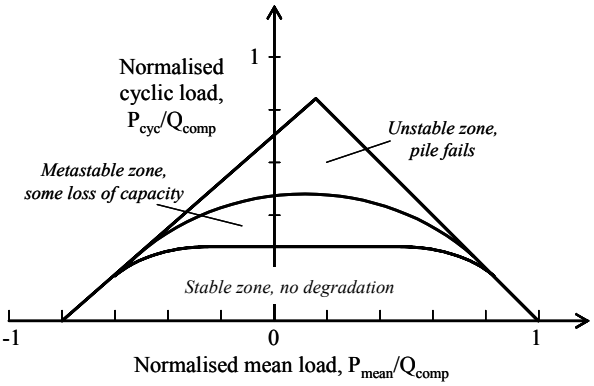

Figure 3.12 Cyclic stability diagram (after Poulos, 1988)

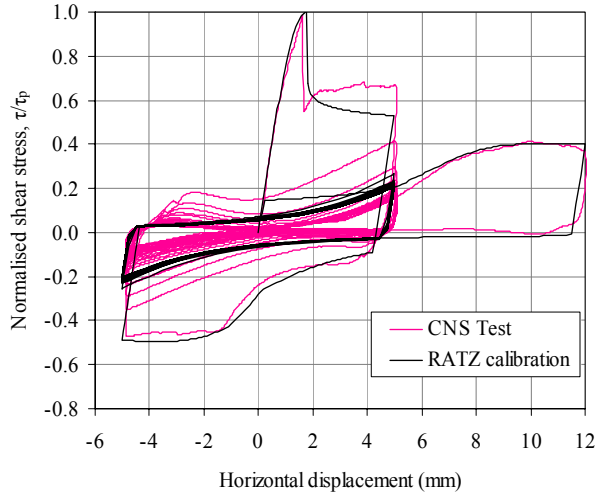

Figure 3.13a Calibration of RATZ against CNS test data

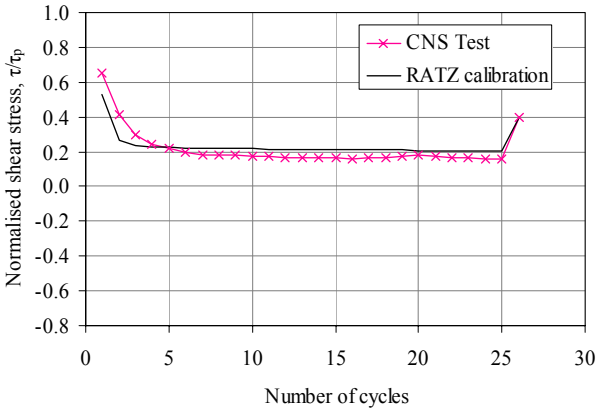

Figure 3.13b Comparison of RATZ with CNS test cyclic degradation data

Analysis of the cyclic response of piles relies on algorithms for cyclic load transfer, calibrated against laboratory element data such as constant normal stiffness (CNS) shearing tests, or from back-analysis of instrumented pile tests. One such software, which has been calibrated for clays and carbonate sediments, is RATZ (Randolph, 2003; Randolph et al., 1996). Recent work has focused on the response observed in cyclic CNS tests between fixed displacement limits (mimicking that undergone by load transfer elements in the upper part of the pile).

Figure 3.13a shows the results of calibration against a CNS test on calcarenite (cemented calcareous sand). The test data show very rapid post-peak softening to about 60 % of the initial peak, τ_p, extremely low shear stresses mobilised during subsequent cyclic displacements, followed by a rise to a residual shear strength of 40 % of the peak strength during final monotonic displacements. The computed response simulates the main features extremely well, and also matches closely the pattern of maximum stress mobilised during each cycle (Fig. 3.13b).

An example application is considered here to illustrate the potential effects of cyclic loading; although based on an actual design in variably cemented calcareous sands, the pile geometry has been changed and the stratigraphy simplified. The pile has been taken as 2 m in diameter and 50 m long, with wall thickness increasing from 40 mm in the lower half, up to 80 mm at mudline (where the bending moments would be greatest). The peak shaft friction increases up to a maximum of 400 kPa at a depth of 25 m, below which it is constant at 300 kPa. The upper 25 m of soil has been assumed to strain-soften abruptly in a similar manner to that shown in Figure 3.13a, while the lower soil strain softens more gradually, but with a lower residual. Figure 3.14 shows the profiles of peak and residual shaft friction.

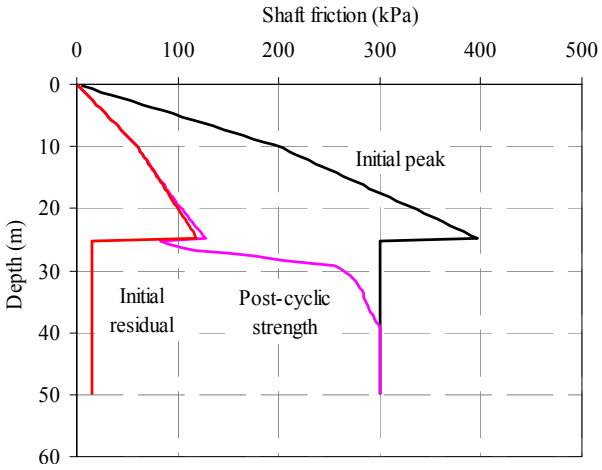

Figure 3.14 Profiles of peak, residual and post-cyclic shaft friction

The theoretical shaft capacity of the piles is 81.7 MN (and end-bearing is ignored, because of the drilled and grouted construction technique). Under monotonic displacement (Fig. 3.15), the actual peak load that can be mobilised is only 57.8 MN (71 % of ideal), due to progressive failure. A hypothetical storm loading has been applied, with 20 'equivalent' cycles applied between loads of -2 and +38.5 MN (67 % of monotonic capacity). As shown in Figure 3.15, this results in further reduction in capacity, with a post-cyclic capacity for the pile of 51.3 MN (89 % of the monotonic capacity, but only 63 % of the ideal shaft capacity).

A typical load transfer response, at a depth of 20 m, is shown in Figure 3.16, with gradual degradation of the available shaft friction occurring. The post-cyclic profile of shaft friction is compared with the peak and residual profiles in Figure 3.14; degradation to residual conditions occurs virtually throughout the upper 25 m, with progressively less degradation below that depth. The degradation in shaft friction in the upper part of the pile is accompanied by a gradual transfer of the axial load to the deeper sections of the pile, as may be seen by the pattern of cyclic load at a depth of 40 m (Fig. 3.15). At the peak in the first cycle, the load in the pile at 40 m is only 3 MN, but this increases to 15 MN by the 20th cycle.

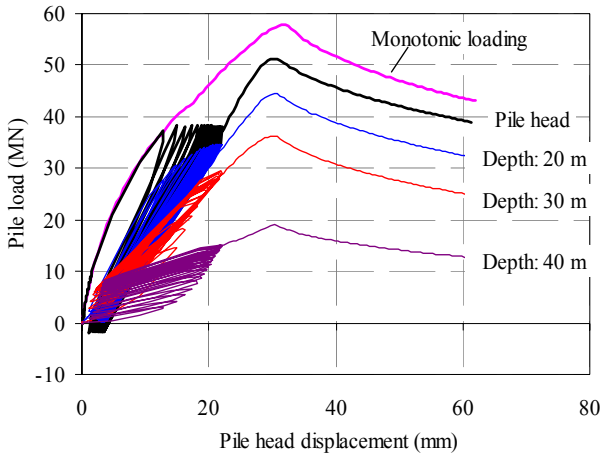

Figure 3.15 Monotonic and cyclic load-displacement responses

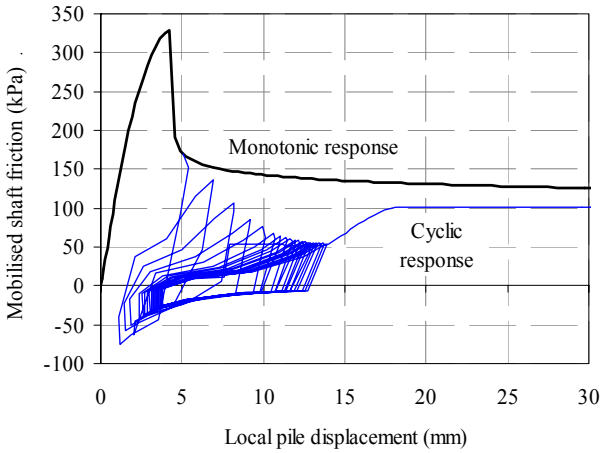

Figure 3.16 Element response at a depth of 20 m down the pile

3.4 *Lateral response*

The lateral response of piles in offshore design is almost universally quantified using a load transfer approach, with the interaction between pile and soil modelled by non-linear P-y curves relating lateral force (P) per unit length down the pile to the lateral deflection (y). The critical design issue is generally the maximum bending moments induced down the pile, rather than the magnitude of deflection, although the latter may be critical in some cases (e.g. the Bass Strait retrofit struts, Wiltsie et al., 1988). Bending moments and lateral deflections are limited to the upper part of the pile, as illustrated in Figure 3.17, and it is common practice to downgrade (or ignore) any axial shaft capacity in the upper few diameters of the pile in order to allow for lateral movements.

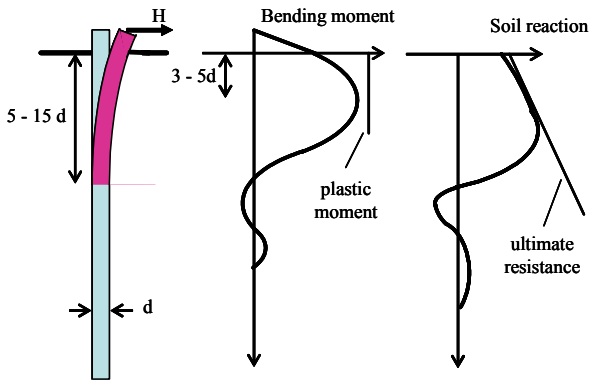

Figure 3.17 Schematic of laterally loaded pile response

Design guidelines prescribe forms for the non-linear P-y curves for standard 'soft clay' and 'sand' categories of seabed sediment. These have evolved from the experimentally derived curves proposed by Matlock (1970) and O'Neill & Murchison (1983). Limiting lateral resistance in clay is taken to vary as

$$P_u = \left[\left(3 + 0.5\frac{z}{d}\right)s_u + \sigma'_{vo}\right]d \;\le\; 9s_u d \qquad (3.14)$$

with the upper limit of $9s_ud$ not being reached until a critical depth, z_r, several diameters below the seabed. The limiting value at depth is conservative in the light of the lower bound plasticity solution (Randolph & Houlsby, 1984), which ranges between $9.14s_ud$ for a smooth pile and $11.92s_ud$ for a fully rough pile. Similarly, the upper bound mechanism proposed by Murff & Hamilton (1993) suggests a much more rapid rate of increase with depth once the soil weight is accounted for.

By contrast, the proposed limiting resistance in sand, which follows a rather complex quadratic variation with depth (API, 1993; ISO, 2004) appears unduly optimistic by comparison with other approaches (Fig. 3.18). Other studies have indicated that adopting a limiting resistance of $P_u = K_p^2\gamma' zd$ (Barton, 1982) provides a good fit to experimental data (Prasad & Chari, 1999)

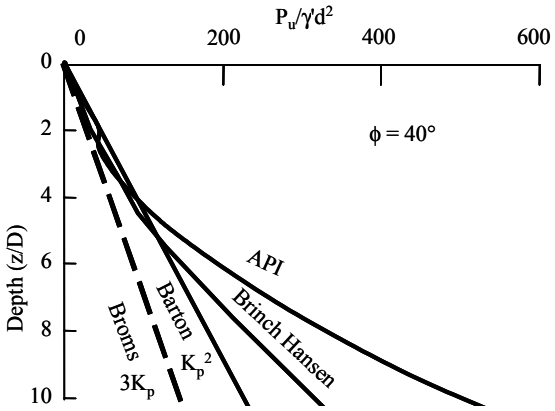

Figure 3.18 Comparison of different approaches for the ultimate soil resistance for laterally loaded piles in sand

The shape of P-y curves in clay recommended in the draft ISO (2004) code may be expressed as

$$\frac{P}{P_u} = 0.5\left(\frac{y}{y_r}\right)^{1/3} \le 1 \qquad (3.15)$$

but with a finite initial gradient of 2 (in the normalised form). The reference deflection, y_r is expressed as $2.5\varepsilon_{50}d$, where ε_{50} is nominally the strain at 50 % peak stress in an unconsolidated undrained test, and generally taken in the range 0.005 to 0.01. Under cyclic loading (the usual design condition), the maximum resistance is reduced to $0.72P_u$ (reached when $y = 3y_r$) at depths less than the critical depth, z_r (where P_u reaches $9s_ud$). At shallower depths the response is taken to soften at displacements greater than $3y_r$, reducing to $0.72z/z_r$ at a deflection of $15y_r$.

Many offshore pile layouts are at large spacings (e.g. with 1 pile at each corner of small platforms). However, for applications such as TLPs, interaction effects may become significant. Doyle et al. (2004) report the results of centrifuge model tests undertaken in relation to the URSA TLP, where the pile spacing was at 3.08 diameters. They found that under static loading the trailing pile gave lateral resistances of about 2/3 that of the leading pile. Under cyclic loading, the lateral soil resistance for a single pile reduced to about 0.6 of the static resistance (i.e. 20 % lower than Matlock's (1970) value of 0.72). Of greater concern, however, was the finding that the soil resistance during cyclic loading of a group of 2 piles reduced to only 29 % of the static value. While further tests are needed to substantiate this, it ap-

pears that the soil was becoming fully remoulded under the cyclic loading, much as in a cyclic T-bar test, giving a reduction in resistance by a factor of $1/S_t$, where S_t is the soil sensitivity.

The form of P-y curve proposed by O'Neill & Murchison (1983) for piles in sand under static loading is

$$\frac{P}{P_r} = A \tanh\left(\frac{kz}{AP_r} y\right) \qquad (3.16)$$

$$\text{where } A = 3 - 0.8\frac{z}{d} \geq 0.9$$

where P_r is a reference soil resistance (API, 1993; ISO, 2004) For cyclic loading, the factor A is taken as 0.9 throughout. The quantity k is the depth gradient of the initial subgrade reaction modulus, $(P/y)_{y=0}$, taken as 45 MPa/m for dense soil (nominally $\phi' \sim 40^o$), and halving with each 5º decrease in the friction angle.

3.4.1 *Carbonate sediments*

An alternative form of load transfer curve was found necessary for piles in carbonate sediments, which are characterised by high friction angles but much greater compressibility than silica sands (Wesselink et al., 1988; Williams et al., 1988). Refinement of the approach arising from those studies led to the alternative load transfer relationships of Novello (1999)

$$\frac{P}{d} = 2\sigma'^{0.33}_{vo} q_c^{0.67} \left(\frac{y}{d}\right)^{0.5} \qquad (3.17)$$

and (Dyson & Randolph, 2001)

$$\frac{P}{\gamma' d^2} = R\left(\frac{q_c}{\gamma' d}\right)^n \left(\frac{y}{d}\right)^m \qquad (3.18)$$

where R, n and m were optimised as 2.7, 0.72 and 0.58. These forms of load transfer curve are not bounded as y increases, and also have an infinite initial gradient (set to a finite value for numerical implementation). For practical values of deflection, with y << d, the net lateral pressure on the pile remains as a fraction of the cone resistance. Thus for q_c = 10 MPa, and $\gamma' d$ = 20 kPa, the latter expression gives a net pressure, P/d, of 1.86 MPa for y = 0.2d, and remains below $0.5q_c$ even for y ~ d.

While this form of load transfer curve has only been proposed for carbonate sediments at this stage, it is attractive to link the load transfer curve to the cone resistance for silica sands as well, avoiding the need to estimate a friction angle. Indeed, similar lateral resistances would be predicted using this expression to those discussed above for silica sand; thus, for q_c = 20 MPa, the above expression would yield P/d ~ 2 MPa for y/d = 0.1, which is similar to the limiting resistance of $K_p^2 \gamma' z$ for a 40º sand at a depth of 10 m.

Carbonate sediments often exhibit cementation in the upper few metres of the seabed, where cap-rock may be encountered. At shallow depths, such cemented material is generally quite brittle, which will lead to reduction in resistance once a failure surface is formed. Abbs (1983) suggested a strain-softening model to simulate this. However, a more rational approach was developed by Erbrich (2004) for application in the carbonate deposits on the North-West Shelf of Australia. The basis of the model (Fig. 3.19) is the concept of wedges of 'chipped' material forming near the surface, and this was combined with the kinematic mechanism of Muff & Hamilton (1993) in order to evaluate the net resistance once a chip has occurred, and to develop a criterion for the maximum depth to which chips, as opposed to deformation of intact rock, will occur.

The 'chipper' model proposed by Erbrich (2004) was calibrated by means of 3D finite element analyses, and also through comparisons with centrifuge model tests. It was found to yield much greater lateral pile capacity than the Abbs (1983) model, but provided a sound physical basis on which to design anchor piles for developments at Bayu-Undan and Legendre.

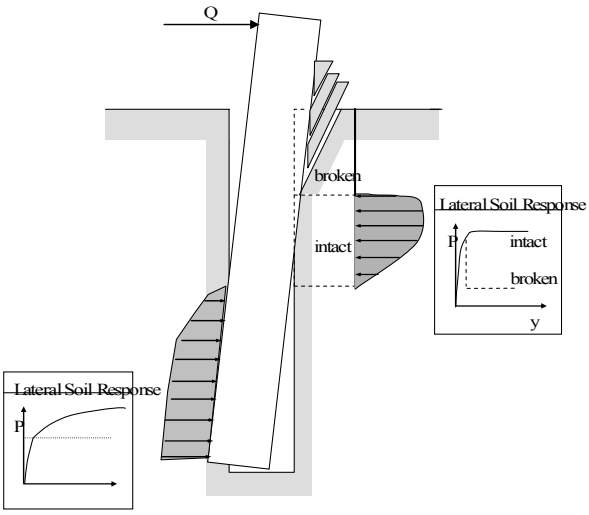

Figure 3.19 Concept of 'chipping' of cemented material near surface (Erbrich, 2004).

4 SHALLOW FOUNDATIONS

4.1 *Skirted foundations and caissons*

Historically offshore shallow foundations either comprised large concrete gravity bases, supporting large fixed substructures, or steel mudmats used as temporary support for conventional piled jackets before the piled foundation had been constructed.

In recent times shallow foundations have become more diverse, and now include concrete or steel bucket foundations used as anchors for floating platforms or as permanent supports for jacket structures instead of piles, or as foundations for a variety of (usually) small sea bottom structures (Fig. 4.1). Skirtless gravity base foundations rest on the surface of competent seabeds, but where softer surficial deposits exist, skirts are provided to confine the soft surface soil and transmit foundation loads to deeper, stronger soil. If the structure is relatively heavy and the soil relatively soft, skirted gravity bases and bucket foundation systems install under self-weight, however for light jackets, dense materials or deep skirts, penetration is assisted with suction (e.g. Tjelta et al., 1986; Bye et al., 1995; Andenaes et al., 1996,).

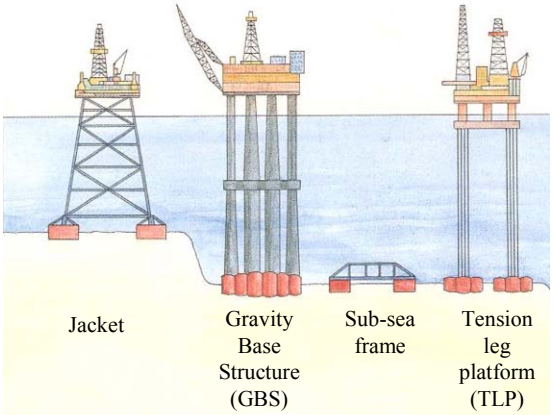

Figure 4.1 Applications of offshore shallow foundations (NGI)

4.2 *Design features of offshore shallow foundations*

There are some clear differences between shallow foundations onshore and offshore:

- Shallow foundations employed offshore are typically much larger than those used onshore.

- Offshore shallow foundations are required to withstand much larger horizontal loads and overturning moments than onshore.
- In the design process more emphasis is placed on capacity of offshore shallow foundations, with less emphasis on displacements than would be typical in onshore foundation design.
- Attention to cyclic loading effects on capacity is critical in design of offshore shallow foundations.
- Soft surface deposits offshore are typically incorporated into an offshore shallow foundation system by the provision of skirts, where onshore soft surficial soils would more often be removed (or treated) prior to construction.

Offshore shallow foundations are larger than those typically required onshore due to the size of the structures they support and the harsher environmental conditions. Even small gravity base structures are often 70 m high (equivalent to an 18 or 20 storey high-rise) with a footprint 50 m by 50 m, and larger structures can be over 400 m tall supported by foundations with a plan area in excess of 15,000 m^2. Even a single bucket foundation may have a diameter in excess of 15 m. Apart from the sheer size of structures offshore, their foundations are required to resist severe environmental forces from wind, waves and currents (and in some cases ice, for example offshore Canada or the Baltics) which impart significant horizontal and moment loads that are not experienced onshore. A schematic of loading conditions of a gravity base platform are shown in Figure 4.2.

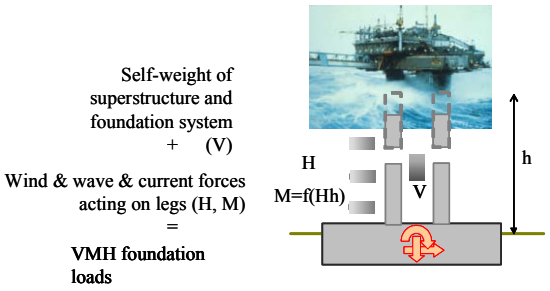

Figure 4.2 Combined loading of a gravity base platform

Design loads for an offshore gravity base structure and an onshore high-rise of similar height are compared in Figure 4.3. The self-weight of the two structures is moderately comparable with the design vertical load of the offshore structure 35 % larger than the onshore high-rise. The live loads, however, are many times greater offshore than onshore; the design horizontal load 1600 % larger and moment 500 % larger, which is reflected in an increased foundation area of around 150 %. More important than the absolute magnitude of the environmental loads is the ratio of horizontal load to moment. For the offshore structure shown in Figure 4.3 M/HD is relatively low (approximately 0.35) compared to the onshore high-rise (approximately 1.6) indicating the high risk of sliding failure for offshore gravity base structures. Limit load, whether sliding, overturning or vertical bearing capacity, is generally the key design criteria for offshore shallow foundations. Allowable settlements of offshore shallow foundations are usually constrained by tolerances of allowable deformation to maintain the integrity of oil wells and pipelines rather than platform stability, and it is feasible to design offshore shallow foundation for settlements of up to several metres.

Due to the dominance of environmental loading, accounting for the influence of cyclic loading on the soil response is much more important than for a typical onshore structure. Environmental forces impart significant cyclic horizontal, vertical and moment loads to offshore foundation systems, and generate excess pore water pressures in the vicinity of the foundation reducing the effective stresses in the seabed. Foundation stability is ultimately compromised by accumulated residual strain and degradation of cyclic shear strength (depending on the combination of average and cyclic stress). If drainage can take place, some pore water pressure dissipation may occur between storm events, although cyclically induced pore pressures may still accumulate from one storm to another (O'Reilly & Brown, 1991).

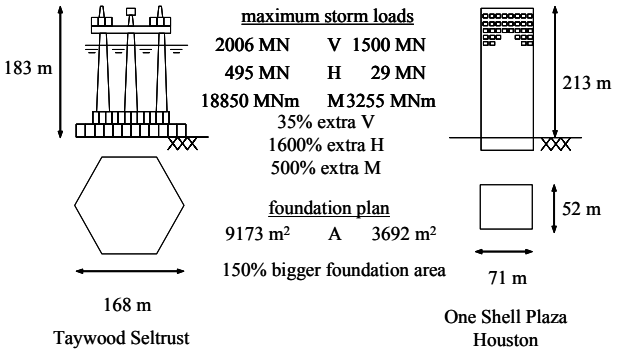

Figure 4.3 Comparison of offshore and onshore design loads (reproduced from Poulos, 1988, after Young et al., 1975)

Foundation skirts have a variety of functions: containing soft surface soils, assisting penetration of the foundation into the seabed, compensating for seabed irregularities and reducing scour around the foundation periphery. Skirts also enable the development of transient tensile capacity during undrained moment or uplift loading which cannot be obtained with conventional shallow foundations. Uplift capacity is well documented by model tests and field observation on clays (e.g. Dyvik et al., 1993, Anderson et al., 1993) as well as sand (e.g. Tjelta & Haaland, 1993, Bye et al., 1995). The duration of the tension load must be relatively short compared to the time required for dissipation of the under-pressure developed in the pore water under the foundation plate. Cyclic uplift loads from ocean waves may safely be resisted even on relatively pervious sand deposits and uplift loads over much longer durations maybe carried by skirted foundations on clays with lower permeability.

4.3 *Evolution of offshore shallow foundation systems*

4.3.1 *Concrete gravity bases*

The first gravity based platform, the Ekofisk tank, was installed in the Norwegian sector of the central North Sea in 1973 (Clausen et al., 1975). Some design details are provided in Table 4.1. The magnitude and nature of the wave-induced forces were unprecedented in geotechnical engineering at the time of the Ekofisk project. The foundation design was based on laboratory and model tests (Lee & Focht, 1975) and the platform was heavily instrumented. Pore water pressure measurements made during storms showed that even for the dense sands at Ekofisk, repeated loading generated excess pore water pressures which was accompanied by large settlements of the tank (Clausen et al., 1975). Experience gained during the project led to the development of a new, and now common, gravity base design, the Condeep (Clausen, 1976). A Condeep gravity base comprises a number of cylindrical cells usually in a hexagonal arrangement as illustrated in Figure 4.4b. The gravity base platform shown in Figure 4.1 is a Condeep style design. As can be seen in Figure 4.4b, the plan geometry of the Condeep foundation is more complex than the Ekofisk tank and this also the case in elevation (Fig. 4.4a). While the Ekofisk tank had short (40 cm) concrete skirts fabricated to a flat base, the Condeep has first steel skirts (to 3.5 m), then concrete skirts. The underside of the Condeep cells has a convex profile and half a metre inside the concrete skirts the top of the dome touches down on the seabed (see Figure 4.4b). The advantage of the Condeep style platform over the Ekofisk tank design is much smaller wave forces acting on the structure (Table 4.1) as the major volume of the Condeep is located deep below the water surface (see Fig. 4.1).

Table 4.1 Details of shallow foundation case studies

Project Year	Foundation type	Location	Water depth m	Soil conditions	Foundation plan	Foundation dimensions m, m^2	Skirts d (d/D)	V (= W') MN	H MN	M MN	M/HD	Reference
Ekofisk Tank 1973	GBS	North Sea (Norway)	70	Dense sand to 26 m, layers stiff clay 16-18 m. >26 m hard clays and sands (s_u ~ 300 kPa)		A = 7,390 D_{eqiv} = 97	0.4 (0.004)	1900	786	28000	0.37	Clausen, 1976 (p.400) Clausen, 1976 (p.263) O'Reilly & Brown, 1991 (p.124)
Beryl A 1975	Condeep	North Sea (Norway)	120	As at Ekofisk but sand layer only to 10 m		A = 6,360 D_{eqiv} = 90	4 (0.04)	1500	450	15000	0.37	Clausen, 1976 (p.263)
Brent B 1975	Condeep	North Sea (Norway)	140	Stiff to hard clays (s_u ~ 300 kPa) with thin layers of dense sands to 45 m		A = 6,360 D_{eqiv} = 90	4 (0.04)	2000	500	20000	0.44	O'Reilly & Brown, 1991 (p.124)
Gullfaks C 1989	Deep skirted Condeep	North Sea (Norway)	220	Soft nc silty clays (s_u ~ 30 kPa) and silty clayey sands with dense sand layers (q_c ~ 4 MPa)		A = 16,000 D_{eqiv} = 143 D_{cell} = 28 (t = 0.4)	22 (0.13)	5000	712	65440	0.64	Tjelta et al., 1990 Tjelta, 1998
Snorre A 1991	TLP with concrete buckets	North Sea (Norway)	310	Very soft to soft nc clays (s_{um} = 0, k ~ 7 kPa/m to 20 m; 0 < q_c < 2 kPa @ 17 m)		A_{total} = 2,724 D_{cell} = 17 (t = 0.35)	12 (0.7) (CFT, 0.4)	142 per CFT	21 per CFT	126 per CFT	0.20	Christophersen, 1993 (p.435) Stove et al., 1992 (p.76)
Draupner E (Europipe) 1994	Jacket with steel buckets	North Sea (Norway)	70	22-25 m dense to very dense fine sand (q_c ~ 60 MPa) over stiff clay		A_{total} = 452 D = 12	6 (0.5)	57 per bucket	10	30	0.25	Bye et al., 1995 (p.870)
Sleipner SLT 1995	Jacket with steel buckets	North Sea (Norway)	70	As at Draupner E		A_{total} = 616 D = 14	5 (0.35)	134 per bucket	22	-	-	Bye et al., 1995 (p.876)
Troll A 1995	Deep skirted Condeep	North Sea (Norway)	305	Soft nc clays (s_{um} = 0, k ~ 3 kPa/m to 60 m; 0 < q_c < 1.5 kPa @ 40 m)		A = 16,596 D_{eqiv} = 145 D_{cell} = 32	36 (0.25)	2353	512	94144	1.27	Andenaes et al., 1996 (p.62) Hansen et al., 1992 (p.924)
Wandoo 1997	GBS	NW Shelf W Australia	54	Thin layer dense calcareous sand (q_c ~ 3 MPa) over thick strong calcarenite (q_c ~ 30 MPa)		A = 7,866 114 x 69 x 17 D_{eqiv} = 100	0.3 (0.003)	755	165	7420	0.45	Humpheson., 1998 (p.362, 365)
Bayu-Undan 2003	Jacket with steel plates	Timor Sea N Australia	80	2 m very soft calcareous sandy silt over cemented calcarenite and limestone (q_c ~ 20 MPa)		A_{total} = 480 A_{plate} = 120 6 x 20	0.5 (0.04)	125 per plate	10	-	-	Neubecker & Erbrich, 2004 (p.2)
Yolla 2004	Skirted GBS/jacket hybrid	Bass Strait S Australia	80	Firm calcareous sandy silt with very soft clay and sand layers (q_c ~ 2 MPa)		A = 2500 50 x 50 D_{equiv} = 56.4	5.5 (0.1)	-	-	-	-	

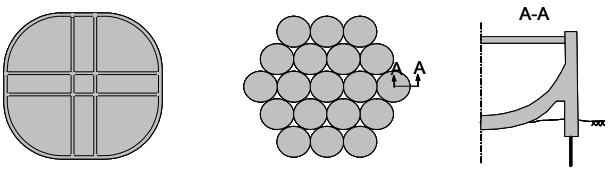

Figure 4.4 (a) Ekofisk tank and (b) Condeep gravity base designs

The first Condeep, Beryl A, was installed in 1975 in the North Sea at a site with similar dense sand conditions to the Ekofisk field. The second Condeep, Brent B, was installed in the same year, also in the North Sea but at a stiff clay site (Table 4.1). The main uncertainties with the new foundation design concerned the penetration of the skirts and contact pressures on the platform base (Clausen, 1976). This is complicated as conditions may vary across the foundation base area due to a sloping seabed profile, varying soil conditions or a combination of the two. At the time of construction of Beryl A and Brent B there were differing opinions as to how geotechnical analyses and design of gravity structures should be carried out, but it was clear that in order to verify and improve the existing design practice instrumentation and monitoring of each project was essential (Clausen, 1976). Both Beryl A and Brent B were instrumented for settlements, inclination, pore pressure and earth pressure measurements and the commitment to instrumentation of platforms has continued to be given a high priority during the construction of subsequent gravity base structures.

As exploration of the North Sea oil and gas reserves moved into deeper water softer normally consolidated clays were encountered and the Condeep gravity base design developed to include the provision of deep skirts to transmit the foundation loads to the stronger deeper soils. To achieve the deeper penetration active suction is required to draw the skirted base into the seabed. Gullfaks C, installed in 1989 at a soft clay site in the Norwegian North Sea, was the first skirted gravity base to use suction to assist its installation. Active suction was also maintained for some time after installation to accelerate consolidation for ground improvement.

At the time of construction Gullfaks C was the largest and heaviest offshore structure ever built (Tjelta, 1993). Some details of the project are summarised in Table 4.1. The combination of the heavy structure and soft soils necessitated a deep skirted foundation and an active drainage system for foundation improvement. One of the primary design concerns was whether the design depth of penetration could be achieved (even with active suction) which prompted large scale penetration tests in the North Sea (Tjelta et al., 1986). In the event, the observed penetration resistance was considerably less than predicted particularly in the hard soil layers.

Following installation, soil drainage was accelerated by applying an under pressure which was reduced incrementally over 15 months. Most of the settlement took place in the first three months when the most active soil drainage operation was in place (approximately 0.5 m) and was similar to predicted values. It was the intention that the majority of settlement was completed before wells and pipelines were in operation (as these can only tolerate limited settlement). The initial three months of very active drainage coincided with the summer months and it was also important that consolidation, and the associated strength improvement, was achieved before the winter storms arrived. When the active under pressure ceased settlements reduced to 1.5 – 2 cm/year. Tjelta (1993) comments that for such a heavy structure on relatively soft soils the reduced settlement rate only 15 months after installation is remarkable and illustrates the benefit of deep skirt foundation systems. Earth pressure measurements showed that immediately after platform installation the entire platform weight was carried as contact pressure between the foundation base and the soil. By the end of the active drainage period pore water pressures had dissipated sufficiently that 100 % of the submerged weight of the platform was carried as skirt wall friction: The platform had changed from being a traditional gravity base structure with all load taken as base contact pressure to a 'piled' type structure where all load was carried as wall friction and tip resistance.

In 1995, a similar but more ambitious deep skirted gravity base platform, Troll A, was installed in the Norwegian North Sea (Table 4.1). Troll A was the deepest skirt pile system to be installed, the previous record having been held by Gullfaks C. Troll A is 100 m taller than Gullfaks C but it is relatively a much lighter structure, and the design overturning moment was the dominating load factor (Hansen et al., 1992). The relatively light weight of Troll A in conjunction with the deep water site led to dynamic effects of the platform to be the main criteria for the foundation design. The consequent sensitivity to, and requirement of foundation stiffness necessitated a larger foundation than needed to fulfil stability requirements. The low permeability clays at the Troll A site in conjunction with the long drainage paths (due to the large plan area of the foundation base and the deep skirts) limit excess pore pressure dissipation. The time for primary consolidation was estimated at approximately 1000 years so only a fraction of the consolidation will take place during the lifetime of the structure. A basic design criterion was a watertight base, ensuring an undrained response and acceptable settlements (dictated mostly by constraints related to the integrity of the oil wells). A reliance on the undrained response of the foundation soils was in contrast to previous experience where foundation performance improved continuously after installation due to consolidation, and was a very different approach compared to at Gullfaks C where active drainage was used to increase the strength of the soil.

Permanent monitoring of Gullfaks C and Troll A has enabled verification of the designs and improved understanding of the response of deep skirted gravity bases. The experience from these projects led to application of the technology to individual suction installed ‘bucket’ foundations (section 4.3.2).

In other offshore regions where gravity base structures have been installed different seabed conditions have necessitated different shallow foundation solutions. In some areas, particularly offshore Australia, calcareous soil deposits predominate on the seabed. These are characterised by spatial variability in terms of particle size and cementation, and high angularity of individual particles causing high void ratios and compressibility. Particular problems for shallow foundation design in calcareous deposits include cemented inclusions impeding skirt penetration and liquefaction and volume collapse under the action of cyclic loading (Randolph & Erbrich, 2000). Also, stratigraphies where low strength material underlies stronger layers may lead to punch-through type failures or large settlements.

Sliding resistance and cyclically induced settlements were the key issues in the design of Wandoo B (Fig. 4.5a, details in Table 4.1), where the seabed comprises a thin surface layer of dense carbonate sand (0.5 - 1.4 m), overlying strong calcarenite (Humpheson, 1998). The competent calcarenite near the surface ensures against vertical bearing capacity and overturning but horizontal shear loads are only resisted by the surface sand layer. Because of the shallow depth of sand, skirts were not provided; instead friction between the base slab and the surficial sand was relied on. Sliding stability is dependent on the level of excess pore pressure in the sand. Excess pore pressures are generated by wave induced cyclic shear loading during design storm events. Cyclic shear tests results carried out to predict the accumulation of excess pore water pressures within the sand layer are shown in terms of average excess pore water pressure per load cycle, β (Bjerrum, 1973), against shear stress ratio τ/σ'_v in Figure 4.5b. A passive drainage system was provided in the base slab of Wandoo B to facilitate dissipation of excess pore water pressures. Finite element dissipation analyses were used for the design to calculate the amount of ballast required to resist the severe environmental loads and ensure against a sliding failure (Humpheson, 1998).

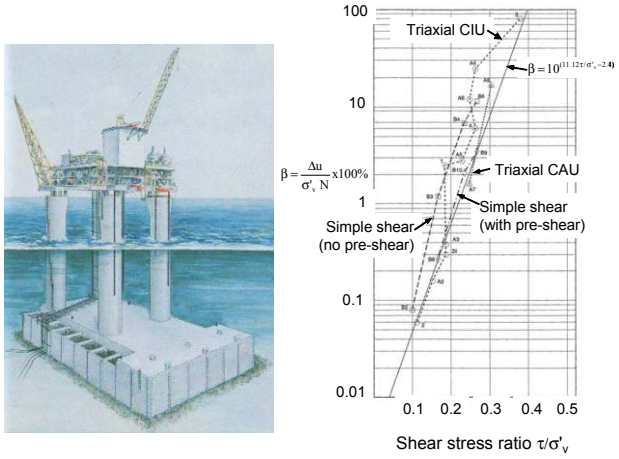

Figure 4.5(a) Wandoo B, NW Shelf, Australia, (b) Anticipated excess pore water pressures in sand layer (Humpheson, 1998)

Two unusual gravity base platforms were installed at Bayu-Undan (Timor Sea, North Australia). These comprised a steel jacket with steel plate foundations provided at each corner (Fig. 4.6, details in Table 4.1) with the weight of the topsides, rather than the substructure providing the dead load required to resist environmental loading (Neubecker & Erbrich, 2004). Conditions at Bayu-Undan are relatively unusual; the central processing platforms have unusually heavy topsides, water depth is moderate and environmental loading is mild. Due to the relatively mild environment, it was the large gravity dead load on the structure rather than the environmental loading that was critical in the foundation design. Soil conditions at the site comprised a shallow layer of very soft calcareous muddy silts and sands, underlain by a sequence of variably cemented calcarenites. Another unusual aspect of the Bayu-Undan project was that seabed preparation works were carried out prior to installation of the jackets in order to remove the surficial silty sand. This was necessary due to the high bearing stresses imposed from the foundation. The silt and sand layer was blasted away and the steel plate foundations were grouted directly onto the underlying caprock (Sims et al., 2004).

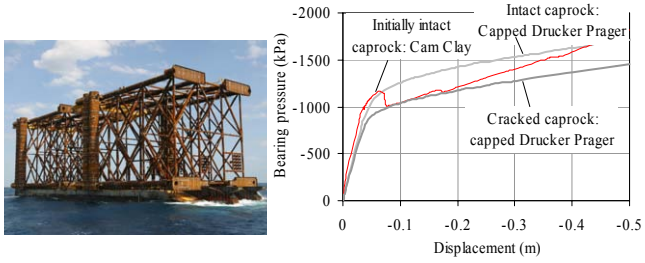

Figure 4.6 Bayu-Undan gravity jacket structure and computed bearing response using different caprock models

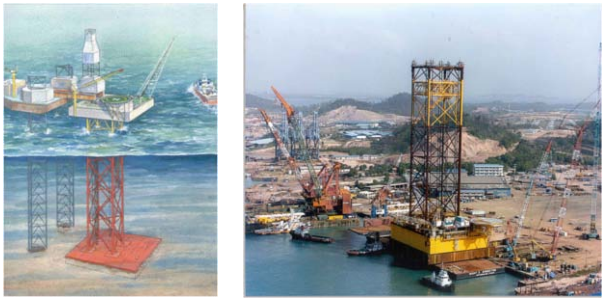

Figure 4.7 Yolla A Hybrid gravity base structure, Bass Strait, Australia (Watson & Humpheson, 2005)

A novel gravity base hybrid structure, the Yolla A platform, was recently installed in the Bass Strait, offshore Australia (Table 4.1), comprising a steel skirted gravity base foundation supporting a steel jacket substructure (see Fig. 4.7). Unlike the Wandoo B ballasted raft foundation the skirted raft for Yolla A relies on the soil inside the skirts to resist the large environmental lateral and overturning loads. Soil conditions consist (mostly) of carbonate sandy silt and silty sand. Randolph and Erbrich (2000) note design studies that show shallow foundations with deep skirts, extending up to 30 m, are viable in regions where the finer grained calcareous silts dominate, however, until Yolla, there had been no practical experience.

Due to the eccentricity of the jacket on the gravity base (necessary due to drilling constraints from the adjacent jack-up) a permanent moment is transferred to the foundation, leading to potential for differential consolidation settlement over the life of the platform. In addition there are high transient overturning loads due to the strong wave forces and low platform self-weight, leading to the potential for high storm induced platform deformation. Another critical aspect of foundation design included likely interaction of the structure with the foundations from the adjacent jackup rig, which was used to drill the wells after the platform was installed.

4.3.2 *Concrete caissons for TLPs*

A progression from the development of suction-installed deep skirted concrete gravity base foundations for Gullfaks C (section 4.3.1), was the use of individual or clusters of small concrete caissons or 'bucket' foundations. The first application of the new technique was for the Snorre A tension leg platform (TLP), installed in 1991 in the Norwegian North Sea (details in Table 4.1). At the time of construction Snorre A was the deepest North Sea installation. An artist's impression of the Snorre A TLP and foundation system is shown in Figure 4.8a.

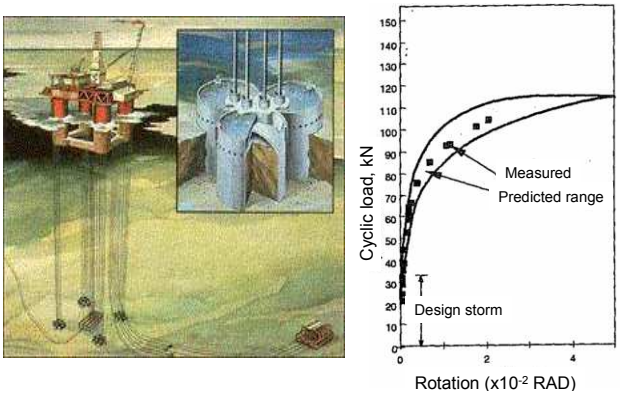

Figure 4.8 (a) Snorre A TLP. Inset, foundation template showing cluster of concrete caissons (b) Predicted and measured load-displacement response (Christophersen, 1993)

The Snorre A foundation system involves a concrete foundation template (CFT) composed of three cylindrical concrete caissons located beneath each of the four corners of the floating pontoon. Resistance to the tether tension is provided by a combination of the self-weight of the CFT and the interaction between the structure and seabed. The average static tension on the tethers is counteracted by the weight of the CFT and ballast to prevent any long term creep effects. Cyclic wave and wind induced loads are transferred to the soil partly by skirt friction and suction under the top cap (Stove et al., 1992). During a storm the TLP will offset from the foundations resulting in a moment on the CFTs which give the most critical load situation (Christophersen, 1993). A series of static and dynamic scale model tests were carried out for the Snorre foundation design (Dyvik et al., 1993; Andersen et al., 1993). Predictions of bearing capacity and displacements made with limit equilibrium and three dimensional finite element analyses agreed well with measured values, shown in Figure 4.8b (Christophersen, 1993).

During installation it was important to ensure a minimum self-weight penetration was achieved to provide a sufficient water tight seal which could withstand the differential pressures applied during suction. Conversely too much self-weight penetration was to be prevented to avoid a costly consolidation phase before water evacuation could be released (Stove et al., 1992). Friction on the interface of the skirt walls and the soil was anticipated to contribute to most of the skirt penetration resistance but uncertainty existed about appropriate prediction methods. The state-of-the-art methods at the time indicated a friction coefficient α in the range 0.5 to 1 should be applied to the soil undrained shear strength. Observations during the self-weight penetration of the Snorre caissons indicated friction coefficients in the range $\alpha = 0.15$ to 0.3 depending on the material.

Following Snorre A, a similar foundation system was employed for the Heidrun TLP, installed in the North Sea in 350 m depth of water in 1995. For concrete caissons to provide a cost-effective foundation solution in deeper waters, tensile resistance under normal working loads would need to be relied on. (By contrast, at Snorre A the dead weight of the CFT and ballast counteracts the tension in the tethers under normal, calm weather, working conditions and only during storm conditions is skirt friction and suction under the top cap relied on to provide resistance to the moment incurred as the platform offsets over the CFTs.) Caissons have certain advantages over piles as anchors for deeper water moorings if they can provide sufficient tensile capacity. For example, the pumps used for installation of caissons do not have the same problems as piling hammers at great working depths, although new systems are being developed for the latter to allow operations in water depths of 3 km; also the larger diameter of caisson foundations provides a larger area for ballast and also mobilises greater reverse end bearing or passive suction during uplift compared to a pile foundation (Clukey et al., 1995).

4.3.3 *Steel buckets for jackets*

The concrete caisson foundations of Snorre A were the precursor to steel 'buckets' (also known as suction cans) used as an alternative to pile foundations for jackets. The Draupner E platform (formerly known as Europipe 16/11E) was the first occasion that steel bucket foundations were provided on a jacket structure. The jacket and bucket foundations can be seen in Figure 4.9 and some platform details are provided in Table 4.1. The foundation concept was developed by Statoil's Morten Baerheim and Tor Inge Tjelta (Tjelta & Haaland, 1993). A unique aspect of this foundation system was the reliance on mobilising tensile capacity (in sands) through 'passive suction' under the baseplate when the foundations were subject to extreme environmental loads.

Figure 4.9 Draupner E jacket with steel bucket foundations (© NGI)

Draupner E was the first time that bucket foundations had been used and the need to penetrate steel skirts into very dense sand also went beyond any previous experience (Tjelta, 1995). An extensive field investigation at the Draupner E site was carried out in 1992, including penetration and capacity tests which provided the basis for the bucket design (Tjelta & Haaland, 1993; Bye et al., 1995). Following the successful use of the suction installed steel bucket foundations on Draupner E a similar foundation solution was employed the following year on the nearby Sleipener Vest SLT jacket. Ground conditions were similar but the jacket was considerably larger with a maximum compression load of 134 MN per leg compared with 57 MN per leg for Draupner E and slightly larger tensile loads (17 MN compared to 13.9 MN). To maintain an economical and practical foundation size a greater percentage of the available capacity had to be relied on than for the Draupner E bucket design. As a result, a comprehensive programme of model testing and numerical analysis was undertaken as part of the detailed design for the Sleipner SLT buckets, as reported by Erbrich (1994) and Bye et al. (1995). Geotechnical concerns also included the potential for buckling of the very thin walled skirts during installation due to the applied suction pressures and lateral soil resistance (Barbour and Erbrich, 1995). .

Figure 4.10a illustrates the stages of installation of a steel bucket foundation supporting a jacket. During the suction penetration phase, pumping creates an under-pressure across the foundation baseplate and, more importantly, sets up seepage flow (Fig. 4.10b) that reduces tip resistance and internal skirt friction. If sufficient suction is applied, skirt tip resistance and internal skirt friction can degrade to approximately zero. The most obvious and serious problem is the potential for sudden liquefaction of the internal soil plug when suction is applied, which could stop further penetration and severely impair the in-place performance of the foundation (Senpere & Auvergne, 1982). The model testing and analytical work carried out for the Sleipner SLT bucket design showed that such sudden failures do not occur under carefully controlled conditions, which was attributed to the increased soil permeability as the initially dense sand loosens within the bucket (Erbrich & Tjelta, 1999).

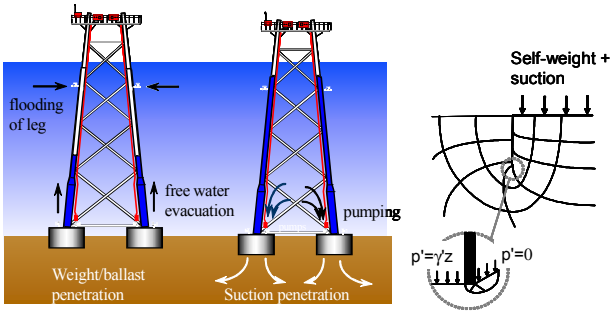

Figure 4.10 (a) Stages of installation of a bucket foundation for a jacket structure (b) Seepage pressures set up during suction installation of bucket foundation (after Erbrich & Tjelta, 1999)

One of the principle in-service design concerns was the reliance on tensile resistance during moment loading. Resistance to substantial tensile forces in sand had previously been considered possible only with the use of active suction, maintained by continuous pumping during the life of a platform while the bucket foundation is a totally passive system in which suction is generated in response to short term tension load (Erbrich, 1994). Previous consideration of tensile resistance had been based on the assumption of idealised elastic and non-dilatant plastic soil, from which it follows that tensile loading causes a decrease in mean effective stress, and therefore a decrease in strength, with time. Once pore water pressures have dissipated tensile resistance is very small, resulting only from skirt friction and the self-weight of the system. In real dense sands the tendency for volumetric expansion during shear is resisted by suctions generated due to the incompressibility of the pore water and expansion of the soil matrix can only occur if water is allowed to flow freely into the pore spaces. If water ingress is inhibited the mean effective stresses will increase mobilising additional shear stress. While this mechanism predicts very high monotonic pull-out capacity for bucket foundations, cavitation of the pore water, which is a function of the water depth at the site, may limit the ultimate achievable pull-out capacity (Bye et al., 1995).

Most of the environmental loading applied to a bucket foundation is cyclic rather than monotonic and for such conditions pore pressure accumulation must also be considered. Although under monotonic shearing a dense sand will tend to dilate contraction always occurs under cyclic loading. Ultimately a state of initial liquefaction may be reached when the effective stresses in the soil reduce to zero. Observations from model tests indicate that once such a state is triggered, a bucket foundation will continuously sink into the soil even if the magnitude of the applied cyclic loads are subsequently reduced. For very dense sands it was found that this condition could only be initiated when the foundation was cycled from compression to tension, and it was this mechanism that limited the design tensile capacity to only a very small component of the monotonic pull-out resistance (Bye et al., 1995). In less dense sands it remains a moot point as to the magnitude of cyclic tensile loads that may be safely resisted.

Much of the current knowledge regarding the performance of steel bucket foundations, both during installation and in-service, is a result of the field, laboratory and numerical work that was carried out for the design of the Draupner E and Sleipner SLT jackets. The acceptance that dense sands can carry moderate transient tensile loads has increased the scope for shallow foundations, particularly where separate caisson foundation are used at each corner of the platform.

4.4 *Design practice*

The design practice for offshore shallow foundations has varied in sophistication depending on the application under consideration. For the early gravity base designs, the foundation bearing capacity was assessed using specialised limit equilibrium methods (e.g. Janbu et al., 1976; Svano, 1981). Various algorithms have also been introduced into these limit equilibrium programs to specifically deal with cyclic loading (e.g. Andersen & Lauritzsen, 1988).

More recently, finite element analyses have become increasingly common for the design of major structures, first using 2D approaches (plane strain and axisymmetric, e.g. Hight & Potts, 1988), then pseudo 3D approaches based on fourier series (e.g. Erbrich, 1994) and most recently full 3D finite element analyses (e,g. Neubecker & Erbrich, 2004).

However, for smaller scale foundations such as temporary mudmats, or subsea foundations, simpler bearing capacity approaches have generally been adopted, such as those outlined in recommended practices (DNV, 1992; API, 1993; ISO, 2000). Interestingly, the shape and design load combinations acting on many of these smaller structures are often even more complex than those acting on larger foundations, and include torsional loads in addition to vertical, horizontal and moment loads about different axes.

Despite the clear differences between offshore and onshore shallow foundation systems and loading conditions the roots of the design methods presented in the recommended practices are the same as adopted for onshore design (e.g. Eurocode 7, 1997). These are ultimately all based on classical bearing capacity equations for failure of a vertically loaded strip foundation on a uniform Tresca soil (Terzaghi, 1943) combined with various modification factors to account for load orientation (in terms of inclination and eccentricity), foundation shape, embedment, and soil strength profile. The shortcomings of the classical design approach and alternative design approaches increasingly gaining favour with industry will be discussed in the following sections.

4.4.1 *Conventional bearing capacity theory*

For the undrained failure of a shallow foundation the ISO guidelines suggest:

$$V_{ult} = As_{u0}\left(N_c + kB'/4\right)FK_c \qquad (4.1)$$

where V_{ult} is the unit vertical bearing capacity, A is the area of the foundation, s_{u0} is the undrained shear strength of the soil at seabed level and N_c is the bearing capacity factor for vertical loading of a strip foundation on a homogeneous deposit, i.e. 5.14 (Prandtl, 1921). k is the gradient of the undrained shear strength profile (equal to zero for homogeneous deposits), B' is the effective width of the foundation (Meyerhof, 1953) and F is a correction factor to account for the degree of heterogeneity (given as a function of a dimensionless non-homogeneity factor kB'/s_{uo} after Davis & Booker, 1973). K_c is a modification factor to account for load orientation, foundation shape and embedment, d, expressed as:

$$\begin{aligned} &K_c = 1 - i_c + s_c + d_c \\ &\text{where:} \quad i_c = 0.5\left(1 - \sqrt{1 - H/A's_{u0}}\right) \\ &\qquad\quad s_c = s_{cv}\left(1 - 2i_c\right)B'/L \\ &\qquad\quad d_c = 0.3e^{-0.5kB'/s_{u0}} \arctan\left(d/B'\right) \end{aligned} \qquad (4.2)$$

The inclination (i_c) and shape factors (s_c) are taken directly from Brinch Hansen (1970). The inclination factor, is based on the exact solution for loading of a strip foundation under a centrally applied inclined load (Green, 1954) in conjunction with the effective width principle (Meyerhof, 1953) to account for moment. The shape factor s_c is dependent on a coefficient s_{cv} which is a function of the degree of heterogeneity kB'/s_{uo} (Salençon & Matar, 1982), the inclination factor and foundation aspect ratio. For uniform deposits $s_{cv} = 0.2$ (Brinch Hansen, 1970). The ISO guidelines do not make explicit provision for specific three-dimensional geometry but suggest equivalence to a rectangle with the same area and areal moment of inertia. The recommended depth factor in Eqn 4.5 is slightly more conservative than the conventional Brinch Hansen (1970) factor. Further, ISO recommend that $d_c = 0$ be used if the installation procedure or other foundation aspects, such as scour, prevent mobilisation of shear stresses in the soil above skirt tip level, or if the in-service horizontal loads lead to large passive earth pressures over the depth of the skirts.

The undrained bearing capacity under uniaxial vertical loading of a strip foundation resting on the surface of a homogeneous deposit calculated by Eqn 4.1 gives $V_{ult} = 5.14As_{u0}$ in agreement with the exact solution (Prandtl, 1921). Incorporation of the shape factor gives $V_{ult} = 6.17As_{u0}$, slightly over-predicting the exact solution for a rough circular foundation of $6.05As_{u0}$ (Cox et al., 1961). The horizontal failure criterion gives $H_{ult}/As_{u0} = 1$ and is independent of foundation geometry or undrained shear strength gradient implying failure by sliding when the applied force is in equilibrium with the undrained shear strength at ground level. For conditions of no vertical load eccentricity and $H/As_{u0} = 1$, the inclination factor $i_c = 0.5$ and the shape factor s_c, if applicable, reduces to zero such that substitution in Eqn 4.1 indicates lateral failure will prevail for vertical loads $V \le 2.57As_{u0}$, i.e. $V/V_{ult} \le 0.5$. The ultimate moment (M_{ult}) is predicted in conjunction with a vertical load $V = 0.5V_{ult}$ (Meyerhof, 1953). At lower vertical loads, application of moment is assumed to result in separation at the foundation/soil interface leading to a reduced bearing area and hence bearing capacity. Solution of the bearing capacity equation in Eqn 4.1 gives $M_{ult} = 0.64ABs_{u0}$ for a strip foundation and $0.61ADs_{u0}$ for a circular foundation, which compare well with plasticity solutions (Houlsby & Puzrin, 1999) and finite element analyses (Taiebat & Carter, 2002a).

For conditions of soil strength homogeneity, classical theory (as outlined in Eqns 4.1 and 4.2) adequately predicts bearing capacity under either centrally applied inclined loads *or* vertical eccentric loads, but is less accurate (but conservative) under superposition of the solutions for inclination and eccentricity (i.e. VHM loading). The validity of this coupling was questioned in the light of bound solutions reported by Ukritchon et al. (1998) for strip foundations and similar shortcomings for circular foundations were confirmed by Gourvenec and Randolph (2003a).

For non-uniform shear strength profiles classical bearing capacity theory will underpredict the capacity even for simple eccentricity with no lateral load. The breakdown of classical bearing capacity theory under combined loading is particularly significant in offshore shallow foundation design due to the large components of horizontal load and moment from the harsh environmental conditions (i.e. wind, wave and current forces, see Fig. 4.2) and the often normally consolidated seabed deposits. The applicability of classical bearing capacity theory to offshore design is also questionable as the approach neglects tensile capacity, which in reality can be mobilised by some offshore shallow foundations provided they are equipped with skirts and sealed baseplates.

4.4.2 *New solution methods for undrained conditions*

In this section, new solution methods for shallow foundation design will be presented and compared with predictions from classical theory (as outlined in Section 4.4.1). Ultimate limit states under combined vertical, moment and horizontal loading are most conveniently expressed by three-dimensional interaction diagrams expressed in VHM load space as shown in Figures 4.11. The surfaces shown are relevant for undrained failure of a single circular foundation under combined vertical moment and horizontal load, as indicated in Figure 4.12.

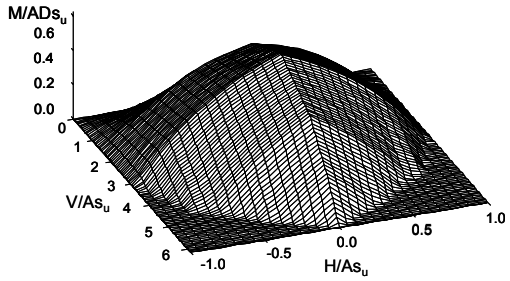

(a) Conventional surface foundation: Classical bearing capacity theory (ISO, 2000)

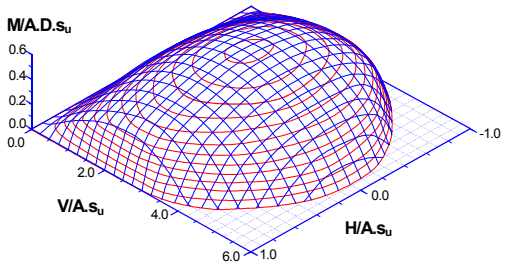

(b) Conventional surface foundation: Finite element results (Taiebat & Carter, 2002b)

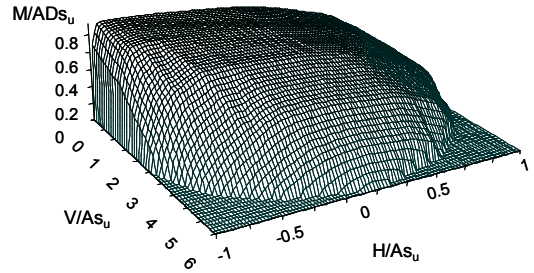

(c) Circular skirted foundation: Finite element results (after Gourvenec & Randolph, 2003a)

Figure 4.11 Three-dimensional failure surfaces for a circular foundation on a Tresca soil under combined vertical, horizontal and moment load

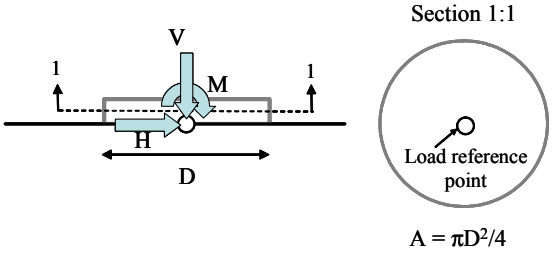

Figure 4.12 Combined VHM loading of a circular foundation – relevant to the failure surfaces shown in Figure 4.11

Figure 4.11a shows a failure surface derived from classical bearing capacity theory (Eqns 4.1 and 4.2). The locus is symmetric and quasi-linear in the HM plane in contrast to the numerically derived loci in Figures 4.11b and c. The locus derived from the classical approach is symmetric in the HM plane as the method assumes equivalence between a combined lateral load and moment acting in the same direction and in opposition. Figure 4.11b represents the same boundary conditions as Figure 4.11a but derived from finite element analyses. The apex points are coincident, but the failure surface is more curved indicating greater load capacity is predicted than with the classical approach under the interaction of horizontal and moment loading. The locus is largely symmetric in the HM plane, supporting the assumption adopted in the classical approach that foundation response is independent of the directions of the coupled loads. It is interesting to note that for the same boundary conditions for a strip foundation Ukritchon et al. (1998) report an asymmetric response in the HM plane indicating a different response to combined horizontal load and moment acting in the same direction and in opposition (see Fig. 4.14)

The failure surface shown in Figure 4.11c is relevant for a shallow foundation with tensile capacity, as would be appropriate where skirts are used. In this case, moment capacity continues to increase as the vertical component of load diminishes. The locus is highly asymmetric in the HM plane and the maximum moment capacity occurs in conjunction with a horizontal load acting in the same sense (i.e. clockwise and left to right or vice versa). In this example foundation skirts were conceptually modelled by allowing tension on the underside of a surface foundation (Fig. 4.13). Similar analyses of skirted foundations on soils with a non-uniform shear strength profile should use the value of undrained shear strength at the level of the skirt tips, $s_{u(tip)}$ (= kd).

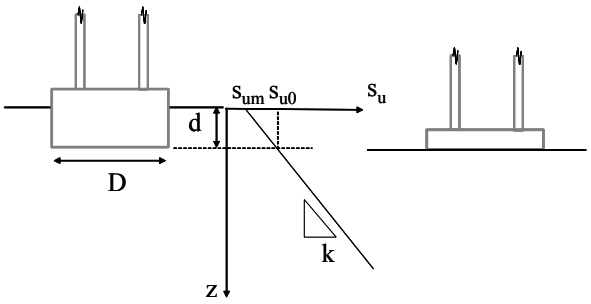

Figure 4.13 Conceptual modelling of foundation skirts in numerical analyses

Three-dimensional failure surfaces of the type shown in Figure 4.11 are useful for qualitative comparison, but for quantitative assessment it is more useful to consider a slice through the three-dimensional surface. Figure 4.14 shows a slice through the surfaces shown in Figures 4.11a and b at a vertical load of half the ultimate uniaxial value. Results for a strip foundation are also shown for comparison. The conservatism of classical theory is clear, with the failure surface lying well inside that predicted by numerical analysis.

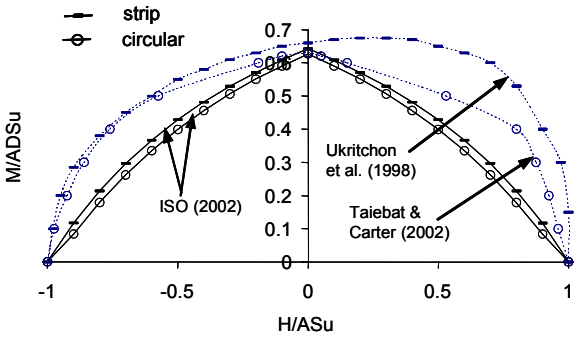

Figure 4.14 Ultimate limit states for strip and circular foundations on a Tresca soil; Classical bearing capacity theory (ISO, 2000) and numerical predictions (from Gourvenec & Randolph, 2003a)

Classical bearing capacity theory and finite element results presented in Figure 4.11a and b and Figure 4.14 represent a no-tension interface between the foundation and the soil, i.e. the foundation lifts up from the soil under moment loading at low vertical loads, reducing the bearing area and hence bearing capacity. As already discussed it is more common for offshore foundations to be equipped with skirts allowing the foundations to withstand some tensile loads, provided the baseplate is also sealed, leading to the form of failure surface in Figure 4.11c, although standard industry design guidelines do not account for this quantitatively. Figure 4.15a and b compare slices through the failure surfaces in MH space at discrete values of vertical load, predicted by classical bearing capacity theory (no-tension interface), and finite element analyses in which tension between the foundation and soil is allowed. The considerable conservatism in the classical predictions is readily apparent.

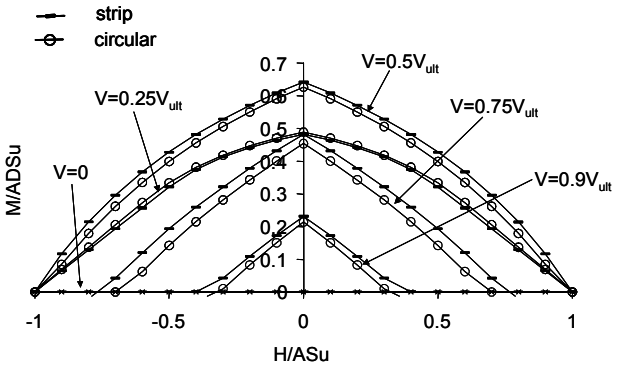

(a) Classical bearing capacity theory (ISO, 2000) (from Gourvenec & Randolph, 2003a)

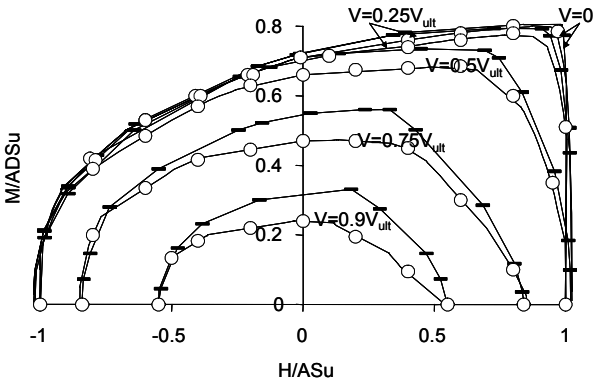

(b) Finite element results (from Gourvenec, 2003)

Figure 4.15 Failure surfaces for strip and circular foundations (Homogeneous Tresca soil). Strip footing

A considerable obstacle to the adoption of failure surfaces such as those shown in Figures 4.11b and c for routine design is that their complex shape (even in two dimensions, cf. Figs. 4.14 and 4.15b) is not conducive to a closed-form solution.

Bransby & Randolph (1998) proposed a simplifying transformation for skirted foundations on Tresca soil with linearly increasing strength with depth:

$$f = \left(\frac{V}{V_{ult}}\right)^{2.5} - \left(1-\frac{H}{H_{ult}}\right)^{\frac{1}{3}}\left(1-\frac{M^*}{M_{ult}}\right) + \frac{1}{2}\left(\frac{M^*}{M_{ult}}\right)\left(\frac{H}{H_{ult}}\right)^{5} \quad (4.3)$$

$$\text{where}: \quad \frac{M^*}{ADs_{u0}} = \frac{M}{ADs_{u0}} - \frac{L}{D}\frac{H}{As_{u0}}$$

This approach was developed based on finite element results of a strip foundation and a material with an undrained strength given by $kD/s_{u0} = 6$, where k is the gradient of the undrained strength profile, D is the width of the foundation and s_{u0} is the undrained shear strength at seabed level. The M* term is a modified moment parameter, defined as a function of the height, L, of rotation above the foundation of the scoop component of the mechanism accompanying failure. An upper bound solution is proposed for all combinations of VHM loading based on a wedge-scoop-wedge configuration, generalising observations from the finite element analyses. Normalised uniaxial capacities (i.e. V_{ult}, H_{ult} and M_{ult}) for other foundation geometry (e.g. circular) can be substituted into Eqn 4.3 to extend the expression from plane strain conditions. Gourvenec (2003) shows that there is sufficient similarity between the shape of the failure surfaces for this approximation to be appropriate for circular foundations. Unfortunately, Gourvenec & Randolph (2003b) and Gourvenec (2004) show the shape of the failure locus is dependent on the shear strength profile and therefore the exponents in Eqn 4.8 need to be re-evaluated (i.e. re-optimised within the upper bound framework) for various different values of kD/s_{u0} before this approach can be used reliably for general design purposes.

The closed-form solution in Eqn 4.3 is based on finite element analyses that conceptually represented foundation skirts by allowing tension (Fig. 4.13), and therefore overlook additional load capacity which would result from the physical embedment. Vertical, moment and horizontal load resistance is enhanced by embedment due to the additional shearing involved in failure (Fig. 4.16). For soils with an increasing shear strength profile with depth the effect is magnified.

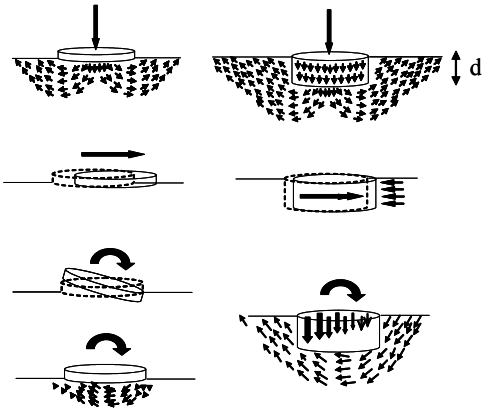

Figure 4.16 Enhanced foundation capacity due to embedment

Recent work has challenged the use of the conventional depth factors (Skempton, 1951; Brinch Hansen, 1970) and explored the extent to which the vertical bearing capacity is enhanced, and the mode of failure changed, by increasing embedment ratio, d/D. Martin and Randolph (2001) present rigorous plasticity solutions of circular foundations with rough-sided

skirts which show, for example, in a homogeneous deposit bearing capacity increases by ~ 50 % as the depth of embedment increases from zero to one diameter, compared to a 20 % increase predicted by Skempton (1951). The trend of increasing capacity with increasing embedment does not continue indefinitely owing to a change in the failure mode. In a homogeneous deposit the transition from a surface failure mechanism to a confined failure occurs at an embedment ratio between 1 and 2 (Hu et al., 1999) while for soils with a high strength gradient the transition will take place at an embedment ratio between 2 and 3 (Hu & Randolph, 2002). An exact solution has not yet be found for shallowly embedded foundations and the bracket between lower and upper bound solutions widens rapidly with increasing embedment ratio. However, lower bounds show good agreement with finite element results (Randolph et al., 2004). Lower bounds for rough-based, smooth-sided embedded shallow foundations in Tresca soil for a range of heterogeneity indicate that as embedment ratio increases, bearing capacity tends to a steady state value of ~ 9.3 for all values of kD/s_{um} (Martin, 2001), as shown in Figure 4.17 (where s_{um} is the strength at seabed level).

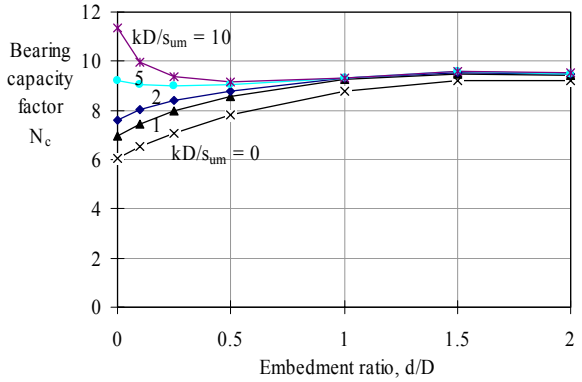

Figure 4.17 Undrained bearing capacity factors for skirted circular foundations (after Martin, 2001)

The horizontal capacity of embedded foundations comprises the sum of base shearing capacity and the passive and active resistance of the skirts. For foundations with skirt depths less than 50 % of the diameter, the latter component is relatively minor and is often ignored. However, for embedment d > 0.5D the resistance around the skirts can be a major component. In terms of the (vertical) projected area of the foundation dD, bearing capacity factor N_c, and average undrained shear strength $s_{u\text{-}avg}$ over the embedment depth, the lateral resistance of an embedded foundation can be given by:

$$H_{ult} = 0.25\pi D^2 s_{u0} + dDN_c s_{u-avg} \qquad (4.4)$$

The value of N_c increases rapidly with the embedment depth, with a minimum value of 2 (or 4 for two-sided failure) and a maximum value of 10 to 11 (Randolph et al., 1998b).

Little investigation has taken place to address the effect of embedment on the capacity of a foundation under rotation. An upper bound solution based on a scoop mechanism (Bransby & Randolph, 1999) suggests an approximately proportional relationship between embedment ratio d/D and moment capacity for normally consolidated soil where $kD/s_{u0} = D/d$, given by:

$$d_m = 1 + 0.3\frac{d}{D} \qquad (4.5)$$

The embedment factor for moment loading is shown in Figure 4.18 for a range of values of kD/s_{u0}.

Figure 4.18 and Eqns 4.4 and 4.5 can be used to evaluate uniaxial collapse loads V_{ult}, H_{ult} and M_{ult} appropriate for embedded foundations. It is then commonly assumed that the shape of the failure surface in V, H, M space will be unaffected by the embedment, such that a normalised surface (derived for a surface foundation with tension allowed) can be scaled to the appropriate apex points, although this has not been verified comprehensively.

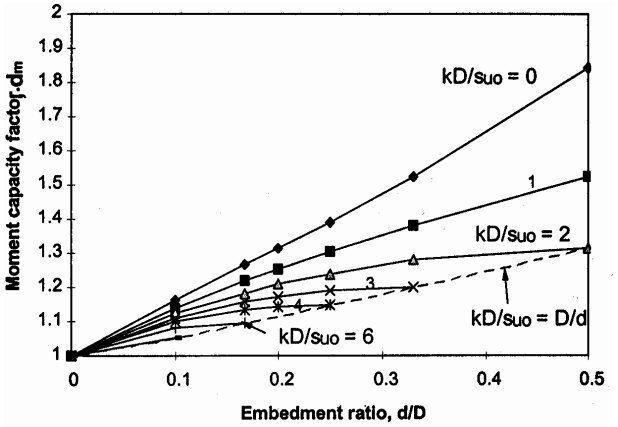

Figure 4.18 Upper bound prediction of moment capacity factor with embedment (Bransby & Randolph, 1999)

In summary, classical bearing capacity theory, based on Terzaghi's equation for uniaxial vertical limit load of a surface strip foundation on a uniform deposit, modified by various multiplicative factors, gives conservative results for conditions relevant to many offshore shallow foundation designs.

New solution methods provide more realistic predictions of foundation capacity for these cases. However, they have yet to be generalised fully for routine application. Theoretically exact plasticity solutions are only available for relatively few simple cases. In practice, therefore, geotechnical engineers still need to resort to other methods. These include empirically derived formulae, which are often of limited accuracy although generally err on the conservative side; limit equilibrium methods, which, similar to upper bound solutions, usually give an unsafe (i.e. high) prediction of bearing capacity; and numerical methods such as finite element analysis with which extreme caution must be exercised if serious errors, usually unconservative, are to be avoided.

4.4.3 *Consolidated undrained bearing capacity*

The previous section has dealt with the undrained bearing capacity of soils where the undrained strength profile can be modelled simply as either uniform or linearly varying with depth. Such conditions occur for foundations that do not consolidate rapidly under the weight of the structure and would be expected to occur in the finest grained soils such as most clays. In onshore applications, the bearing capacity of coarse grained soils such as sands would be generally evaluated assuming fully drained conditions, but a characteristic feature of the offshore environment is that the governing load condition acting on most foundations involves a significant magnitude of cyclic loading applied over short durations (i.e. wave periods of generally less than about 16 seconds). Under these conditions, even fairly coarse materials, such as most sands, exhibit an undrained response during the passage of a wave (which is the basis for the bucket foundation tension capacities discussed earlier). For sands and silts it is therefore usually necessary to assess the 'consolidated' undrained bearing capacity – that is where the peak loads are applied undrained but the soil has consolidated and strengthened under the weight of the platform before the peak loads are applied. For these conditions, the distribution of undrained shear strength beneath the foundation is complex and there are no simple solutions available in the literature that address such behaviour. Inevitably, the design engineer must resort to either limit equilibrium methods (eg. Svano, 1981; Randolph & Erbrich, 2000) or finite element methods (eg. Bye et al., 1995) to address these types of problem.

4.4.4 *Cyclic bearing capacity*

As already discussed, most loads of importance to offshore shallow foundation design have a significant cyclic load component. The 'cyclic bearing capacity' is generally assessed by first prescribing a cyclic strength to the soil that should not be exceeded in order to avoid either excessive progressive settlement or the triggering of a more catastrophic sudden subsidence of the foundation. The derived cyclic strength profile is then integrated to obtain the 'cyclic bearing capacity', using methods such as those outlined in the previous sections.

The cyclic soil strength is not unique and is a function of several variables including the number of cycles of load, the ratio of cyclic and static shear stresses, the stress path direction and the acceptable magnitude of shear strain or excess pore pressure. A comprehensive state-of-the-art review on the assessment of the cyclic soil strength for clay soils is presented by Andersen (2004). Since clay soils do not generally exhibit any drainage during a design storm, the cyclic strength is normally derived with reference to limiting strains. However, in sands the accumulated pore pressure is usually used instead since the influence of on-going dissipation of excess pore pressures can then be readily accounted for. This is an important factor for relatively permeable sands since accumulated excess pore pressures may dissipate within the duration of a design storm.

Carbonate soils are generally highly susceptible to degradation under cyclic loads. This can be particularly significant in carbonate silts or silty sands, which degrade much more substantially than soils comprised mostly of clay minerals, but have permeabilities that are sufficiently low to preclude any drainage during the design storm event. Non-carbonate silts may also be troublesome if they comprise mostly non-clay minerals.

5 MOBILE DRILLING UNITS

5.1 *Mobile drilling units (jack-ups)*

Most offshore drilling in shallow to moderate water depths is performed from self-elevating mobile (jack-up) units. Although the earliest reference to a jack-up platform is in the description of a United States patent application filed by Samuel Lewis in 1869 (Veldman and Lagers, 1997), it was not until 85 years later in 1954 that Delong McDermott No. 1 became the first unit to utilise the jack-up principle for offshore drilling. Delong McDermott No. 1 was a conversion of one of the successful 'Delong Docks': a mobile wharve with a number of tubular legs which could be moved up and down through cut-outs in the pontoon. However, it was only two years later that former entrepreneur in earthmoving equipment R.G. LeTourneau revolutionised the design of jack-ups by reducing the number of legs to three and introducing an innovative electrically driven rack and pinion jacking system (Ackland, 1949; Stiff et al., 1997).

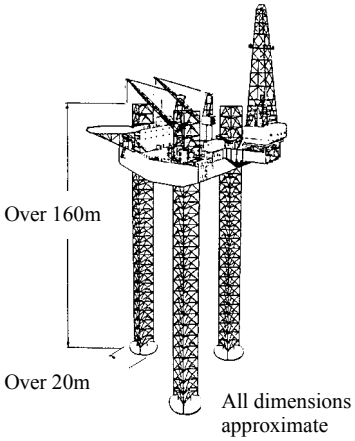

Figure 5.1 Typical jack-up unit used today (after Reardon, 1986)

Units today are similar in concept and consist of a buoyant triangular platform resting on three independent truss-work legs, each with a rack and pinion system used to jack the legs up and down through the deck (Fig. 5.1). The foundations of independent-leg jack-up platforms approximate large inverted cones and are commonly known as 'spudcans'. Roughly circular in plan, spudcans typically have a shallow conical underside (in the order of 15 to 30° to the horizontal) with a sharp protruding spigot. In the larger jack-ups in use today the spudcans can be in excess of 20 m in diameter, with shapes varying with manufacturer and rig. Figure 5.2 shows some more typical shapes.

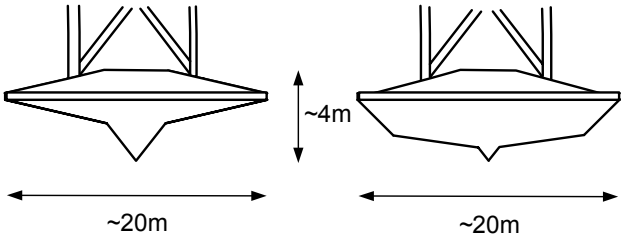

Figure 5.2 Some example spudcan shapes

Jack-ups play a vital role in the offshore industry with proven flexibility and cost-effectiveness in field development and operation. This is mainly due to their self-installation capacity. Jack-ups are towed to site floating on the hull with the legs elevated out of the water (Fig. 5.3a). On location, the legs are lowered to the sea-bed, where they continue to be jacked until adequate bearing capacity exists for the hull to be lifted clear of the water. The foundations are then effectively 'proof' tested by pumping sea-water into ballast tanks in the hull (Fig. 5.3b). The reasoning is to expose them to a larger pure vertical load than would otherwise be expected due to a combined loading combination during service. The ballast tanks are emptied before operations on the jack-up begin (Fig. 5.3c).

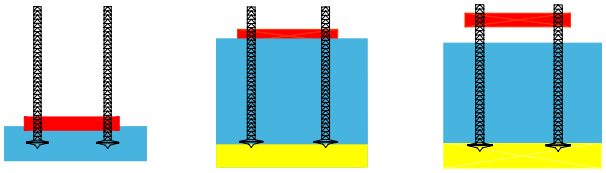

Figure 5.3 Jack-up installation procedure

Before a jack-up can operate at a given location a site-specific assessment of its operation must be performed. This continual assessment is what differentiates jack-up analysis from that of conventional fixed platforms and most onshore operations. For any new site two separate analyses are required: a prediction of the footing penetration during installation and preload and an assessment of its capacity to withstand a design storm. In the past, with jack-ups used in relatively shallow and calm waters, it has been possible to use simple but conservative analysis techniques for these assessments. However, as jack-ups have moved into deeper and harsher environments, there has been an increased need to understand jack-up behaviour and develop more sophisticated analysis techniques. The publication of the "Guidelines for the Site Specific Assessment of Mobile Jack-Up Units" (SNAME, 1997) was an attempt by the offshore industry to standardise jack-up assessment procedures. However, jack-ups are still perceived to have lower reliability then fixed offshore platforms (Sharples et al., 1989; Boon et al., 1997; Morandi, et al., 1997), with many of the accidents attributed to geotechnical 'failures'. Hunt and Marsh (2004) attribute 52 fatalities between 1955 and 2000 to these failures. They also highlight the significant economic cost and the continuation of accidents, as shown by the 15 more 'widely known incidents' reported during the last seven years (Table 5.1).

Table 5.1 Jack-up 'structural' incidents 1996-2003 (after Hunt and Marsh, 2004)

	Rig	Incident	Location	Weather	Date
Pre-loading	Victory	Punch-through	South Australia	Fair	1996
	Harvey Ward	Punch-through	Indonesia	Fair	1998
	Al Mariyah	Slewed / dropped	PG	Fair	2000
	Monitor	Leg damage from uneven sea-bed	CNS	Fair	2000
	101	Leg damage from adjacent footprint	CNS	Fair	2001
	Ekhabi	Punch-through	PG	Fair	2002
	57	Rapid leg penetration	SCS	Fair	2003
In-situ	Harvey Ward	Ship impact	Indian ocean	Fair	1996
	Wijslift 6	Stern dropped	CNS	Fair	2002
	Monarch	Uneven sea-bed scour	SNS	Fair	2002
	Arabdrill19	Overturned / sank	PG	Fair	2002
	Roger Mowell	Leg damaged	SCS	Fair	2002
	Dolphin 105	Overturned	GOM	Hurricane Lili	2002
	Houston	Overturned	GOM	Hurricane Lili	2002
	John Sandifer	Leg damaged	GOM	Hurricane Lili	2002

PG – Persian Gulf; CNS – Central North Sea; SNS – South North Sea; SCS – South China Sea; GOM- Gulf of Mexico

Both installation and combined storm-loading analysis will be considered in this paper.

5.2 *Spudcan foundations*

5.2.1 *Effect of installation method and load path*

With jack-up and spudcan sizes fixed, the installation method and the pre-loading level reached are critical to any site-specific assessment. With the foundations exposed to a vertical load prior to operation it is argued that a combined loading 'failure' surface is established and is proportional to the vertical pre-load.

In the offshore industry, the calculation of the bearing capacity under combined loading (see Fig. 5.4) initially evolved from the onshore procedures described by Meyerhof (1951, 1953), Brinch Hansen (1970) and Vesic (1975). However, their reliance on numerous *ad hoc* factors (shape, inclination, depth) made them somewhat impractical and they are rapidly being replaced by surfaces formulated explicitly in combined load space. Further, in comparison to the design of shallow foundations onshore, where the vertical loads dominate, spudcans are subjected to proportionately higher horizontal and moment to vertical loads. This has driven more accurate understanding of the combined loading behaviour, with the interaction surfaces reflecting this development.

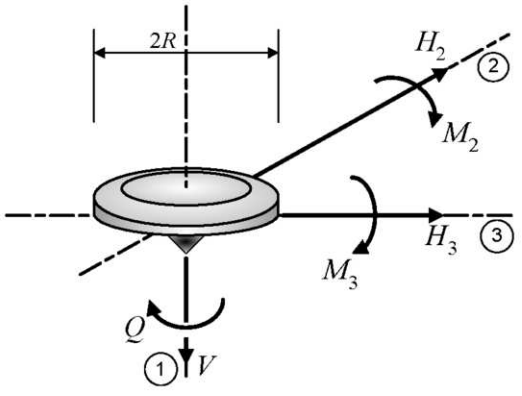

Figure 5.4 Combined loads on a spudcan footing

The load path of the jack-up legs has a critical effect on the factor of safety. During installation and pre-load an interaction 'failure' (or yield) surface for each spudcan is theoretically produced and is proportional to the vertical load applied ($V_{pre\text{-}load}$). After the pre-load water has been dumped the load settles inside such a surface ($V_{self\text{-}weight}$). Under environmental wind and wave loading, load paths for each leg and spudcan can be predicted and safety factors are then evaluated based on the proximity of the expected load paths to the yield envelope (Georgiadis, 1985). For a typical jack-up case shown in Figure 5.5, the additional load for a windward spudcan failure is between the windward leg design (WL_d) point and the windward leg failure (WL_f) point, and for the leeward leg between points LL_d and LL_f. This produces a drastically different factor of safety than if the more traditional constant combined load to vertical load ratio was applied from the origin (lines WL_d to A and LL_d to B respectively). Further, for design cases where additional pre-load is required, although the expansion of the surface may-be uniform the additional capacity along the load paths may not. This is shown in Figure 5.6, with $LL_{f1} \rightarrow LL_{f2}$ requiring more additional load than $WL_{f1} \rightarrow WL_{f2}$.

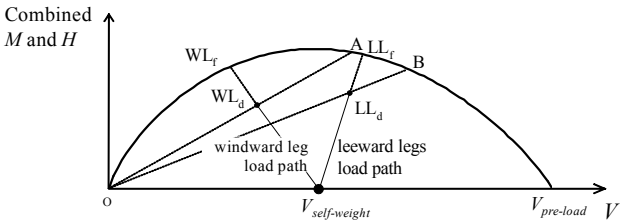

Figure 5.5 Expected load paths during a typical site-assessment

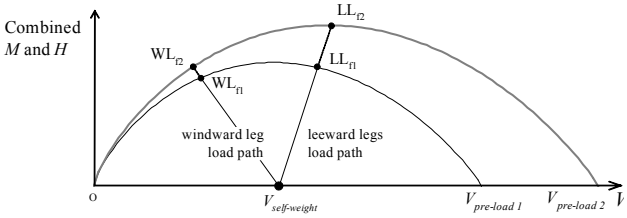

Figure 5.6 Role of extra pre-load in a combined loading assessment

5.2.2 *Other differences from onshore situations*

Other aspects of jack-up and spudcan behaviour that differentiate them from onshore situations include:

- quality and level of detail of the site-investigation of a typical jack-up installation is significantly poorer. This is also the case when compared to other permanent offshore designs (Houlsby & Martin, 1992);
- cyclic nature of environmental wind and wave loads complicates any jack-up analysis;
- dynamic response and significant non-linearities, requiring an integrated analysis approach to environmental loading, structural and foundation modelling;
- higher levels of uncertainty in all of the modelling inputs (e.g. loading conditions at an offshore site are less certain).

5.2.3 *Spudcan installation*

During installation, the vertical self-weight of a jack-up is the dominant loading on its spudcan footings and under most pre-loading circumstances it is assumed to act directly through the spudcan load reference point (the centre of the plan of the conical footing). Maximum leg loads of a modern jack-up can exceed 140 MN and produce average vertical bearing pressures in excess of 400 kPa for a fully embedded spudcan. These can be significantly higher in very stiff soils where the penetration may limit the contact area. Accurate prediction of the installation and preloading is required, such that:

- the final penetration depth allows for adequate air gap between the maximum predicted wave elevation and underside of the deck; and
- overall stability is maintained, avoiding potential punch-through problems or eccentric loading instabilities due to existing footprints or sea-bed depressions (discussed in Section 5.2.5).

Vertical load in uniform sands: Spudcan preloading is usually performed sufficiently slowly to ensure that fully drained conditions will occur in sandy seabed soil. The drained ultimate vertical bearing capacity of a circular foundation on the surface of homogeneous frictional material (with no effective surcharge), can be expressed as:

$$V = \gamma' N_\gamma \pi R^3 \tag{5.1}$$

where R is the footing radius, γ' the effective unit weight of the soil and N_γ the dimensionless bearing capacity factor calculated for the axi-symmetric case. Various bearing capacity and shape factors are given in the literature for the analysis of bearing capacity in silica sands. Traditionally, the value of the dimensionless bearing capacity N_γ has been calculated for strip footings, and applied to circular foundations by using an empirical shape factor. However, more recently values for the axi-symmetric case have been determined directly. Recent tabulated lower bound solutions have been provided by Cassidy and Houlsby (2002) for circular conical foundations of radius, R, cone angles between 30 and 180° (flat plate), a range of roughness from smooth to fully rough and angles of friction (ϕ) between 5 and 50°. Other values for rough circular footings have been provided by Martin (2004) and are discussed in the context of the load carrying capacity of a foundation by Randolph et al. (2004). For the rough circular plate the suggested values of Martin (2004) are given in Table 5.2.

Table 5.2 Bearing capacity factors for circular rough plate (after Martin, 2004)

Friction angle ϕ: degrees	Bearing factor, N_γ
5	0.081
10	0.32
15	0.93
20	2.42
25	6.07
30	15.5
35	41.9
40	124
45	418

Footing penetrations in a thick layer of clean silica sand are usually minimal with the maximum diameter of the spudcan rarely coming into contact with the soil. It is therefore not usual to need any N_q term unless soft clay overlays sand. With different shaped spudcans it is important for the purpose of analysis (particularly during partial penetration) to be able to establish an equivalent area and conical angle. A method where the volume of the equivalent cone is equal to the volume of the penetrated portion of the spudcan and the planar area in soil contact is consistent (i.e. the radius of the equivalent cone is equal to the maximum radius of the spudcan in contact with the soil) is recommended (Osborne et al., 1991; Martin, 1994). This is shown diagrammatically in Figure 5.7 for all penetration conditions (noting that once the maximum spudcan radius has been passed the equivalent conical footing is constant, Fig. 5.7(d)).

Consideration of the effect of the compressibility of sands and its effect on bearing capacity should also be made. Recent numerical studies by Frydman and Burd (1997) and Erickson and Drescher (2002) for strip and circular footings respectively have indicated that the dilation angle has little effect on the bearing capacity at small friction angles, but becomes significant for friction angles above 35°. This may mean that bearing capacity values derived through rigorous plasticity analysis using the assumption of associated flow (angle of friction equal to the angle of dilation) could be significantly affected by the effect of soil compressibility (*i.e.* due to excessive displacements the tabulated values of Cassidy and Houlsby (2002) and Martin (2004) are unlikely to be achievable in practice (Randolph et al., 2004)).

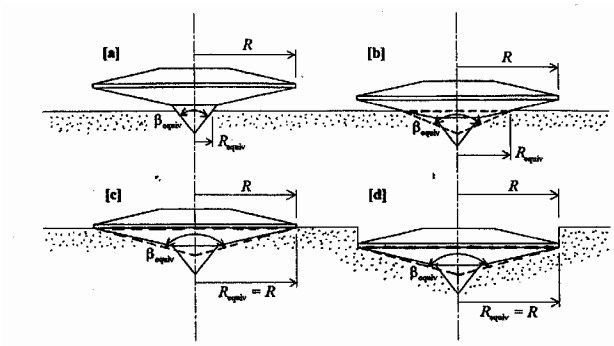

Figure 5.7 Calculating an equivalent conical footing for various embedments (after Martin, 1994)

Therefore, reduced angles of friction ϕ have been recommended by various practitioners for use in bearing capacity calculations on sand (Graham & Stewart, 1984; James & Tanaka, 1984; Kimura et al., 1985). Based on centrifuge model tests on spudcan footings, Murff et al. (1992) proposed a reduction of the bearing capacity factor itself. Uncemented carbonate sands are generally much more compressible than silica sands, but these materials also have a high friction angle. Application of the classical Eqn 5.1 would lead to a substantial under estimate of actual spudcan penetrations in such soils. Alternative methods, such as the empirical approach recommended by Finnie (1993) have therefore been developed to assess spudcan penetration in carbonate sands.

Vertical load in uniform clays: Calculation of the ultimate vertical bearing capacity of a foundation in clay of uniform shear strength (undrained failure in clay, $\phi = 0$) follows bearing capacity theory (as outlined in Section 4.4.1). As in the sand case, traditionally the value of N_c has been determined from solutions for strip footing on homogeneous clay, with shape and depth factors based on Skempton (1951). However, these factors are significantly affected by the gradient of shear strength with depth. To improve predictions during pre-load assessments, the jack-up industry manipulated the location at which the undrained shear strength was chosen. For example, based on back calculations of monitored installations, and while using the Skempton factors, Young et al. (1984) recommended using a shear strength averaged over the zone of soil from the spudcan tip to a depth of half a diameter. This reduced the former recommendation of one whole diameter by Gemeinhardt & Focht (1970).

Such approximate methods are inappropriate as rigorous plasticity solutions for axisymmetric circular footings that include strength varying linearly with depth become available. The bearing capacity at a specific depth can be expressed by:

$$V = \left(s_u N_c + \sigma'_{v0}\right)\pi R^2 \tag{5.2}$$

Appropriate tabulated lower bound solutions of N_c have been provided by Houlsby and Martin (2003) for circular conical foundations of diameter, D, cone angles between 60 and 180° (flat plate), different embedment depths (zero to 2.5 diameters) in soil with different strength gradients (expressed as kD/s_{um} from 0 to 5, where k is the rate of increase in shear strength with depth, from a value of s_{um} at the mudline).

When calculating the maximum pre-load the effect of back-flow must be considered. The maximum preload is equal to

$$V_{pre-load} = V_{bc} - F_0' A + \gamma' V \tag{5.3}$$

where V_{bc} is as calculated in Eqn. 5.2 and the effect of backflow, F_o'A, and the effective weight of the soil replaced by the spudcan, $\gamma'V$ are also accounted for.

For a more thorough review of bearing capacity of shallow foundations in both sands and clays reference can be made to Randolph et al. (2004). For clay layers with distinct strength differences methods for layered soils should be used (e.g. Meyerhof & Hanna (1978); Wang & Carter, 2002).

'Difficult' Soils: The methods discussed above are considered appropriate to probably the majority of locations where jack-ups will be installed. However, a number of important exceptions exist, where the utmost caution is required. Erbrich (2005) presents two such cases which occurred recently in the Bass Strait, offshore Australia. In the first instance (at the Yolla A location), spudcan penetrations proved to be much larger than had been predicted by four independent a-priori assessments, even though the available soils data was of exceptional quality compared to that available for most jackup installations. These poor predictions have been principally attributed to the very high sensitivity of the carbonate sandy silt found at this location and the influence of partial drainage during CPT and T-bar testing, compared to the more undrained response that occurs during spudcan penetration.

The second case (Trefoil) involved a site close to Yolla but in slightly shallower water depth, which resulted in the predominant material being carbonate silty sand rather than sandy silt. This slight coarsening of the grain size enabled enough partial drainage to develop, such that the initial spudcan penetration under the maximum preload was only around 25% of that achieved at Yolla. However, it was known that the monotonic undrained strength would be insufficient to support the jackup at this depth, and that even this inadequate monotonic strength would be severely degraded by cyclic action during a design storm. In what is believed to be a unique operation, the spudcans were therefore 'worked' downwards (from about 6 m initial penetration to 14 m) through the application of cyclic preload until their embedment had increased to a 'safe' depth (how the 'safe' depth was determined is discussed in Section 5.3.10).

The following features should be seen as a warning of a potentially 'difficult' soil where extreme caution is required:

1. Any soils where the coefficient of consolidation lies between 1000 m^2/yr and 250,000 m^2/yr.
2. Any soils with high sensitivity (say > 7).
3. Any soils that are susceptible to severe strength degradation under cyclic loading

The most likely soil types to have these properties are those which would be described as silts, sandy silts and silty sands, with either non-carbonate or (particularly) carbonate mineralogy. Alternative methods for assessing the spudcan penetration in such soils are presented in Erbrich (2005).

Predicting Backflow: The methods used to assess spudcan penetration resistance discussed previously have assumed failure based on a footing 'wished into place'. Care must be taken in ensuring the factors represent the preferential mechanism. Recently, the application of Particle Image Velocimetry (PIV) and close range photogrammetry methods have provide exciting opportunities to investigate continual modes of soil displacement and failure (White et al., 2001a,b, 2003). One successful application has been the investigation of deep penetrating spudcans in clays (Hossain et al., 2003, 2004; Hossain, 2004), where a half-plane spudcan was penetrated against a transparent window a drum centrifuge (Stewart et al., 1998). Images were captured in-flight (in this case at an acceleration of 300 earth gravities) by a high resolution (2270×1704 pixel) digital still camera. Example digital image and interpreted particle flow velocity vectors are shown in Figure 5.8.

The tests have revealed that backflow on-top of a spudcan is governed by the transition from shallow penetration with soil heaving on the soil surface to a localised flow-around mechanism. Importantly, this latter deep penetration mechanism is the result of a preferential 'flow failure' and not a 'wall failure' of an open cavity as assumed in current guidelines (SNAME, 1997). Conditions for back flow may be expressed simply as

$$\frac{H}{D} = \left(\frac{s_u}{\gamma' D} \right)^{0.55} \tag{5.4}$$

where H is the limiting cavity depth and D the spudcan diameter. Figure 5.9 shows the resulting design chart and compares results for a flow failure (both finite element and centrifuge) and those of a wall collapse, where N_s is a stability ratio defined as

$$N_s = \left(\frac{H\gamma}{s_u} \right) \tag{5.5}$$

Under certain circumstance the traditional collapse assumptions (as detailed in site-assessment guidelines SNAME, 1997) may overestimate the depth of collapse by factors as large as four.

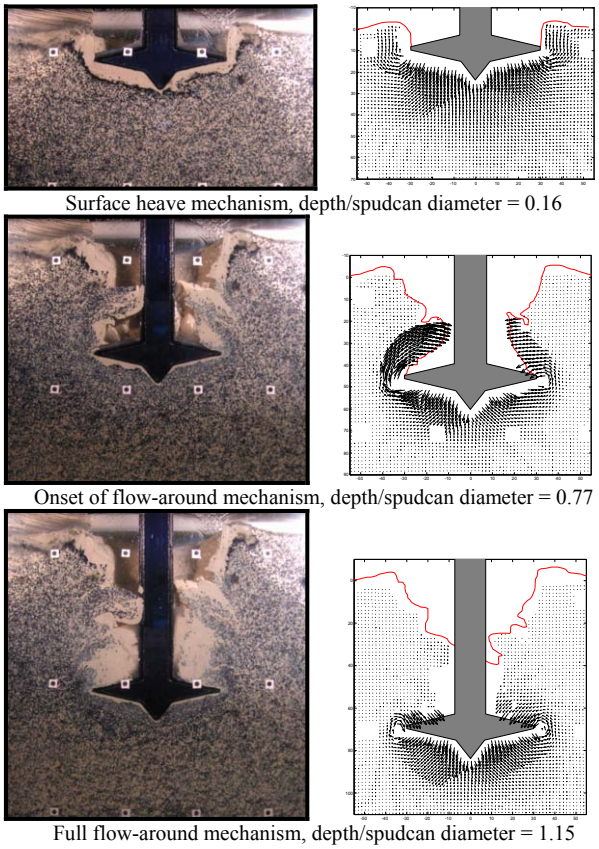

Figure 5.8 Digital images and PIV analysis of flow vectors from centrifuge tests (after Hossain et al., 2004)

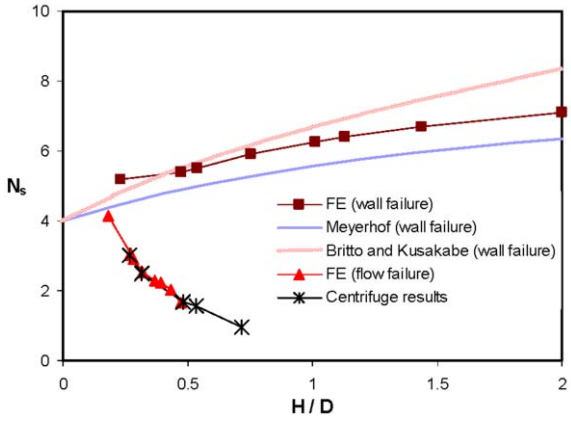

Figure 5.9 Stability ratios for flow and wall failure (Hossain et al., 2004)

The results of Hossain et al. (2004) are highly significant as a more accurate prediction of the onset of backflow should allow for:

- improved evaluations of penetration resistance;
- tensile capacities due to transient suctions, and additional horizontal and moment capacities, to be accounted for in any combined loading analysis.

As shown in Figure 5.10, these additional capacities were observed by Cassidy et al. (2004a) during combined loading tests on spudcan in normally consolidated clay, where backflow was always observed. Due to the backflow, longer drainage paths were thought to guarantee undrained conditions thereby increasing the horizontal capacity at zero vertical loads. Increased horizontal and moment resistance can also occur due to bearing on the sides of the spudcan, shear resistance on the top, and even (Springman & Schofield, 1998) encasing of the lattice legs in very soft clays. It is believed that the additional capacities are invoked after flow around has occurred.

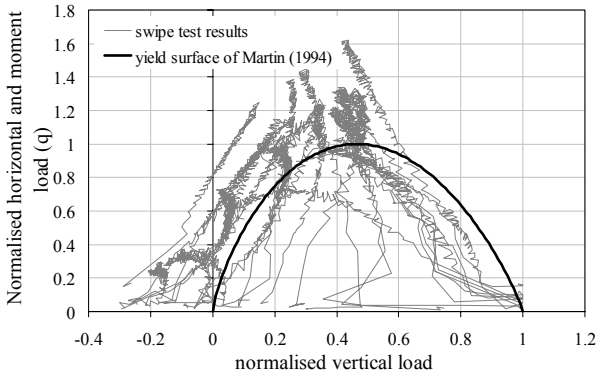

Figure 5.10 Observed tensile capacity observed in drum centrifuge tests of Cassidy et al. (2004a)

Visualisation experiments and PIV analysis is also being applied to the investigation of flow mechanisms of spudcans pushing stiffer clay soil into an underlying softer layer (Hossain, 2004; Hossain et al., 2004).

5.2.4 *Spudcan punch-through*

During installation and pre-loading the potential for unexpected 'punch-through' failure of a jack-up exists. This occurs when the spudcan uncontrollably pushes a locally strong zone of soil into underlying softer material (Fig. 5.11). Such failures can lead to buckling of the leg, effectively temporarily decommissioning the platform, and even toppling of the unit. Soil conditions of a thin layer of sand (or cemented material) overlaying a weaker stratum of clay and stiff-over-soft clay are particularly hazardous.

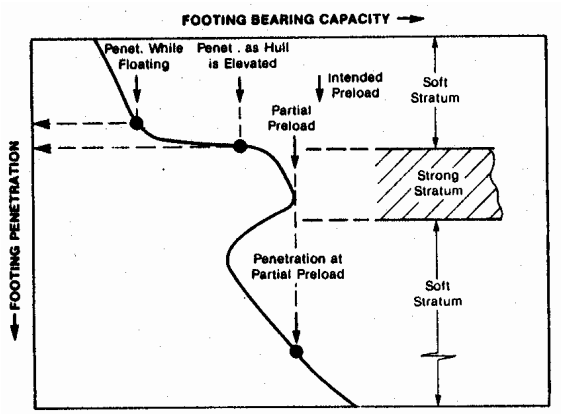

Figure 5.11 - Punch-through failure during pre-load (after Young et al. 1984)

Current industry analysis guidelines (SNAME, 1997) recommend the mechanism developed by Hanna and Meyerhof (1980) for calculating the bearing capacity of the footing for sand-over-clay conditions. For a flat footing at one particular depth (i.e. wished into place), the failure mechanism is assumed to comprise of a truncated cone in the sand layer being depressed into the underlying clay. However for calculation purposes, the simpler vertical shear plane is always used, although it is known to be a deviation from reality (Craig & Chua, 1990). The 'projected area' method is a suggested alternative (SNAME, 1997). Here the load is assumed to spread through the upper sand layer to an imaginary footing of increased size at the sand-clay boundary. However, for this case there still remains debate as to appropriate values of the assumed angle of spread, which is critical to this calculation, with inconsistency between small-scale model test data (Young & Focht, 1981; Higham, 1984) and the lower angles required to fit measured spudcan penetrations offshore (Baglioni et al., 1982). Both recommended mechanisms are significantly different from post-failure observations of four centrifuge tests performed by Craig and Chua (1990).

Jack-up site assessment guidelines (SNAME, 1997) recommend the solutions of Brown and Meyerhof (1969) and Meyerhof and Hanna (1978) for the other potential punch-through condition of a strong clay layer over a soft clay. Unfortunately, the validity of these methods have not been confirmed by either field or laboratory measurements of failure mechanisms (with the majority of laboratory floor model tests not maintaining stress similitude). As an alternative, Wang and Carter (2002) used large deformation finite element analyses to develop bearing capacity factors for circular footings penetrating strong over soft clay. Further, a recent centrifuge study by Hossain et al. (2005) has commenced investigating soil failure mechanism under these conditions, with Figure 5.12 revealing a truncated cone of stronger soil consistently penetrating the underlying layer.

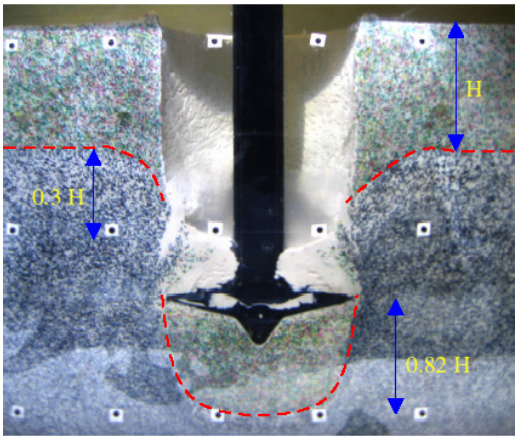

Figure 5.12 Captured image of a penetrating half-spudcan in two-layered clay (after Hossain et al., 2005)

Inadequate site investigation techniques and the lack of accurate information regarding the seabed stratigraphy and strength profile also contribute to the large number of jack-up punch through failures. Information on the seabed conditions is often extrapolated from investigations several kilometres away (Geer et al., 2000). It is also extremely rare for a continuous profile of soil strengths to be determined, even though this information would be the most useful in predicting punch-through events. Improved analysis techniques for predicting punch-through will prove ineffectual if the soil stratigraphy remains ill-defined during site-investigations, and improved techniques and methodologies should be pursued by jack-up owners and operators.

5.2.5 *Existing footprints and eccentric loading*

Locating a jack-up unit at a site where previous jack-up operations have occurred can be hazardous because the new jack-up may need to negotiate the spudcan footprints left on the sea-bed from the previous operations (see Fig. 5.13). In soft clay soils the footprints can be in excess of 10m deep and wide, with varying strengths distributions from the new surface to a depth below which the original spudcan penetrated (Stewart & Finnie, 2001). This scenario is shown diagrammatically in Figure 5.14. Pre-loading close to these footprints can result in uncontrolled penetration (through softer remoulded soils) and slewing of the legs as the spudcan slips into the footprint. Overstressing of the structural legs, collision with adjacent platforms and even injury to personnel may result from such uncontrolled activities (Foo et al., 2003a,b; Hunt & Marsh, 2004). The growing concern of builder, owners and operators of jack-ups to this difficult problem is reflected in a joint industry project established in 2002 to investigate the issue (Sumrow, 2002). Initially, a survey of operator experience on sites where spudcan interaction was considered problematic was conducted. Based on this experience, large strain finite element analysis and scale model testing has been proposed, though no significant results outlining new analysis techniques or guidelines have yet been published.

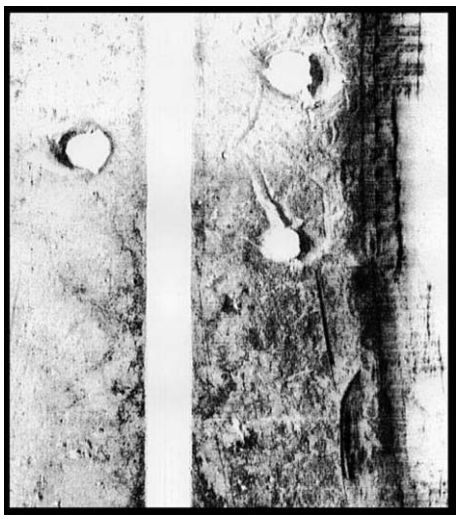

Figure 5.13 Survey of spudcan footprints on sea-bed (after Hefer, 2004)

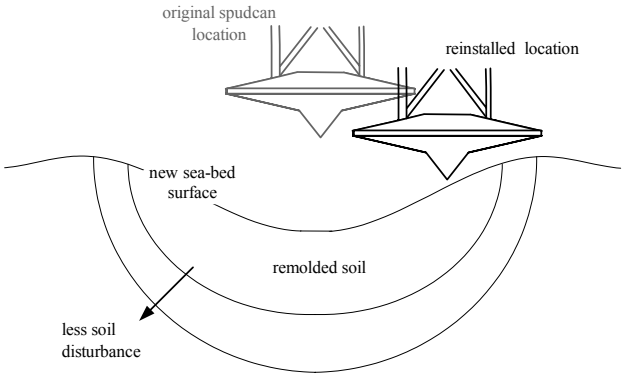

Figure 5.14 Possible footprint reinstallation

Experimental studies have given some insight into the installation of spudcans next to existing footprints in clay soils (Clunie-Ross, 1999; Stewart & Finnie, 2001; Treacy, 2003; Cassidy, 2003; Foo et al., 2003b). The tests performed by Stewart and Finnie (2001) were of an equivalent 12m diameter prototype spudcan attached to a rigid leg. On the other hand, the experiment detailed by Tracey (2003) and Cassidy (2003), and also reported in Foo et al. (2003b) modelled 1:250 scale 116C and ModV spudcans. They also varied the relative leg stiffness in order to investigate its affect (and subsequently also that of water depth) on induced loads and movements. Example combined loads measured during an installation and re-installation at an offset of half a diameter are shown in Figure 5.15.

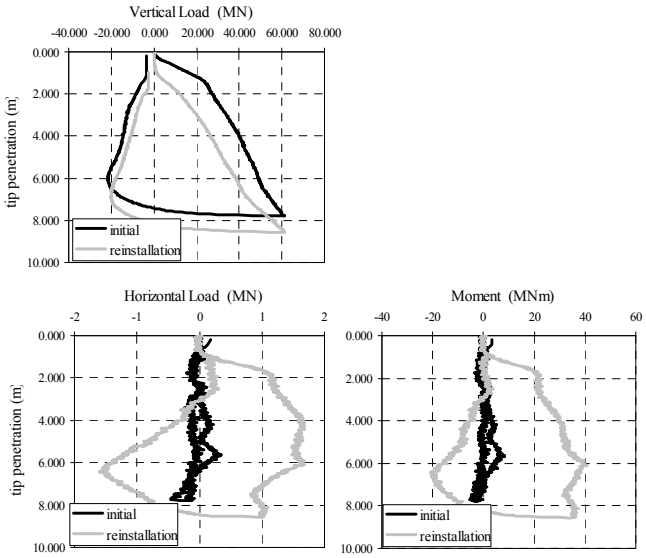

Figure 5.15 Measure combined loads on spudcan during reinstallation experiment (in scaled prototype units)

Using results such as these, a measure of the critical offset distance between installations was the major outcome of both experiments, with Figure 5.16 showing this to be at 0.75 diameters for the Stewart and Finnie (2001) experiments. Interestingly, the tests on the flexible legs did not indicate significantly different results (Tracey, 2003; Foo et al., 2003b). However, as discussed below, the modelling condition of a single footing and fully fixed connection between the leg and actuator is thought to contribute to this slightly surprising result.

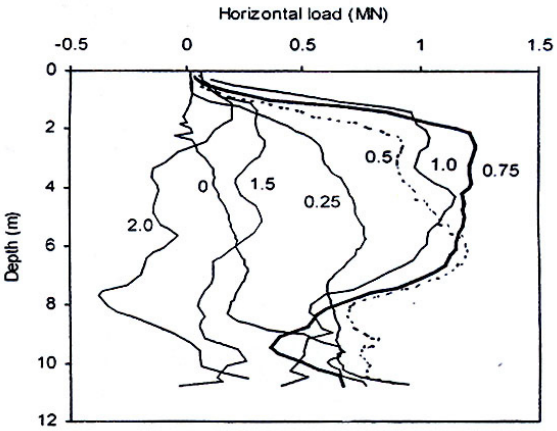

Figure 5.16 Measured horizontal loads at offset distances (expressed as a multiple of spudcan diameter) (after Stewart & Finnie, 2001)

Unfortunately, all of these experimental studies utilised a similar highly idealised modelling technique − a single spudcan and loading leg re-installed at a fixed distance from a prior penetration. With a fixed connection between the top of the loading leg and the centrifuge actuator lateral and rotational movement at this connection were restricted. The movement of the jack-up structure as a system is discounted and it is believed that the spudcan loads and displacement measured are potentially significantly lower than if the system behaviour was accounted for. Experimental studies of a full three-legged jack-up are recommended.

With further understanding of the problem preventative measures are now being taken offshore. It is hoped that installations of systems measuring Rack Phase Difference (RPD) will alert operators to eccentric loading conditions and translation of the spudcan (Foo et al., 2003a). RPD is simply the difference in elevation between the chords of any one leg and is a direct measure of the inclination of the leg with respect to the hull. Though an early alert to an inclined leg and spudcan may mitigate buckling of the leg braces and stability problems, there are still no guidelines available to operators to help in a safe reinstallation (Dean & Serra, 2004). Further studies of spudcan stomping, use of sand or gravel infilling (Jardine, et al., 2001), spudcan configuration (Dean & Serra, 2004) or simply improved analysis models and installation procedures are urgently required.

Eccentric loading of spudcans can also arise due to slopes on hard sandy sea-beds, partial scour around a spudcan, or the spudcan hitting rock or boulder formations. An interesting case study of jack-up damage due to these types of loading conditions is described by Stoner et al. (2004).

5.3 *General multi-footing structures*

5.3.1 *Wave-structure-soil interaction*

During a storm environmental wind, wave and current forces impose horizontal, sometimes moments and even torsion loads on the spudcans, as well as altering the vertical load between them (Fig. 5.4). Traditional methods of separating the environmental loading, structural, and geotechnical modelling components into individual analyses has proved inadequate in analysing the overall system response, with highly non-linear stiffnesses and a dynamically responsive system simultaneously affecting all analysis components. More recently, methods for combining models for geotechnical, structural and environmental load in a consistent manner have been receiving attentions. These have concentrated on describing the shallow foundation behaviour of spudcans in a plasticity framework and in terms of the forces and displacement on the spudcan footing. This allows direct integration within conventional structural analysis programs, as will be shown herein.

5.3.2 *Force-resultant modelling*

During storm loading, an understanding of the complex state of stress and strain under a spudcan is essential to any integrated structural analysis. However, it is rarely possible to conduct a combined finite element analysis in which the sea-bed is modelled in detail using continuum elements and the full jack-up structure is accounted for (depicted in Fig. 5.17a). This is especially infeasible when, as is the case in many jack-up site-specific assessments, little or no site-investigation has been performed.

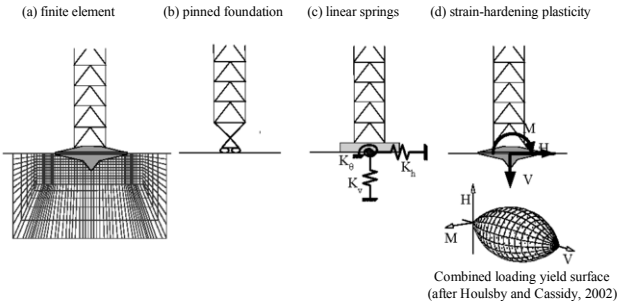

Figure 5.17 Spudcan – soil interaction analysis methods

The simplest alternative approach is to model the spudcan-soil interaction as either a pinned joint (infinite translational stiffness but no rotational stiffness as depicted in Fig. 5.17b) (Reardon, 1986; Frieze et al., 1995) or a set of uncoupled springs (Fig. 5.17c). The former is generally thought to be conservative (Chiba et al., 1986; Norris & Aldridge, 1992). However, this is not always the case, particularly during dynamic loading (Williams et al., 1998; Cassidy et al., 2001, 2002c). Further, the assumption of infinite translational stiffness enforces no differential movement of the footings, and in the analysis of three legged jack-up systems this can rapidly cause unconservative results (Martin & Houlsby, 1999; Cassidy, 1999; Vlahos, 2004). The use of linear springs is often favoured because the inclusion of any rotational spudcan fixity reduces the critical member stresses at the leg/hull connection (shown in Fig. 5.18), and other responses such as the lateral hull deflection. Unfortunately, while springs are easy to implement into structural analysis programs, this simplistic approach cannot capture many important features. For instance, capturing of shallow sliding of a windward spudcan and/or 'plunging' of a leeward spudcan is not possible with simple springs (Cassidy et al., 2004b).

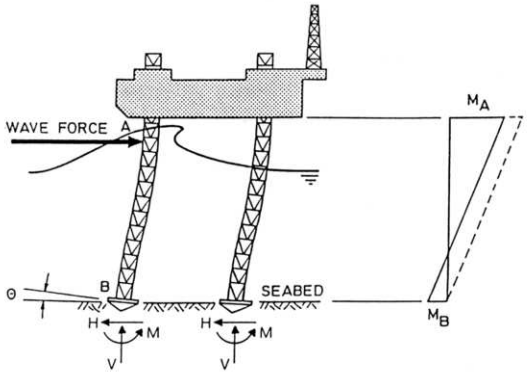

Figure 5.18 The effect of rotational fixity (after Santa Maria, 1998)

Recent developments in modelling soil-foundation behaviour (known as 'force-resultant' modelling) offers a practical alternative. 'Force-resultant' models attempt to capture the entire behaviour of a foundation in terms of the combined forces on it, and their resultant displacements. As the response of the foundation is expressed in terminology consistent with structural mechanics, the significant non-linear behaviour of soils can be coupled directly to the numerical analysis of a structure.

5.3.3 *Strain-hardening plasticity models*

The framework of single-surface strain-hardening plasticity has allowed the behaviour of the spudcan to be described in an elegant and comprehensive manner (Fig. 5.17d). The load-displacement behaviour is determined in essentially the same way that a constitutive law of a metal or soil relates stresses and strains. Loading is applied incrementally, and the numerical plasticity model computes updated tangent stiffnesses for each step. The hardening concept adopted is that at any given plastic penetration of the foundation into the soil, a yield surface of a certain size is established in combined loading space. Any changes of load within this surface will result only in reversible elastic deformation. However, plastic deformation can result when the load state touches the surface, with the irreversible footing displacements calculated from a flow rule. During this event the size of the yield surface is directly related to the 'backbone' curve of vertical bearing capacity against plastic vertical penetration (which is determined either theoretically or empirically). The expansion of a VHM yield surface during an elasto-plastic step is diagrammatically illustrated in Figure 5.19.

Schotman (1989) first described a complete incremental plasticity model for a spudcan foundation in terms of force resultants. The model was framed in planar (VHM) load space, though it still relied heavily on numerous assumptions. For instance, the yield surface and hardening law were derived from Brinch Hansen's semi-empirical bearing capacity formula, and the elasticity constants and plastic potential were calibrated using finite element analyses of a plane strain 'spudcan'. How-

ever, Schotman did succeed in incorporating his spudcan model into a (linear elastic) jack-up structural analysis, and some useful insights into the behaviour of the overall soil-structure system were obtained.

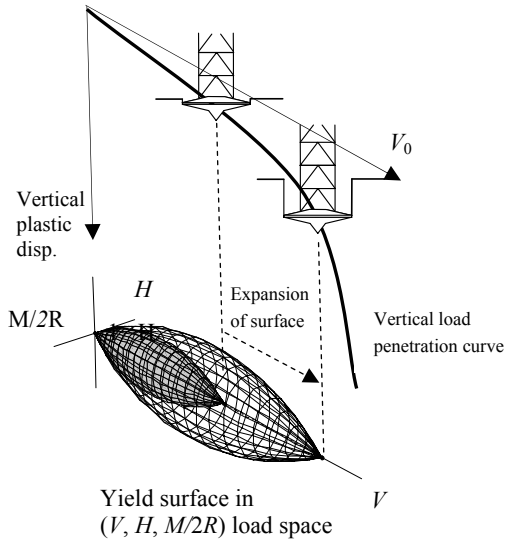

Figure 5.19 Expansion of the combined loading yield surface with spudcan penetration

5.3.4 *Experimental procedures to develop plasticity models*

Since Schotman's original development there have been a number of experimental investigations designed to provide the data necessary to support a fully strain-hardening plasticity model. Most of this research has concentrated on dense silica sands (Tan, 1990; Nova & Montrasio, 1991; Gottardi & Butterfield, 1993, 1995; Gottardi et al., 1999; Byrne, 2000), uncemented loose carbonate sands (Byrne & Houlsby, 2001) and clays with increasing strength with depth (Martin, 1994, Martin & Houlsby, 2000; Byrne & Cassidy, 2002; Cassidy et al., 2004b).

Central to the experiment programs were swipe tests (Tan, 1990), where the footing is penetrated vertically to a prescribed level, then subjected to a radial displacement excursion (horizontal, rotational or torsional displacement, or a combination thereof). For a spudcan footing this excursion results in the accumulation of horizontal (and/or moment/torsion) loads combined with a reduction of vertical load. Tan (1990) argued that the load path followed (with some minor adjustments for soil elasticity and experimental rig stiffness) can be assumed to be a track across the yield surface appropriate to that penetration (shown in Fig. 5.20).

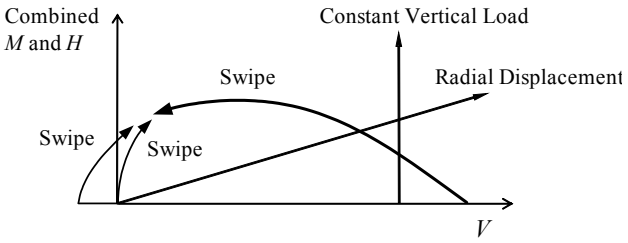

Figure 5.20 Experimental load paths followed to develop strain-hardening plasticity models

Swipe tests were used to detail the combined vertical-horizontal load (VH) yield loci for various conical and spudcan footings by Tan (1990) and then, using an improved loading system, for combined vertical-horizontal and moment (VHM) loads by Martin (1994). Example swipe test results on sand are shown in Figure 5.21. Also shown is an investigation of the yield surface at low stress, achieved by loading vertically to the same penetration then unloading to a low vertical force and displacing radially in the same manner (see also Fig. 5.20).

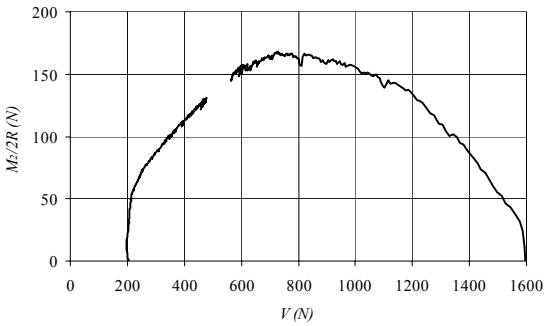

Figure 5.21 Load paths followed during rotation swipe test of a flat 100mm circular footing on sand (after Gottardi et al., 1999)

With the yield surface established, the behaviour during an elasto-plastic step may be explored through a combination of constant vertical load (also referred to as probe tests) and radial displacement tests. Incremental plastic displacements are measured and the results related to a suitable flow rule. Constant vertical load tests are similar to a swipe test except rather than holding the vertical penetration constant, the vertical load is fixed while the footing is driven horizontally or rotated (Fig. 5.20). According to plasticity theory, the yield surface should expand or contract according to the strain hardening relationship. Similar results (though for a different load path) can be achieved when straight (radial) displacement paths of different combinations of vertical, horizontal and rotational displacements are applied to the footing.

Similar testing programs have been successfully used in other offshore foundation applications including caissons (Watson, 1999; Byrne, 2000; Cassidy et al., 2004a), and for partially embedded pipelines (Zhang, 2001).

5.3.5 *Numerical formulation of spudcan strain-hardening plasticity models*

A series of force-resultant models describing spudcan behaviour on clay (Martin, 1994; Martin & Houlsby, 2001), dense silica sand (Cassidy, 1999; Houlsby & Cassidy, 2002) and loose carbonate sand (Cassidy et al., 2002a) have been described. The models are similarly structured within strain-hardening plasticity theory, but in order to simulate experimental observations, they maintain subtle differences in their hardening law, yield surface shape, elasticity relationship and flow rule. These details and typical parameter values are given in Table 5.3.

The yield surface of the plasticity models is defined in three-dimensional (*VHM*) loading space by the best fit of experimental swipe test data obtained for overconsolidated clay and sand (Gottardi et al., 1999, Martin & Houlsby, 2000, Byrne and Houlsby, 2001). The shape of the surface is shown in Figure 5.22 and can be described as an eccentric ellipse in section on the planes of constant V, and approximately parabolic on any section including the V-axis.

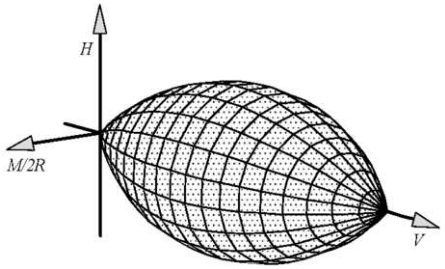

Figure 5.22 Yield surface shape (after Houlsby & Cassidy, 2002)

Table 5.3 Strain-hardening plasticity models developed for inclusion in jack-up analysis (typical values after Martin & Houlsby, 2001; Houlsby & Cassidy, 2002; Cassidy et al., 2002a)

Model Comp.	Constant (dimension)	Explanation	Main Equations	Typical values			Notes
				Clay	Dense sand	Loose carbonate sands	
Geometry	R (L)	Footing radius					For partially embedded spudcans defined as the embedded radius (see Fig. 5.7).
Elasticity	G (F/L^2)	Representative shear modulus	$\begin{pmatrix}\delta V\\ \delta M/2R\\ \delta H\end{pmatrix}=2GR\begin{bmatrix}k_v & 0 & 0\\ 0 & k_m & k_c\\ 0 & k_c & k_h\end{bmatrix}\begin{pmatrix}\delta w^e\\ 2R\delta\theta^e\\ \delta u^e\end{pmatrix}$ where δw^e, $\delta\theta^e$ and δu^e represent the conjugate pairs of the footing incremental elastic displacements.	Eqns 5.5 & 5.6	Eqns 5.7 & 5.8		Suggestions for calculating a representative shear modulus are based on calibration with monitored offshore jack-ups, as outlined in Cassidy et al. (2002[b]).
	k_v (-)	Elastic stiffness factor (vertical)		see Bell (1991), Ngo-Tran (1996) and Doherty & Deeks (2003)	2.65	2.65	These dimensionless elasticity coefficients may-be derived using finite element analysis of a footing. They depend on the geometry of the footing (e.g. depth of embedment and shape) as well as the Poisson's ratio of the soil. The values given here for the sand cases were derived by Bell (1991) for a flat surface footing and a Poisson's ratio of 0.2. Other factors for rigid conical footings have been published by Ngo-Tran (1996) and more recently Doherty & Deeks (2003) extended the range of geometries and conditions by using the scaled boundary finite element method.
	k_h (-)	Elastic stiffness factor (horizontal)			2.3	2.3	
	k_m (-)	Elastic stiffness factor (moment)			0.46	0.46	
	k_c (-)	Elastic stiffness factor (horizontal/moment coupling)			-0.14	-0.14	
Yield Surface	h_0 (-)	Dimension of yield surface	$f=0=\left(\frac{H}{h_0V_0}\right)^2+\left(\frac{M/2R}{m_0V_0}\right)^2-\frac{2aH\,M/2R}{h_0m_0{V_0}^2}-\left[\frac{(\beta_1+\beta_2)^{(\beta_1+\beta_2)}}{\beta_1^{\beta_1}\beta_2^{\beta_2}}\right]^2\left(\frac{V}{V_0}\right)^{2\beta_1}\left(1-\frac{V}{V_0}\right)^{2\beta_2}$	0.127	0.116	0.154	In the yield surface equation V_0 determines the size of the yield surface and indicates the bearing capacity of the foundation under purely vertical loading (H = 0 and $M/2R$ = 0). Furthermore, V_0 is governed by the vertical plastic penetration and is determined from the strain-hardening law (Fig. 5.18). h_0 and m_0 represent the dimensions of the surface in the horizontal and moment directions and a accounts for eccentricity (rotation of the elliptical cross-section) in the $M/2R$:H plane. In clay the eccentricity varies slightly with V/V_0 and takes the form $a=e_1+e_2\left(\frac{V}{V_0}\right)\left(\frac{V}{V_0}-1\right)$ with $e_1=0.518$ and $e_2=1.180$ recommended by Martin & Houlsby (2001). For flat footings on sand the ellipse is rotated in the other direction in $M/2R$:H space. The parameters β_1 and β_2 round off the points of surface near V/V_0 = 0 and V/V_0 = 1. It is interesting to note that the yield surface shape does not vary greatly for the different soil types.
	m_0 (-)	Dimension of yield surface		0.083	0.086	0.094	
	a (-)	Eccentricity of yield surface		See notes	-0.2	-0.25	
	β_1 (-)	Curvature factor for yield surface (low stress)		0.764	0.9	0.82	
	β_2 (-)	Curvature factor for yield surface (high stress)		0.882	0.99	0.82	
Flow Rule	ζ	Non-association parameter	$\partial w_p=\zeta\partial w_{p\,associated}$	0.6	-	-	Both the clay and sand experiments showed associated flow only in the MH plane. With differences in the non-association shown in the deviatoric planes, different flow rules have been suggested. For the clay case, Martin (1994) used an "association parameter" ζ to adjust vertical displacements to match those observed experimentally. The horizontal and rotational displacements were assumed associated. For the sand case, a plastic potential (g) different to the yield surface was required. A similar expression to that of the yield surface is applied, but scaled in shape and size by two association factors (α_h and α_m). The "best-fit" values of α_h and α_m have shown variability to displacement path by Cassidy (1999) and Cassidy et al. (2002a), with the values here representing a compromise solution.
	β_3 (-)	Curvature factor for plastic potential (low stress)	$g=0=\left(\frac{H}{\alpha_h h_0 V_0'}\right)^2+\left(\frac{M/2R}{\alpha_m m_0 V_0'}\right)^2-\frac{2aH\,M/2R}{\alpha_h\alpha_m h_0 m_0 {V_0'}^2}-\left(\frac{(\beta_3+\beta_4)^{(\beta_3+\beta_4)}}{(\beta_3)^{\beta_3}(\beta_4)^{\beta_4}}\right)^2\left(\frac{V}{V_0'}\right)^{2\beta_3}\left(1-\frac{V}{V_0'}\right)^{2\beta_4}$	-	0.55	0.82	
	β_4 (-)	Curvature factor for plastic potential (high stress)		-	0.65	0.82	
	α_h (-)	Association factor (horizontal)		-	2.5	3.25	
	α_m (-)	Association factor (moment)		-	2.15	2.6	
Hardening law	Discussion of appropriate hardening laws are given in section 5.2.3. More details can be found for the sand cases in Cassidy and Houlsby (1999, 2002) and Cassidy et al. (2002a).						

The elastic response of the soil needs to be defined for any load increments within the yield surface. With small elastic displacements extremely difficult to measure within a laboratory experiment, generic non-dimensional stiffness factors derived from finite element analysis combined with an appropriate choice of shear modulus is recommend. An appropriate expression for the three-degrees of freedom case is given in Table 5.3. An appropriate shear modulus is still one of the most difficult parameters to establish. As the mobilized shear stiffness is strongly dependent on the shear strain, it should represent typical shear strains under the footing. Current recommendations are based on findings of the back-analysis of case records of jack-up platforms in the North Sea. The records relate to three jack-ups, Santa Fe's Magellan, Monitor and Galaxy-1, which have since 1992 had their dynamic behaviour and environmental loading conditions monitored (reported in Temperton et al., 1997; Nelson et al., 2000). At the time of the back analysis eight sites of varying soil conditions (3 clay sites of OCR 5-60 and 5 sands of friction angles 27-31 º) and water depth (28.3-98.1 m) had been subjected to substantial storm conditions (H_s of 4.1-9.85 m) (Nelson et al., 2000; Cassidy et al., 2002b).

For each storm, horizontal deck movements of the jack-up and recorded sea-state and wind speed and direction were available (Nelson et al., 2000). In order to compare the monitored jack-up units with numerical simulations of the most severe storm events, a suite of random time domain analyses were performed for each site with adjustments in soil stiffness made. A best-fit of one monitored and simulated response is shown in Figure 5.23.

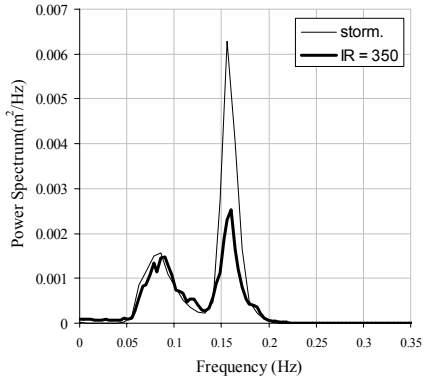

Figure 5.23 Comparison of storm and simulated response in frequency domain (after, Cassidy et al., 2002b)

Resulting from these analyses were the following formulations for the shear modulus for the clay and sand cases. The shear modulus (G) linearly scales all of the stiffness coefficients according to the elastic stiffness matrix in Table 5.3, and for clay can be determined by

$$G = I_r s_u \tag{5.5}$$

where s_u is the undrained shear strength measured at 0.15 diameters below the reference point of the spudcan (taken at the level at which the maximum diameter is reached). I_r is the rigidity index and can be calculated from:

$$I_r = \frac{G}{s_u} = \frac{600}{OCR^{0.25}} \tag{5.6}$$

In sands the shear modulus can be estimated by

$$\frac{G}{p_a} = g\left(\frac{V}{Ap_a}\right)^{0.5} \tag{5.7}$$

where V is the spudcan vertical load, A the spudcan contact area and p_a atmospheric pressure. The recommended value for the dimensionless constant g for a relative density D_R is

$$g = 230\left(0.9 + \frac{D_R}{500}\right) \tag{5.8}$$

Although the shape of the yield surface is assumed constant, the size may vary, with it expanding as the footing is pushed further into the soil and contracting with footing heave. This expansion (or contraction) is defined by an empirical strain-hardening expression and this process is depicted diagrammatically in Figure 5.19. Discussion of an appropriate hardening law was discussed for clays and sands in Section 5.2.3.

All of the experiments used to derive the flow rule of the plasticity models indicate associated flow in the moment-horizontal load plane, but non-association in the horizontal-vertical and moment-vertical planes (Martin & Houlsby, 2000; Gottardi et al., 1999; Cassidy et al., 2002a). However, differences between the clay and sand cases were observed, necessitating a slightly different approach. In the clay case, for high vertical load ratios (post yield surface peak) lower ratios of vertical plastic displacements than associated flow would predict were observed. However, the opposite was found for lower vertical load ratios (pre-peak). This allowed a relatively simple adjustment to the associated flow predictions using a single "non-association" factor, as detailed in Table 5.3. The experimental results on sand exhibited more complex behaviour. Larger ratios of vertical plastic displacements than associated flow would predict were observed for nearly the entire range of vertical loads. To account for this, a plastic potential surface (on which a normal vector defines the plastic displacement ratio) of a similar expression to that of the yield surface, but scaled in shape and size by two association factors, was defined. The expressions for the flow rule and association factors are detailed in Table 5.3 and the expanded surface shape shown in Figure 5.24.

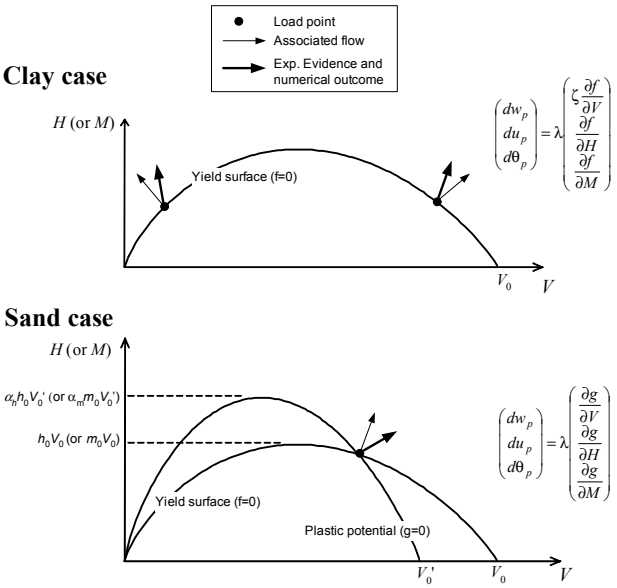

Figure 5.24 Non-associated flow rules for both the clay and sand case

Though only discussed here for spudcans loaded in planar three-degrees of freedom, the models have recently seen extension to the full six-degrees of freedom case (Cassidy & Bienen, 2002; Bienen & Cassidy, 2004). This latter extension is an obvious requirement before three-dimensional jack-up structural analyses can be conducted.

5.3.6 *Example analysis*

The advantage of the plasticity models described is that by formulating them in combined VHM load and wuθ displacement space they can be easily implemented within a conventional structural analysis program. To show this, two example analyses of a jack-up unit will be outlined. The first is a quasi-static

pushover, and this is followed in section 5.3.8 with a dynamic wave loading example. The sign convention adopted is shown in Figure 5.25.

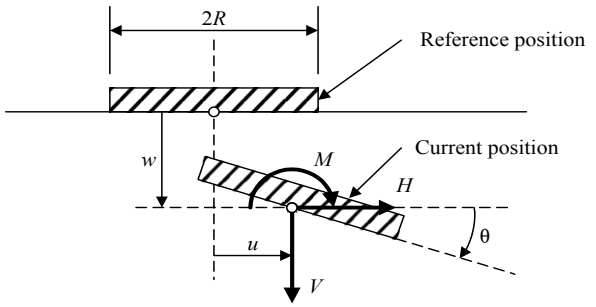

Figure 5.25 - Sign convention adopted for loads and displacements (after Butterfield et al., 1997)

To ensure non-conservative modelling of jack-up response, it is widely acknowledged that structural non-linearities must be taken into account. Non-linear frame analysis based on the Eulerian formulation of Kassimali (1983) has been used for the structural modelling here. P-Δ, Euler and shear effects (using the extension of Martin, 1994) are also accounted for. For the dynamic analysis in section 5.3.8 the Newmark ($\beta = 0.25$, $\delta = 0.5$) solution method is used to solve the dynamic equations (Bienen & Cassidy, 2004).

Figure 5.26 shows the idealised plane frame model of the jack-up analysed, which represents a size typical of a large modern jack-up rig. Structural node locations and member stiffnesses are also detailed in the figure. Both the legs and hull are represented using equivalent beam elements and a rigid leg/hull connection is assumed. Although non-linearities in the leg/hull jack houses are sometimes significant, no attempt was made to include such effects in this study.

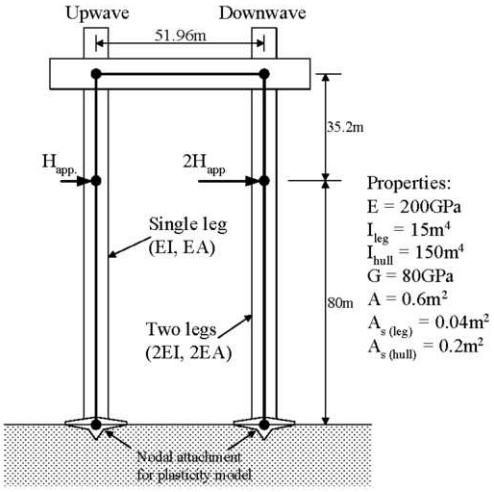

Figure 5.26 Jack-up model and loading for pushover analysis

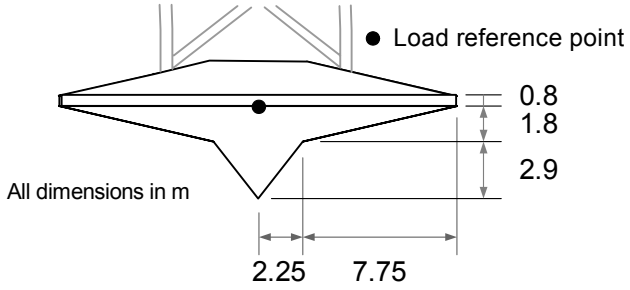

Figure 5.27 Assumed spudcan shape in numerical examples

The plasticity models are 'attached' as point elements on the bottom node of each leg and the spudcans assumed to be resting on dense silica sand (see Table 5.3 for model parameters). Their shape is depicted in Figure 5.27, with the load reference point also shown. A preload of 143 MN per spudcan was applied representing a multiple of two on the jack-up's self-weight. Assuming sand with a friction angle of $\phi = 40^\circ$ a vertical plastic penetration of 3.34 m was evaluated according to the bearing capacity formulation outlined in Cassidy and Houlsby (1999, 2002).

5.3.7 *Quasi-static analysis*

The pushover analysis consisted of the jack-up loaded vertically to the preload level, unloaded to its self-weight and then the simplified environmental loads applied. These applied loads ($H_{app.}$) were increased linearly until failure in the system occurred. Since the structural elements were elastic this constrained the failure to occur in the foundation. This pushover analysis follows a similar simulation for jack-ups on clay in Martin and Houlsby (1999). Figure 5.28 shows the simulated spudcan loads and displacements during the pushover event. The initial load steps are elastic.

The downwave spudcans yielded first at an applied horizontal load of H_{app} = 2.78 MN (indicated on Fig. 5.28 as Y_d and noting the total applied load is always $3H_{app}$). The subsequent change in load paths is also easily observed. Yielding of the upwave spudcan follows at H_{app} = 2.95 MN (Y_u) and in both cases the reduction in moment resistance at the spudcan can be immediately observed. The moment that is shed is redistributed into increased incremental vertical loads (the change of slope can be observed in Fig. 5.28). The spudcan reaches its ultimate load at H_{app} = 8.33 MN. Allowing for strain-hardening within the model has significantly increased the capacity of the system from the point of first yield. Failure occurs due to sliding of the upwave spudcan. Larger vertical displacements and rotations of all footings are observed during the elasto-plastic steps due to the reduction in the spudcan tangential stiffness that occurs.

The horizontal hull displacements during this event are shown in Figure 5.29. Again the reduction of stiffness due to yielding of the footings is evident in the increased magnitude of hull displacement after yielding. Comparisons to the assumption of pinned and encastré footings are also shown in Figure 5.29. Pinned and encastré footings represent infinite horizontal and vertical stiffness, but with no or with infinite rotational stiffness respectively. An expected factor of four difference in displacement magnitude is observed between these two cases. Initially the plasticity model response lies between these (so called) extremes. However, after H_{app} = 7.55 MN the sand case exhibits a larger hull sway than the pinned case, which highlights the importance of modelling all of the degrees of freedom.

5.3.8 *Dynamic analysis*

Conventionally, jack-up assessments have used the same quasi-static analysis methods employed for fixed structures (and shown in the previous example). However, due to their relative flexibility the need to consider dynamic effects has long been recognized (e.g. Hattori et al., 1982; Grenda, 1986; Bradshaw, 1987). With use in deeper water, the contribution of dynamic effects to the total response has become more important as the natural period of the jack-up approaches the peak wave periods in the sea-state. Time domain techniques provide the most complete analysis option with the ability to reflect the actual physical processes and non-linearities within the system.

The same jack-up and spudcan conditions have been used for the dynamic analysis example as used in the previous quasi static analysis. The additional structural masses and hydrodynamic criteria required for a dynamic analysis are shown in Figure 5.30. A mean water level of 90m was assumed and wave loading was applied using a NewWave model (Tromans et al.,

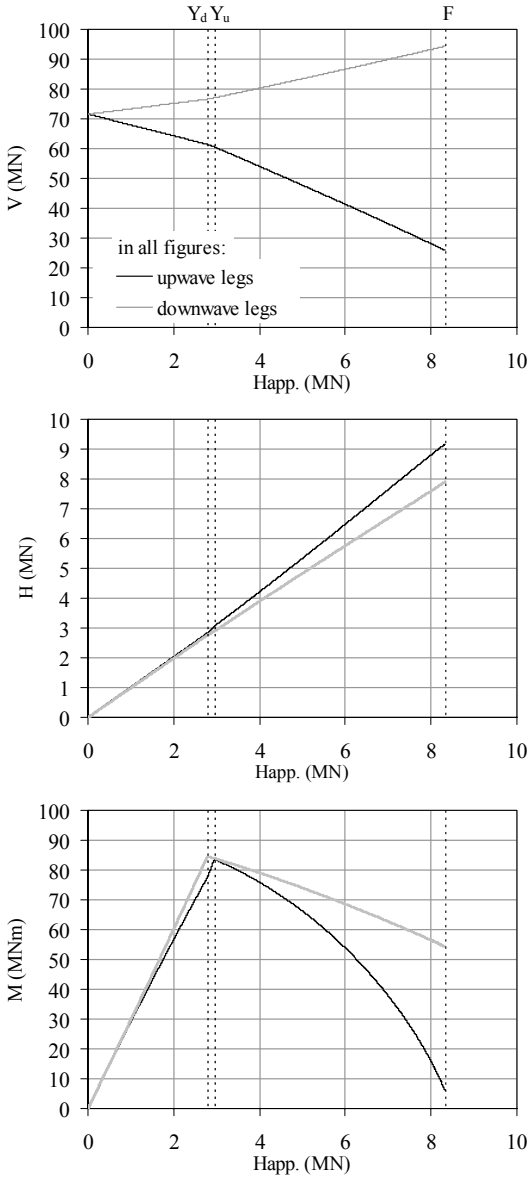

Figure 5.28 Load and displacement paths followed by spudcans during quasi-static pushover.

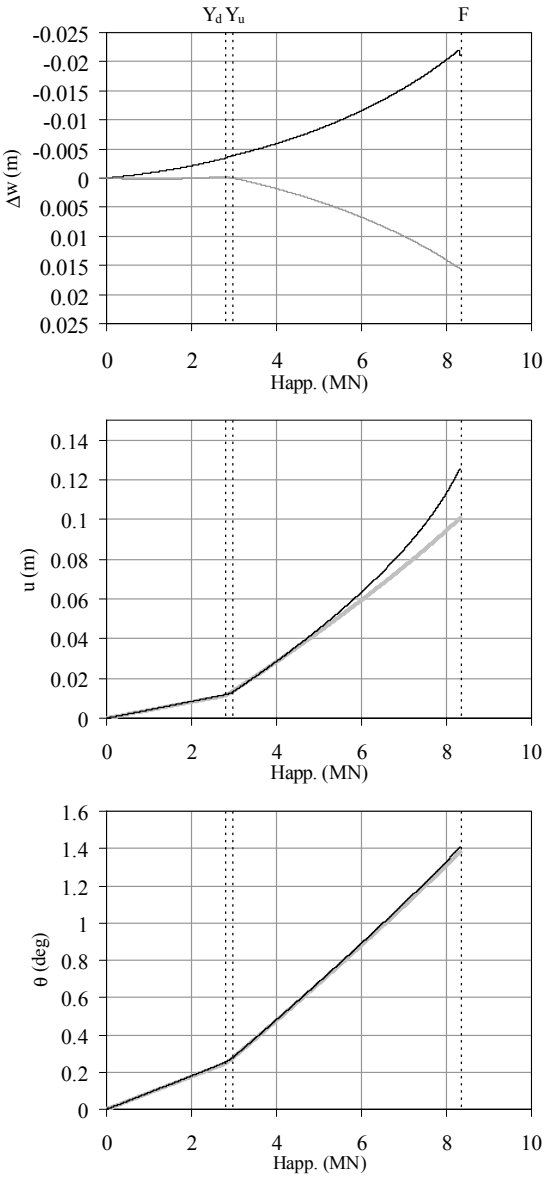

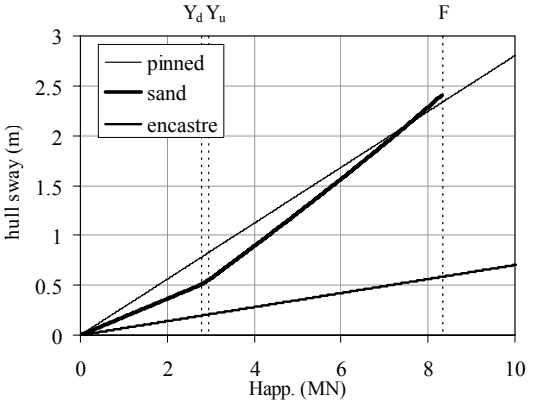

Figure 5.29 Horizontal hull displacement predicted in quasi-static pushover analysis

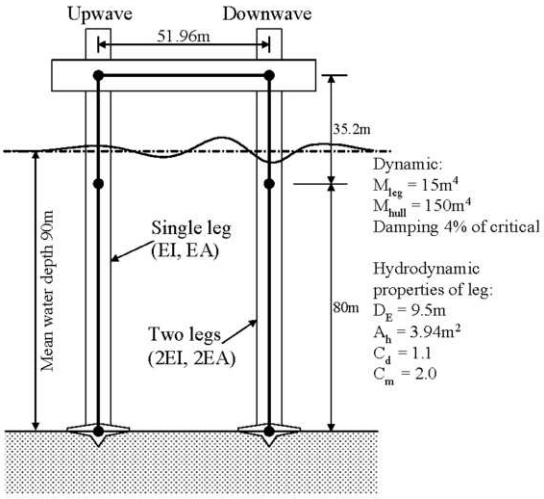

Figure 5.30 Properties used in dynamic environmental loading example

1991). The elevation of the wave relative to the mean-water level is shown in Figure 5.31 for both upstream and downstream legs. Hydrodynamic loading was evaluated using the extended Morrison's equation, including relative motion effects.

The corresponding horizontal deck displacements due to this wave loading are also shown in Figure 5.30 for the same three foundation cases considered previously: pinned, sand plasticity model and encastré. After the wave passes, the structure can be seen to be vibrating at its natural period. With increased rotational fixity the natural periods decrease, with approximate values of 9, 7.5, and 4 seconds for the pinned, sand and encastré footings respectively. During an elasto-plastic step the natural period of the jack-up increases. This and the finite stiffness imposed for the other degrees of freedom (particularly vertically) can result in longer natural periods than for the pinned case. As expected the pinned footings give the largest horizontal deck displacement and the encastré case the lowest. Further, the pinned case can be seen, for this example, to be rather conservative compared to the predictions for spudcans on sand. However, in the sand model, plastic yielding of the foundation occurs leading to a permanent offset in the displacement of the deck. This yielding of the sand footings occurred during the peak of the wave.

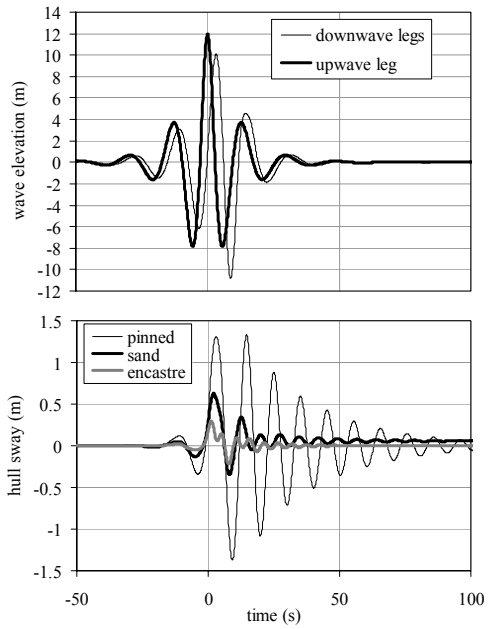

Figure 5.31 Horizontal hull movement during wave loading event

5.3.9 *Summary of benefits of plasticity approach*

The major advantages of using a strain-hardening plasticity approach for the analysis of jack-up response are:

- it is formulated in a form amenable to numerical analysis, allowing it to be implemented into structural analysis programs. This was shown by two examples in this paper;
- it accounts for the non-linearities of combined loading of a spudcan on soils in a consistent manner (though some loss of detail is possible);
- a direct indication of yielding is given. Furthermore, movement of the spudcan footings can be evaluated, with differentiation between upwave and downwave leg behaviour possible. Failures due to sliding or plunging of spudcan footings can be evaluated directly;
- a realistic interpretation of spudcan fixity allows for more accurate dynamic analysis. It was shown that this can give significantly different dynamic response to that obtained using pinned and encastré footing assumptions;
- only a limited number of soil conditions require definition before modelling (hardening law parameters, shear modulus), with the majority of the model parameters predetermined (yield surface size, flow rule, elasticity matrix).

5.3.10 *Development of cyclic loading models*

Although a major improvement on pinned, encastré or sets of springs for simulating jack-up response under monotonic loading conditions, the framework of strain hardening plasticity is still inadequate as far as the modelling of cyclic behaviour is concerned. One reason for this is that the models incorporate only a single discrete yield surface, whereas it is now increasingly recognised that yielding of a foundation is more gradual, and can be represented by an infinite number of yield surfaces. When used for numerical prediction of jack-up behaviour the models described in section 5.3.3 to 5.3.9 have a number of shortcomings:

- they predict a sudden reduction in stiffness where as in reality the process of spudcan yielding entails a gradual reduction of stiffness;
- experimental load displacement response upon unloading and reloading is hysteretic and not linear elastic as predicted by these models.

The development of models that provide realistic modelling of behaviour during cycling, including a gradual degradation of stiffness with strain amplitude, is a priority and is currently seeing attention by researchers (e.g. Cremer et al., 2001; Houlsby, 2003; Cassidy et al., 2004b; Nguyen-Sy & Houlsby, 2005).

Significant developments still need to occur before such models could be made applicable to soil types where pore pressure accumulation during design storms is significant. For example the Trefoil case history reported by Erbrich (2005) (and discussed in section 5.2.3) is an extreme example of the potential effect of cyclic loading on spudcan foundations. Similar behaviour was observed by Finnie (1993) in centrifuge model tests.

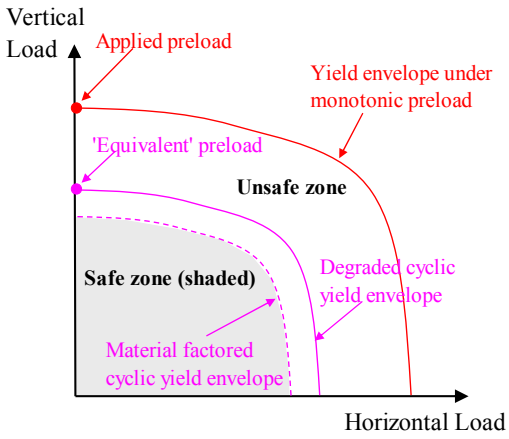

Figure 5.32 Modified yield envelope approach for jack-ups in cyclically degradable soils

In susceptible soils, a different approach to ensuring adequate jack-up stability is suggested (and further detailed in Erbrich, 2005). It is essential to ensure that a 'cyclic failure' is not triggered, since this can lead to catastrophic failure of the jack-up foundations (i.e. uncontrollable and ongoing large progressive settlement). A key feature of such cases is that the static pre-load cannot be relied on to define the 'vertical bearing capacity' of the foundation (and to define a combined loading surface inside which design loads are considered 'safe'). It is possible that under undrained cyclic loading a lower vertical load will trigger a cyclic failure. For these cases, Erbrich (2005) has recommended the yield envelope be maintained but anchored by a calculated 'cyclic vertical bearing capacity' rather than the applied static preload (Fig. 5.32). This is termed the 'equivalent

preload' and is calculated using approaches such as those discussed in Section 4.4.4. The factored design storm loads should not exceed the yield envelope defined using the 'equivalent preload' after accounting for an appropriate material factor. It is recommended that conventional material factors (1.25 to 1.3) should be applied to such cases rather than the reduced values permitted in the SNAME guidelines, since there is effectively no load-testing of the foundations under these conditions.

6 ANCHORING SYSTEMS

6.1 *Types of offshore anchors*

Anchoring systems are used to moor buoyant facilities such as tension leg platforms (TLPs) like Snorre A discussed in section 4.3.2, semi-submersible production systems (FPSs), floating production storage and offloading vessels (FPSOs) and Spar platforms. A selection of buoyant facilities is shown in Figure 6.1. Anchors may also be employed to provide extra stability to fixed or flexible structures, such as a jacket or compliant tower platform.

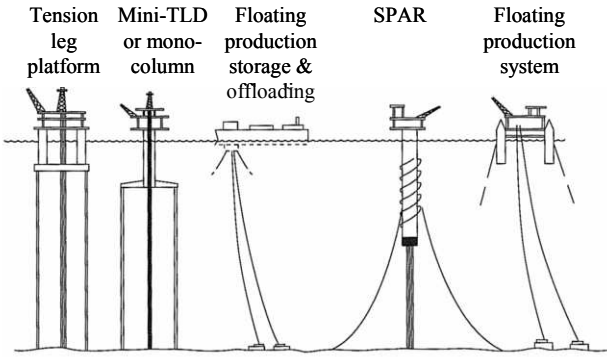

Figure 6.1 Floating system options (Leffler et al., 2003)

The floating facility is connected to the seabed via a mooring system. For TLPs this comprises vertical tendons attached either directly to anchor piles (or caissons in the case of Snorre) or via a sea-bed template. For other floating systems a catenary chain mooring is used in moderate water depths, resulting in loads on the anchor that are quasi-horizontal (~20º or less). With deeper water applications, however, there is a trend towards taut-line moorings, based on a combination of steel wire and synthetic rope, resulting in much higher angles of loading (typically 30 to 40º) and therefore significant vertical capacity is required. A variety of anchors exist but they can be divided into two types, gravity anchors or embedded anchors (see Table 6.1).

Table 6.1 Types of anchors

Gravity anchors	Embedded anchors
Box	Anchor pile
Grillage and berm	Suction caisson
	Drag anchor (fixed fluke)
	Vertically loaded drag anchor (VLA)
	Suction embedded plate anchor (SEPLA)
	Dynamically penetrated anchor (DPA)

Analysis and design of suction caissons, drag anchors and dynamically penetrated anchors are considered in the following sections. The design of anchor piles and gravity anchors follows similar principles to those discussed previously in Sections 3 and 4. A brief comment on offshore construction issues for gravity anchors is included here.

In order to minimise crane capacity for the installation of gravity anchors, they are generally designed as a structural component, for example an empty box, together with bulk granular fill (either rock-fill, or heavier material such as iron ore). The structural element is placed first, and then the bulk fill is added (deposited down tubes extending from the vessel to close to the seabed, guided by ROVs). Figure 6.2 shows two different configurations: a conventional box anchor and a novel 'grillage and berm' solution that was adopted for the Stag field on the North-West Shelf of Australia (Erbrich & Neubecker, 1999). The latter is considerably more efficient in terms of quantity of steel for a given holding capacity (and hence can be installed with smaller crane vessels) but is much less efficient in terms of the quantity of ballast required. Design of this type of anchor is also more complex since a variety of failure modes must be considered, ranging from sliding of the complete berm, pulling out of the grillage, or combinations involving asymmetric mechanisms.

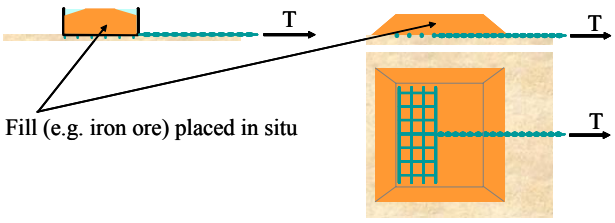

(a) Box anchor (b) Grillage and berm anchor

Figure 6.2 Gravity anchors

6.2 *Suction caissons*

Suction caissons have been used widely as anchoring solutions for a variety of floating facilities all over the world. A comprehensive report on suction caissons has been prepared by Andersen et al. (2005), the culmination of a collaborative project sponsored jointly by the API and Deepstar project and completed in 2003. The details given below draw substantially from that work.

Suction caissons comprise large diameter cylinders, open at the bottom and closed at the top, and generally with a length to diameter ratio (L/d) in the range 3 to 6. Although concrete caissons have been used, the vast majority of suction caissons are fabricated from steel (Fig. 6.3), with very high ratios of diameter to wall thickness (d/t ~ 100 to 250). Internal stiffeners are included to prevent structural buckling (a) during installation, and (b) due to the mooring loads and soil resistance during operation. Mooring loads are applied by an anchor line attached to the side of the caisson at a depth that optimises the holding capacity. Generally this requires the line of action of the load to pass through a point on the axis at a depth of 60 to 70 % of the embedded depth.

Figure 6.3 Suction caissons for the Laminaria field in the Timor Sea.

Suction caissons are installed initially by penetration into the seabed under self-weight with the lid vented, and then the remaining penetration is achieved by pumping water from inside the caisson using demountable pumps connected to a valve in the lid and operated by ROVs. The suction (strictly underpressure relative to the large hydrostatic water pressure) created by pumping creates a differential pressure on the caisson lid to force the caisson further into the soil. After installation the caisson lid is sealed allowing internal suctions to develop under vertical loading, hence maximising the end-bearing resistance.

Design issues for suction caissons can be divided conveniently into those associated with installation, and those concerned with operational conditions, principally capacity. In both areas, structural integrity of the caisson must be considered although that is not considered further here.

6.2.1 *Installation of suction caissons in clay*

The installation resistance during penetration of caissons comprises external and internal friction along the shaft, and along any extended plate stiffeners within the caisson, and end-bearing resistance on the tip of the caisson and any external or internal protuberances (e.g. the padeye, or internal stiffeners). This resistance is estimated using conventional soil mechanics principles, generally taking an end-bearing factor of $N_c \sim 7.5$ for the caisson tip (since it is closer to a deeply embedded strip than a circular foundation), and shaft friction based on the remoulded shear strength of the soil. An effective stress approach may be used to estimated the shaft friction during installation, and is particularly relevant where painted sections render the caisson surface smooth (Colliat & Dendani, 2002; Dendani & Colliat, 2002) or in unusual soil conditions (Erbrich & Hefer, 2002).

Figure 6.4 shows a comparison of measured installation pressures required for suction caissons in two different soft clay sites, drawn from 6 case histories described in detail by Andersen et al. (2005). The predictions were provided by 4 internationally experienced practitioners, and the range of results is indicative of current uncertainties in estimating parameters (even for Class C predictions!). As an example, the lowest prediction for the Diana site was based on an effective stress approach using an interface friction angle δ of 12º based on correlations with plasticity index (in the absence of direct measurements). Increasing δ to 17º below a depth of 20 m, where the PI of the soil reduces to less than 35%, would provide a much improved fit and is consistent with other data from the Gulf of Mexico (Jardine & Saldivar, 1999).

Note that for the Diana site, there was a significant delay between self-weight penetration and the application of suction, during which consolidation has led to an increase in capacity, as noted by the step increase in suction before further penetration occurred. By contrast, without such delay, only a small amount of suction is necessary, as in the Girassol example. In this example, and by contrast with the Diana predictions, the measured data tend to fall below any of the predictors' estimates.

Andersen et al. (2005) identified two main areas of variation in practice for estimating installation performance, other than estimating key soil parameters. These concern (a) treatment of ring stiffeners in regard to soil flow; and (b) choice of end-bearing coefficient, N_c, for internal stiffeners, and the degree to which this coefficient may be affected by friction transferred above the stiffener. As noted by Erbrich and Hefer (2002), soil may not flow fully around ring stiffeners, but will tend to be extruded as a self-supporting inner plug, until such point as the self-weight stresses in the plug cause collapse. By that point, however (and particularly for closely spaced stiffeners), trapped water will prevent the soil from relaxing against the inner caisson wall. For such cases the internal frictional resistance may be extremely low, with a mixture of softened soil and water providing lubrication adjacent to the caisson wall.

Penetration of the caisson will give rise to heave of the inner soil plug to accommodate (partly) the wall thickness of the caisson and also the full volume of any internal stiffeners. The plug heave will be enhanced by using suction, as opposed to self-weight or other external force, to install the caisson. There has been debate over the proportion of the caisson wall that is accommodated by flow of soil inwards into the caisson, or outwards. It is customary to assume a 50:50 split during self-weight penetration, but up to 100:0 split (in favour of inward flow) once suction is applied (Andersen & Jostad, 2002; 2004). Measurements of radial stress changes, and long-term axial capacity, suggest that the difference between suction and jacked installation is minimal (Chen & Randolph, 2005). Field data reported by Newlin (2003) reported measurements of soil plug heave consistent with less than 25 % (on average) of the total caisson steel volume being accommodated by inward soil flow; these data may have been influenced by an external chamfer on the thickened shoe of the caisson.

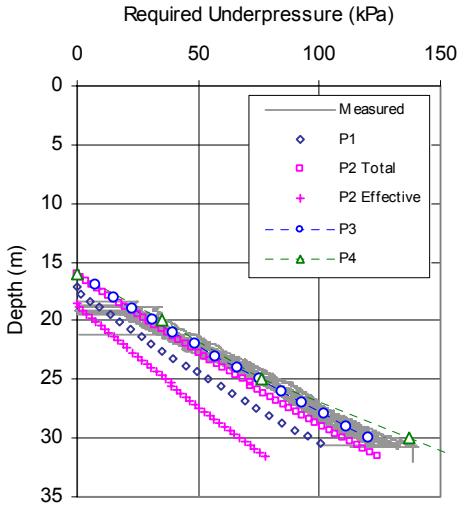

(a) Diana (Gulf of Mexico)

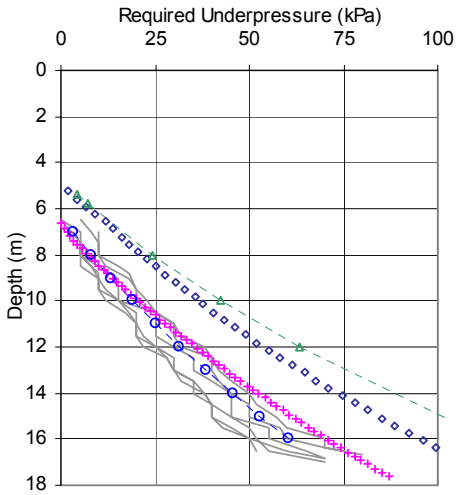

(b) Girassol offloading buoy (West Africa)

Figure 6.4 Measured and (Class C) predictions of penetration resistance for suction caissons at two soft clay sites (Andersen et al., 2005)

In practice, the amount of soil flow into the caisson is likely to be strongly affected by the proximity to internal plug failure, which is one of the essential design calculations (Andersen & Jostad, 1999). During initial penetration by suction, the factor of safety against plug failure is high, and soil flow at the caisson tip is likely to be similar to that during self-weight penetration. Towards the end of penetration, however, the soil plug will be closer to failure, with end-bearing resistance required for stability, and a greater proportion of the soil displaced at the caisson tip is likely to flow inwards.

The resistance of the internal soil plug against failure during suction installation comprises internal friction (as used to evaluate the caisson penetration resistance) together with the end-bearing resistance of the soil plug. Andersen et al. (2005) suggest that, since the internal friction contributes equally to penetration resistance and to soil plug stability, an appropriate design procedure is to adopt a soil strength material factor greater than unity for external caisson resistance (representing a worst case of required suction) and less than unity for the plug base resistance (again representing a worst case estimate). A consensus appeared to be for a minimum material factor of ~1.5 against soil plug failure during suction installation.

6.2.2 *Horizontal and vertical capacity of suction caissons*

The early suction caissons were designed for catenary moorings, where the chain load was close to horizontal at the seabed, increasing to angles typically of 10 to 20º at the padeye, positioned a depth, D, down the caisson. The horizontal capacity is maximised by positioning the padeye such that the caisson translates at failure without rotating. Essentially this is dictated by the centre-line intersection of the line of action of the load, as indicated in Figure 6.5. For normally or lightly overconsolidated clay, where the strength gradient is significant, the optimal depth is for $D^*/L \sim 0.65$ to 0.7, with the optimal depth decreasing slightly with increased loading angle (Andersen et al., 2005). Andersen and Jostad (1999) suggest positioning of the padeye just below the optimal depth in order to ensure backward rotation at failure, thus reducing the potential for a crack to open on the trailing edge of the caisson.

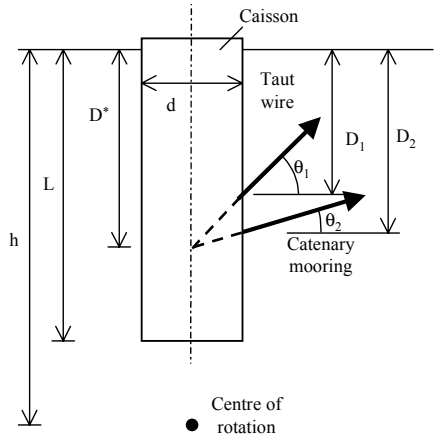

Figure 6.5 Variation of padeye depth with loading angle for given centre of rotation (Randolph & House, 2002)

Finite element analysis is generally used to evaluate the capacity of suction caissons, either full 3-dimensional analyses (e.g. Sukumaran et al., 1999; McCarron & Sukumaran, 2000) or 2-dimensional analyses that have previously been calibrated and are incorporated in design software such as HVMCap (NGI, 2000). The failure modes identified by 3-dimensional analysis are very similar to that suggested by Murff and Hamilton (1993) for laterally loaded piles. The main features of this mechanism are a conical wedge extending from the edge of the caisson at depth, z_o, to a maximum radius of R at the seabed (Fig. 6.6). The radial soil velocity within the wedge is then expressed as

$$v_r = v_o\left(\frac{r_o}{r}\right)^{\mu}\left(\frac{h-z}{h-D^*}\right)\cos\psi \qquad (6.1)$$

where h is the depth to the centre of rotation and ψ is the circumferential angle in plan view.

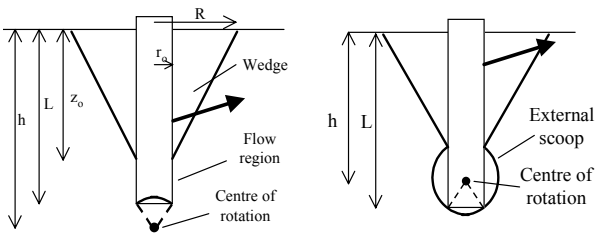

(a) Conical wedge and flow region (b) External base rotational scoop

Figure 6.6 Elements of soil failure mechanism for suction caisson

Below the conical wedge, a confined flow mechanism is assumed with the net resistance given by the plasticity solution of Randolph and Houlsby (1984). For caissons loaded above the optimal depth, where the centre of rotation falls within the caisson, an external scoop mechanism can replace the flow region, as shown in Figure 6.6b.

The above upper bound mechanism has been incorporated in the software AGSPANC (AG, 2001), and has been found to give results that are mainly within 12 % for long caissons (L/d > 3), but with the over-prediction increasing for short caissons (Andersen et al., 2005). Figure 6.7 shows how the caisson capacity calculated using AGSPANC varies with embedment ratio, for the two extreme cases of optimal loading (no rotation) and horizontal loading at seabed level with free rotation. Interestingly, compensating contributions of base shear and lateral resistance gives a net resistance for the optimal case of

$$H_u \approx 10Ld(s_u)_{average} \qquad (6.2)$$

This is a useful working rule for the early stages of design. Note that the capacity allowing free rotation is only about 25 % of the optimal capacity, for normally consolidated soil where the shear strength is proportional to depth.

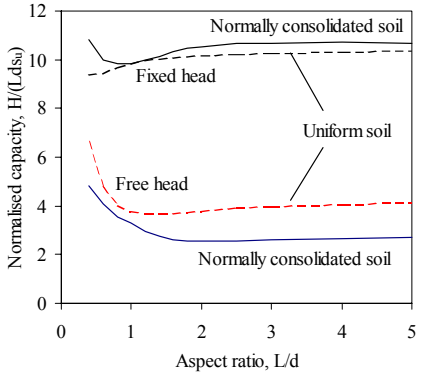

Figure 6.7 Capacity of suction caissons in soil with uniform strength and with strength proportional to depth (Randolph et al., 1998)

The project reported by Andersen et al. (2005) included a comparison between a number of predictors and rigorous finite element computations, with particular attention on the interaction between vertical and horizontal capacity. Two extreme geometries were studied, with L/d = 1.5 and 5, and two different soil profiles: a normally consolidated profile with $s_{u,SS} = 1.25z$ kPa and $\gamma' = 6$ kN/m^3; and a lightly overconsolidated profile with $s_{u,SS} = \max(10, 2z)$ kPa and $\gamma' = 7.2$ kN/m^3. For each profile, anisotropic soil properties were assigned, with the shear strengths in triaxial compression and extension taken respectively as 20 % above and below the simple shear strength, $s_{u,SS}$. The interface friction was taken as $\alpha s_{u,SS}$, with $\alpha = 0.65$.

Detailed results and discussion of predictions are given by Andersen et al. (2005), with results for one case shown here in Figure 6.8. The lines represent separate 3-dimensional finite element analyses conducted by the Norwegian Geotechnical Institute (NGI), the Centre for Offshore Foundation Systems (COFS), and the Offshore Technology Research Center (OTRC). Individual points are predictions made prior to the f.e. solutions, using simplified approaches such as HCMCap, AGSPANC and profiles of lateral resistance based on Murff and Hamilton (1993).

It may be seen that the interaction (or failure) envelope lies significantly within the rectangular boundary defined by the uniaxial vertical and horizontal capacities. The sensitivity to the loading depth, for a 30º loading angle, is shown in Figure 6.8b. In practice, the mooring line will be attached to a padeye on the caisson at a fixed depth, but the loading angle will vary for different design cases, resulting in a variation in the centre-line intercept for the applied load. As may be seen, while the optimum capacity is attained for a centre-line depth of 0.7L (note that D was used by Andersen et al. rather than L), significant reduction in capacity, by 20 %, occurs as the loading depth is varied by ±0.15L. A further point is that, for typical loading angles applied by taut and semi-taut mooring systems, which are generally in excess of 30º giving V > 0.58H, the caisson capacity is essentially governed by the vertical capacity of the caisson.

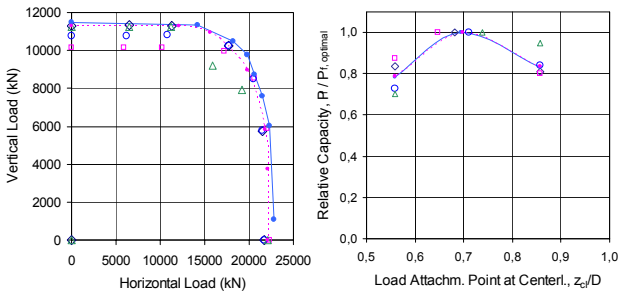

(a) Interaction diagram in V-H space (b) Effect of padeye depth

Figure 6.8 Results from hypothetical capacity analyses for suction caissons (L/d = 5, normally consolidated soil) (Andersen et al. 2005)

The shape of the failure envelopes has been modelled by a relationship of the form

$$\left(\frac{H}{H_u}\right)^a + \left(\frac{V}{V_u}\right)^b = 1 \qquad (6.3)$$

where H_u and V_u are the uniaxial capacities. Senders and Kay (2002) suggested taking the powers a and b as 3, but Supachawarote et al. (2004) found that better agreement with f.e. computations was obtained by varying the powers with the aspect ratio, L/d, of the caisson according to

$$\begin{aligned} a &= L/d + 0.5 \\ b &= L/3D + 4.5 \end{aligned} \qquad (6.4)$$

The high value of the power, b, implies that the vertical capacity is much less affected by the horizontal load than vice versa.

The study reported by Andersen et al. (2005) also considered the effect of a crack forming along the trailing edge of the caisson, and this has been explored further by Supachawarote et al. (2005). Figure 6.9 compares results obtained using 3-d f.e. analysis with and without allowing a crack to form, in soil where the strength gradient was taken as $s_u = 10 + 1.5z$ kPa, with $\gamma' = 7.2$ kN/m^3 and $K_0 = 0.65$. The f.e. results are compared with results obtained using AGSPANC, with either a 2-sided (uncracked), or a 1-sided (cracked) Murff-Hamilton mechanism.

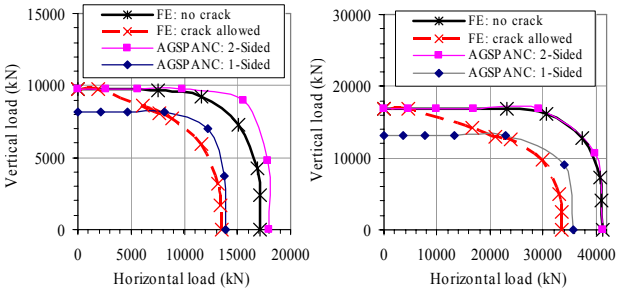

(a) L/d = 3 (b) L/d = 5

Figure 6.9 Comparison of failure envelopes for suction caisson, with and without crack formation (Supachawarote et al., 2005)

The f.e. results show a reduction of between 20 and 22 % in the pure horizontal capacity, which is maintained for loading angles of up to about 45º for L/d = 3 and 30º for L/d = 5. While loading close to vertical produces no reduction due to the formation of a gap, in any practical case the loading direction would range over several degrees from vertical. It therefore seems prudent to design suction caissons with allowance for a gap to form, and the potential for a reduction in capacity by around 20 %. Comparing Figures 6.8b and 6.9, the reduction in capacity due to locating the padeye below optimal level in order to force reverse rotation of the caisson, thus minimising potential gapping, is similar in magnitude to the loss in capacity due to gapping itself. Either way, therefore, the design capacity will be significantly lower than the theoretical optimum.

6.3 *Drag embedment and plate anchors*

6.3.1 *Evolution of anchors*

High capacity offshore anchors for semi-permanent moorings have evolved from conventional ship anchors into very sophisticated designs, spearheaded by companies such as Bruce Anchors and Vryhof (see Fig. 6.10a). Offshore anchors are generally fixed-fluke, with a predetermined angle between shank and fluke, though this may be adjusted prior to anchor placement on the seabed. This angle is typically around 50º for clay conditions (provided soft material occurs near the seabed) and 30º in sand or where clay of high strength occurs at the seabed. High angles in such material lead to instability of the anchor.

For installation, the anchor is placed on the seabed in the correct orientation (with the aid of ROVs) and then embedded by pretensioning the chain to an appropriate proof load. The level of proof load should be such that only limited further movement of the anchor will occur under a design operating condition (Lloyd's, 1999). For soils that are susceptible to cyclic loading, such as many carbonate soils, the industry 'standard' preload requirements may not be adequate to ensure that future anchor movements are minimal. In such cases considerably higher preloads may be required (Neubecker et al., 2005).

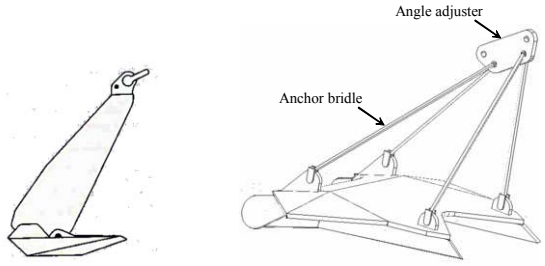

(a) Fixed fluke Stevpris (b) Stevmanta VLA

(c) Bruce DENNLA anchor (resting on shank)

Figure 6.10 Alternative types of Vryhof anchor

Fixed-fluke anchors such as the Bruce FFTS or the Vryhof Stevpris families cannot withstand significant vertical load components at the seabed, indeed these anchors are withdrawn by applying vertical load to the anchor chain. They are therefore suitable for catenary moorings but not for deep-water applications using taut or semi-taut polyester rope moorings. The vertically loaded anchor or VLA was developed to overcome this limitation. The VLA is similar to the conventional drag anchor except the fluke is a plate with much lower profile and the shank is replaced by either a much thinner shank (as in the Bruce DENNLA) or a wire harness (Vryhof Stevmanta) as shown in Figure 6.10. The VLA is installed like a conventional drag anchor with a horizontal chain load at the mudline and then different mechanisms are used to allow the fluke to rotate until it is perpendicular to the applied load, mobilizing the maximum possible soil resistance, and enabling the anchor to withstand both horizontal and vertical loading. VLAs have been the subject of a recent project sponsored by by the API and Deepstar project, completed in 2003, and a report summarising the outcomes has been provided by Murff et al. (2005).

The DENNLA and Stevmanta VLAs achieve the desired effect of installing a plate anchor at a sufficient depth below the seabed in order to resist the mooring loads, but there is an inherent problem with these kinds of anchors in knowing exactly where they are in the soil. An alternative means of installing a plate anchor, overcoming this limitation, is the SEPLA (suction embedded plate anchor, Dove et al., 1998). The plate sits in a vertical slot in the tip of the suction caisson, which is installed in the usual manner. Provision is made for the plate to disconnect from the caisson and the caisson is retrieved leaving the plate at the design penetration depth. As the anchor line is then tensioned, the plate rotates to become perpendicular to the line.

6.3.2 *Anchor chain response*

The anchor chain takes up a reverse curvature through the soil, so that the loading angle is greater (relative to the horizontal) than at the mudline. It is therefore necessary to consider the mechanics of the anchor chain (or wire) in assessing the performance of a given anchoring system, and indeed the chain response is particularly critical in determining the kinematics of drag anchor embedment.

The governing equations for the anchor chain are illustrated in Figure 6.11. A typical element of chain is acted on by the chain tension, T, the normal resistance of Q per unit length, a friction resistance of F = μQ, and the chain weight of w (again, per unit length). Typically, the friction coefficient μ is taken in the range 0.3 to 0.5, although lower values have also been recommended in clay soils. The pair of equations must be solved iteratively, adjusting the boundary conditions at the seabed in order to match the known position of the attachment point on the anchor (Vivatrat et al., 1982).

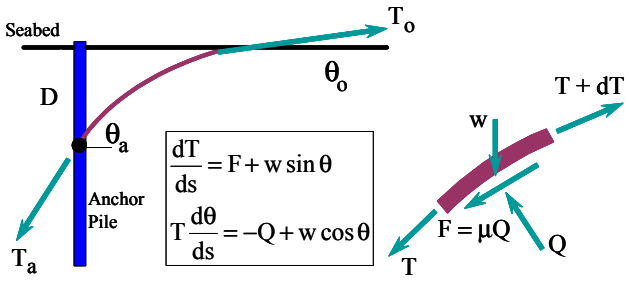

Figure 6.11 Governing equations for anchor chain

Neubecker & Randolph (1995) pointed out that the chain self-weight, w, is essentially negligible except at shallow depths in very soft soil, and hence can be ignored. If necessary, the profile of normal chain resistance, Q, can be adjusted to compensate for ignoring the chain self-weight. This allows closed form solutions to be obtained for the change in angle of the chain, approximated by

$$\frac{T_a}{2}\left(\theta_a^2 - \theta_o^2\right) \approx \int_0^D Q\,dz = D\overline{Q} \tag{6.5}$$

where $\overline{Q}$ is the average bearing resistance (per unit length of chain) over the depth interval from the seabed down to the attachment point a depth D. A corresponding expression was derived for the change in tension along the anchor chain, expressed in terms of the friction coefficient, μ, and the angle change, as

$$\frac{T_o}{T_a} = e^{\mu(\theta_a - \theta_o)} \tag{6.6}$$

This expression is similar to the standard solution for the change in tension in a rope wrapped around a frictional bollard.

The above two expressions, although containing some approximations, are sufficiently accurate to use directly in calculating the installation performance of drag anchors, or the gradual tautening of an anchor chain attached to a suction caisson (Fig. 6.12). For most drag anchor installations, or for standard catenary moorings, the chain angle at the seabed, θ_o, may be taken as zero. By contrast, for taut-wire mooring systems, the change in angle (or in load) between seabed and attachment point becomes insignificant.

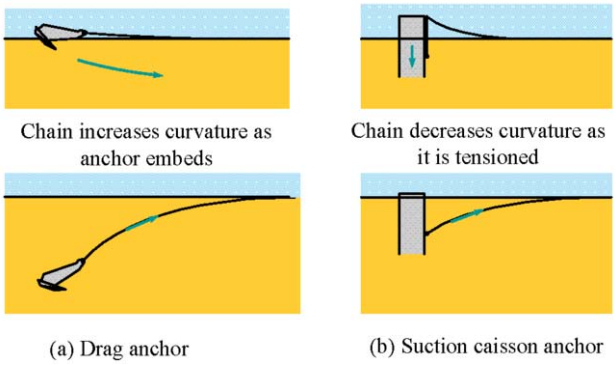

Figure 6.12 Chain response during installation of (a) a drag anchor and (b) a suction caisson

6.3.3 *Embedment process for drag anchors and VLAs*

The holding capacity of a drag anchor or a more recent VLA is a direct function of the depth to which the anchor can be installed. As pointed out by Murff et al. (2005), while predicted embedment depths and capacities for drag anchors show a significant degree of scatter, there is much closer agreement on the anchor capacity for a given embedment depth. Thus accurate prediction of anchor performance relies on being able to simulate the installation process accurately.

Neubecker and Randolph (1996) followed a limit equilibrium approach where the anchor resistance was taken as a function of the anchor area projected at right angles to the direction of travel (assumed approximately parallel to the flukes), using a conventional bearing capacity approach. As the anchor was dragged through the soil, the resisting force was assumed to maintain a fixed angle with the flukes, while the magnitude varied according to the local (average) shear strength. By coupling this approach with their chain solution, the complete embedment response of the anchor could be simulated.

While full 3-dimensional finite element analysis of anchor embedment remains a major challenge, a number of finite element based methods have emerged in recent years (Thorne, 1998; Bransby & O'Neill, 1999; O'Neill et al., 2003). As documented by Murff et al. (2005), the most attractive approach appears to be a combination of the Bransby & O'Neill methodology for the anchor fluke, coupled with limit equilibrium analysis of the forces acting on the anchor shank or the wire harness that serves for a shank in the Vryhof Stevmanta VLA.

Figure 6.13 illustrates the various forces acting on the anchor as it embeds. The first step, using conventional soil mechanics approaches to estimate the resisting forces along the shank, is to transfer the shackle force F, and the overall shank forces, f_{bn} and f_{sn}, to equivalent normal (f_{dn}), parallel (f_{ds}) and moment (m_d) resultants acting at the mid-point of the fluke. Then, a failure envelope derived from finite element analysis (generally for a simplified fluke shape) is used to assess (a) conditions for plastic motion of the fluke, as determined by the size of the failure envelope; and (b) the relative normal, parallel and rotational motion of the plate, determined from the local gradients of the failure envelope (Bransby & O'Neill, 1999).

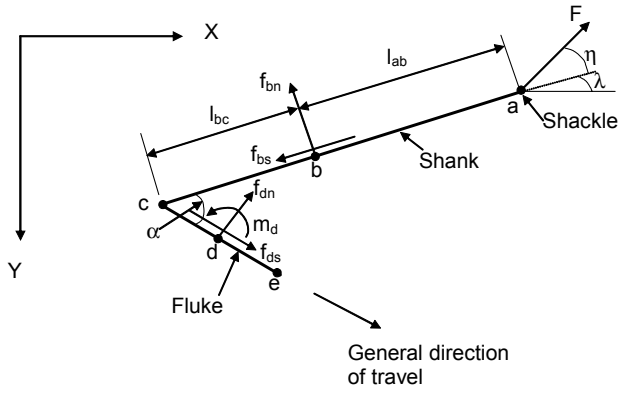

Figure 6.13 Schematic of anchor for transfer of shackle force to fluke (Murff et al., 2005)

Typical failure envelopes for an anchor fluke, modelled as a 2-dimensional strip with length (across the width of the strip) to thickness ratio of L/t = 7 are shown in Figure 6.14. The normal, parallel and moment load factors are defined respectively as

$$N_n = \frac{f_n}{Ls_u}; N_s = \frac{f_s}{Ls_u}; N_m = \frac{m}{L^2 s_u} \tag{6.7}$$

Maximum values of these factors, for uniaxial loading, may be estimated from upper bound analyses as (Bransby & O'Neill, 1999; O'Neill et al., 2003):

$$N_{n\,max} = \frac{f_{n\,max}}{Ls_u} = 3\pi + 2\frac{t}{L}\left(\alpha + \frac{1+\alpha}{\sqrt{2}}\right) \tag{6.8}$$

$$N_{s\,max} = \frac{f_{s\,max}}{Ls_u} = 2\left(\alpha + N_{tip}\frac{t}{L}\right) \approx 2\alpha + 15\frac{t}{L} \tag{6.9}$$

$$N_m = \frac{m_{max}}{L^2 s_u} = \frac{\pi}{2}\left[1 + \left(\frac{t}{L}\right)^2\right] \tag{6.10}$$

where α is the interface friction ratio.

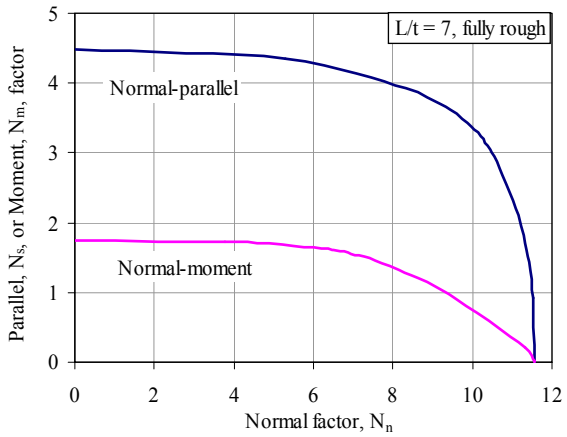

Figure 6.14 Interaction curves in normal-parallel and normal-moment space (Murff et al., 2005)

For general loading combinations, a 3-dimensional failure envelope is required; a form suggested by Murff (1994) was adopted by Bransby and O'Neill (1999), given by:

$$\left(\frac{f_n}{f_{n\,max}}\right)^q + \left[\left(\frac{m}{m_{max}}\right)^r + \left(\frac{f_s}{f_{s\,max}}\right)^s\right]^{\frac{1}{p}} - 1 = F - 1 = 0 \tag{6.11}$$

with coefficient values optimized to fit the results of finite element computations, summarized in Table 6.2.

Table 6.2 Exponents for the Bransby-O'Neill equation

Parameter	p	q	r	s
Value	1.22	3.68	1.37	3.74

An example kinematic analysis using the above failure envelope is shown in Figure 6.15, based loosely on a 32 tonne Vryhof Stevpris anchor, with 50º fluke angle, fluke length of 5 m and a total fluke area of about 25 m^2, penetrating soft clay with s_u = 1.5z kPa. The plots show the evolution of the forces at the mid-point of the fluke, which rapidly move towards a location on the failure envelope corresponding to m ~ 0, and with f_n and f_s close to 80 % of their maximum values. Note that the limiting efficiency of around 20 (ratio of holding capacity to anchor weight) takes a significant distance to be mobilised, in excess of 100 m, with the padeye reaching a depth of around 15 m.

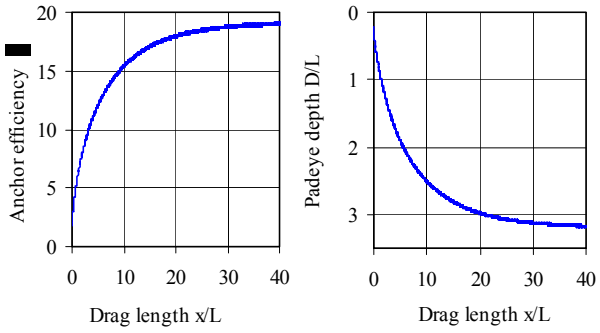

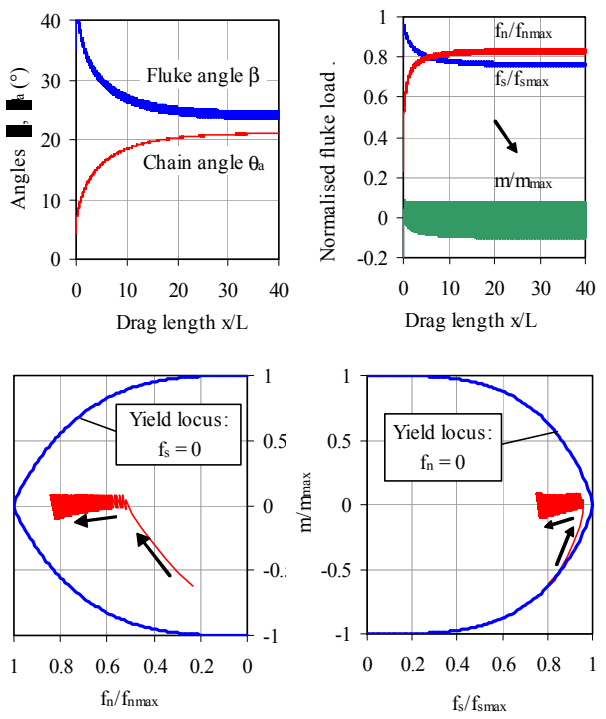

Figure 6.15 Example kinematic analysis using failure envelope for rectangular anchor (O'Neill et al., 2003)

Conventional drag anchor design is usually based on design charts that give the holding capacity as a power law of the anchor weight (e.g. NCEL, 1987; Vryhof, 2000). However, in reality the actual weight of the anchor is largely irrelevant except in determining the initial penetration, and the capacity is primarily a function of the fluke area (Murff et al., 2005). This has become increasingly important with the advent of VLAs, with their low weight to area ratio. Thus the design chart for the Stevpris family of anchors (Vryhof, 2000) may be expressed alternatively as:

$$T_{hc} \approx 48W^{0.92} \qquad (6.12)$$

or

$$T_{hc} \approx 100A^{1.4} \qquad (6.13)$$

where T_{hc}, W and A are the holding capacity (kN), weight (kN) and fluke area (m^2) respectively.

6.3.4 *Capacity of plate anchors*

As noted previously, the challenge in estimating anchor capacity is more in prediction of the embedment, than in estimating the capacity for a given depth below the seabed and soil shear strength. Early finite element solutions for strip anchors at different embedments, together with the exact solution of N_{nmax} = 11.42 for deep embedment, were provided by Rowe & Davis (1982). The corresponding exact solution for a deeply embedded circular plate ranges from 12.42 for a fully smooth interface to 13.11 for a fully rough interface (Martin & Randolph, 2001), with N_n expressed as f_n/As_u. Merifield et al. (2003) have given lower bound solutions for square and rectangular plates at different embedments, with N_{nmax} = 11.9 for a deeply embedded square plate. They also showed that the normalised anchor capacity increases very rapidly with depth once the overburden stress is allowed for, particularly for strength ratios s_u/σ'_{vo} typically encountered in deep-water offshore sediments.

The narrow range of bearing capacity factors given above for loading normal to the plate is also true of the normalised moment capacity, $N_{nmax} = m_{max}/ABs_u$ where A is the plate area and B the width (or diameter) in the plane of rotation. For a thin plate, the normalised moment capacity for both strip and circular plates is close to 1.60. The broadest range in capacity is for sliding parallel to the plate, where the resistance derives from a combination of sliding over the upper and lower surfaces, and bearing at the leading and trailing edges of the plate. The capacity is thus strongly dependent on the interface friction ratio, α. For a given value of α, Eqn 6.9 may be applied to plates of different geometry, replacing t/L by the ratio of projected area perpendicular to the plate, to the area, A, of the plate.

All offshore plate anchors, such as a VLA or SEPLA, undergo some degree of rotation as the operating load is applied, and this gives rise to two effects: (a) the anchor will move upwards as it rotates, thus reducing the embedment (moving into softer soil); and (b) the soil will be (further) remoulded in the immediate vicinity of the anchor. The reduction in soil strength due to the latter effect may be recovered in due course by consolidation, but the loss of embedment is crucial. Wilde et al. (2001) report upward movements ranging between 0.5 and 1.7 times the plate height, which is a disconcertingly wide range.

6.4 *Dynamically penetrating anchors*

The cost of installing anchors in deep water has led to the development of anchors that embed themselves into the seabed under free-fall, such as the 'Deep Penetrating Anchor' (Lieng et al., 1999, 2000). It comprises a rocket-shaped anchor, 1 to 1.2 m in diameter, with a dry weight of 500 to 1000 kN and a height of 10 to 15 m, and is designed to be released from a height of 20 to 40 m above the seabed. Field trials with the anchor (Fig. 6.16a) are proceeding and it has yet to be used in practice.

A less sophisticated 'Torpedo Anchor' has been used by Petrobras in the Campos Basin (Medeiros, 2001, 2002). The dimensions of the anchor range from 0.76 to 1.1 m in diameter by 12 to 15 m long, with a weight of 250 to 1000 kN. Some versions of the anchor have been fitted with 4 flukes at the trailing edge, ranging in width from 0.45 to 0.9 m, and 9 to 10 m long (Fig. 6.16b).

Both of the above anchors are referred to here as dynamically penetrating anchors. They are designed to reach velocities of 25 to 35 m/s at the seabed, allowing tip penetrations of ~3 times the anchor length, and holding capacities after consolidation that are anticipated in the range 5 to 10 times the weight of the anchor. While such efficiencies are lower than would be obtained with other sorts of anchor, the low cost fabrication and installation compensates.

Centrifuge model studies have been reported by O'Loughlin et al. (2004), allowing relationships to be developed between impact velocity, penetration depths and holding capacity. Some results are shown in Figure 6.17, comparing the vertical component of holding capacity (normalised in Fig. 6.17a by the shear strength at the anchor padeye and the total bearing area of shaft and flukes) from the model tests with field data and f.e. predictions. The centrifuge data show a similar range of normalised capacities, although the efficiencies were quite low, typically between 2 and 4.

Figure 6.16 Dynamically penetrating anchors (a) field trial (O'Loughlin et al., 2004); (b) installation of torpedo anchor (Medeiros, 2002)

Table 6.2 Advantages and disadvantages of different deep water anchor types. Reproduced from Ehlers et al. (2004).

Anchor	Advantages	Disadvantages
Suction caisson anchor	• simple to install accurately with respect to location, orientation and penetration • leverage design experience with driven piles • well developed design and installation procedures • anchor with the most experience in deep water for mooring MODUs and permanent facilities	• heavy: derrick barges may be required • large: more trips to shore to deploy full anchor spread • requires ROV for installation • requires soil data from advanced laboratory testing for design • concern with holding capacity in layered soils • lack of formal design guidelines • limited data on set-up time for uplift
Drag embedment vertically loaded anchor (VLA)	• lower weight • smaller: fewer trips to transport the full anchor spread to a site • well developed design and installation procedures	• requires drag installation, keying and proof testing; limited to bollard pull of installation vessel • requires 2 or 3 vessels and ROV • no experience with permanent floating facilities outside of Brazil • difficult to assure installation to, and orientation at, design penetration
Suction embedded plate anchor (SEPLA)	• uses proven suction caisson installation methods • cost of anchor element is the lowest of all the deepwater anchors • provides accurate measure of penetration and positioning of anchor plate • design based on well developed design procedure for plate anchors	• proprietary or patented installation • installation time about 30 % greater than for suction caissons and may require derrick barge • requires keying and proof testing: limited to bollard pull of installation vessel; also requires ROV • limited field load tests and applications limited in numbers to MODU only
Dynamically penetrating anchor	• simple to design: conventional API RP 2A pile design procedures used for prediction of capacity; thus capacity calculations are likely to be readily acceptable for verification agencies • simple and economical to fabricate • robust and compact design makes handling and installation simple and economical using 1 vessel and no ROV • accurate positioning with no requirements for specific orientation and proof testing during installation	• proprietary or patented design • no experience outside Brazil • lack of documented installation and design methods with verification agencies • verification of verticality

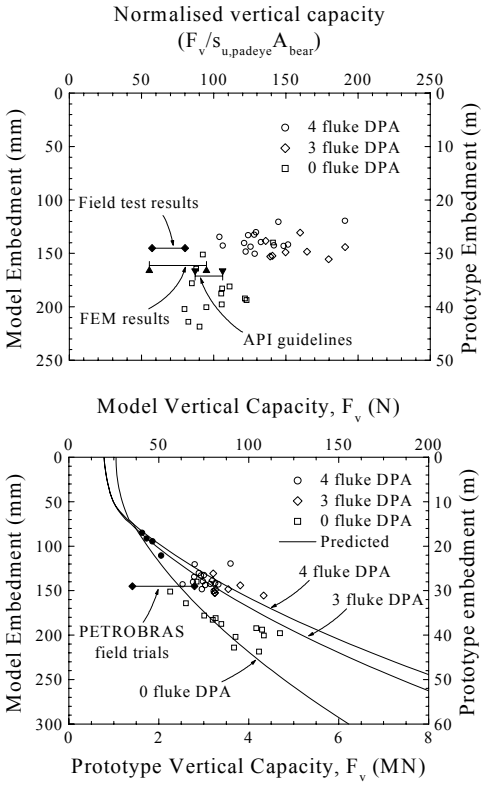

Figure 6.17 Normalised (a) and absolute (b) capacities from anchor tests and theoretical studies (O'Loughlin et al., 2004)

A key aspect of predicting the penetration depth, and thus the eventual holding capacity (Fig. 6.17b) for dynamically penetrating anchors, is understanding the penetration resistance at such high velocities. The resistance will be dominated by fluid mechanics drag resistance a shallow depths, and viscous-enhanced shearing resistance as the anchor penetrates further (O'Loughlin et al., 2004).

6.5 *Comparison of different anchor types*

Ehlers et al. (2004) have provided a comprehensive overview of deepwater anchoring and the relative merits of each type of anchoring system from an industry perspective. These are summarised here in Table 6.3. The very rapid development of different types of anchor over the last few years means that design methods, and the confidence with which some of the anchor types are viewed, have lagged behind. The coming years are likely to bring some rationalisation in the variety of anchor types, as experience starts to favour particular systems.

7 CONCLUDING REMARKS

This paper has covered a wide range of offshore geotechnical design, although many areas, for example geohazard assessment, pipeline and riser design, have been omitted. The objective has been to compare onshore and offshore geotechnical design practice, with the latter dominated by capacity considerations with particular emphasis on cyclic loading.

Over the last decade, offshore design practice has moved from 'Working Stress Design' (based essentially on a global factor of safety, as in API, 1993) to 'Load and Resistance Factor Design', using partial factors for different load types and for the material strength (ISO, 2000, 2004). This shift has occurred in parallel with similar developments in onshore practice (Eurocode 7, 1997). The use of a partial factor approach is considered to be essential when assessing the performance of foundation systems that are subjected to both tensile and compressive loads, but where the foundation capacity under compressive loads is significantly greater than under tensile loads.

Onshore design for urban developments has become extremely sophisticated in treating the interaction of new projects on existing buildings or services, with the emphasis on simulat-

ing the intact (and particularly small-strain) response of soils and rock. By contrast, much of offshore design is focused on the large-strain response of soils, with increasing emphasis on the soft sediments encountered in deep-water developments. The potential softening of soil as it is destructured under monotonic or cyclic deformations is a critical aspect, both in interpretation of in situ site investigation data and the behaviour of foundation or anchoring systems.

Future challenges include developments in water depths extending to 3 km, with a design focus on relatively small (shallow) foundations for subsea systems (manifolds, flow-lines etc) and different anchoring options. Accurate characterisation of the shear strength profile in the upper 1 or 2 m of the seabed, which often shows a pronounced crust with strengths of 5 to 15 kPa, will be critical, as will be evaluation of the potential for small foundations or pipelines to break through that crust.

ACKNOWLEDGEMENTS

The authors gratefully acknowledge input to this paper from colleagues at the Special Research Centre for Offshore Foundation Systems, established and supported under the Australian Research Council's Research Centres Program, and also from Advanced Geomechanics.

REFERENCES

Aas, G., Lacasse, S., Lunne, T. and Høeg, K. 1986. Use of in situ tests for foundation design on clay. *Proc. In Situ '86: Use of In situ Tests in Geotechnical Engineering*, ASCE, New York, 1-30.

Abbs, A.F. 1983. Lateral pile analysis in weak carbonate rocks. *Proc. Conf. on Geotechnical Practice in Offshore Engineering*, ASCE, Austin, 546-556.

Abbs, A.F. 1992. Design of grouted offshore piles in calcareous soils. *Proc. 6th ANZ Conf. on Geomech.,* Christchurch, 128-132.

Ackland, D.F. 1949. Moving Heaven and Earth, R.G. LeTourneau. *Marshall, Morgan and Scott*, London.

AG. 2001. *Suction pile analysis code: AGSPANC Users' Manual, Version 3.0*. Advanced Geomechanics Internal Report, Perth.

Alm, T., Snell, R.O., Hampson, K.M. and Olaussen, A. 2004. Design and installation of the Valhall piggyback structures, *Proc. Annual Offshore Tech. Conf*., Houston, Paper OTC 16294.

Al-Shafei, K.A., Cox, W.R. and Helfrich, S.C. 1994. Pile load tests in dense sand: Analysis of static test results. *Proc. Annual Offshore Tech. Conf.,* Houston, Paper OTC 7381.

Andenaes, E., Skomedal., E. and Lindseth, S. 1996. Installation of the Troll Phase 1 Gravity Base Platform. *Proc. Annual Offshore Technology Conf., Houston*, Paper OTC 8122.

Andersen K.H. 2004. Cyclic clay data for foundation design of structure subjected to wave loading. Invited keynote lecture: *Proc. Int. Conf. on Cyclic Behaviour of Soils and Liquefaction Phenomena*, CBS04, Bochum Germany, Balkema: Rotterdam.

Andersen, K.H., Dyvik, R., Schroeder, K., Hansteen, O.E. and Bysveen, S. (1993). Field tests of anchors in clay. II: Predictions and interpretation. *J. Geot. Eng. Div., ASCE*, 119(10), 1532-1549.

Andersen K.H. and Lauritzen R. 1988. Bearing capacity for foundations with cyclic loads. *J. Geot. Eng. Div., ASCE*, 114(5), 540 - 555.

Andersen, K.H. and Jostad, H.P. 1999. Foundation design of skirted foundations and anchors in clay. *Proc. Annual Offshore Technology Conf*., Houston, Paper OTC 10824.

Andersen, K.H. and Jostad, H.P. 2002. Shear strength along outside wall of suction anchors in clay after installation. *Proc. 12th Int. Offshore and Polar Engrg. Conf*., ISOPE'2002, 785-794.

Andersen, K.H. and Jostad, H.P. 2004. Shear strength along inside of suction anchor skirt wall in clay. *Proc. Annual Offshore Tech. Conf.,* Houston, Paper OTC 16844.

Andersen, K. H., Rawlings, C. G., Lunne, T. and Trond, H. 1994. Estimation of hydraulic fracture pressure in clay. *Canadian Geotechnical Journal*, 31, 817-828.

Andersen, K.H., Murff, J.D., Randolph, M.F., Clukey, E., Erbrich, C.T., Jostad H.P., Hansen, B., Aubeny, C.P., Sharma, P. and Supachawarote, C. 2005. Suction anchors for deepwater applications. *Proc. Int. Symp. on Frontiers in Offshore Geotechnics (ISFOG),* Perth.

Angemeer, J. Carlson, E. and Klick, J.H. 1973. Techniques and results of offshore pile load testing in calcareous soils. *Proc. Annual Offshore Tech. Conf.*, Houston, Paper OTC1894.

API. 1993. *Recommended practice for planning, designing and constructing fixed offshore platforms - working stress design, API-RP-2A*, 20th edition, American Petroleum Institute, Washington.

Baglioni, V.P., Chow, G.S. and Endley, S.N. 1982. Jack-up rig foundation stability in stratified soil profiles. *Proc. 14th Offshore Technology Conf*., Houston, Paper OTC 4408.

Barbour, R.J. and Erbrich C.T. 1994. Analysis of in-situ reformation of flattened large diameter foundation piles using ABAQUS. *Proc. UK ABAQUS Users Conf*., Oxford.

Barbour, R.J. and Erbrich, C. 1995. Analysis of soil skirt interaction during installation of bucket foundations using ABAQUS. *Proc. ABAQUS Users Conf*., Paris, June 1995.

Barton, Y.O. 1982. *Laterally Loaded Model Piles in Sand: Centrifuge Tests and Finite Element Analyses*. PhD Thesis, University of Cambridge.

Bell, R.W. 1991. *The Analysis of Offshore Foundations Subjected to Combined Loading*. M.Sc. Thesis, University of Oxford.

Bienen, B. and Cassidy, M.J. 2004. Three-dimensional analysis of jack-up structures. *Developments in Mechanics of Structures and Materials: Proc. 18th Australasian Conf. on the Mechanics of Structures and Materials*., A.A. Balkema, Perth, 1, 345-351.

Bjerrum, L. 1973. Geotechnical problems involved in foundations of structures in the North Sea, *Géotechnique* 23(3), 319-358.

Boon, B., Vrouwenvelder, A., Hengst, S., Boonstra, H., and Daghigh, M. 1997. System reliability analysis of jack-up structures: possibilities and frustrations. *Proc. 6th Int. Conf. Jack-Up Platform Design, Construction and Operation*, City University, London

Borel, D., Puech, A. and de Ruijter, M. 2002. High quality sampling for deep water geotechnical engineering: the STACOR experience. *Proc. Conf. on Ultra Deep Engineering and Technology*, Brest.

Bradshaw, I.J. 1987. Jack-up structural behaviour and analysis methods. *Mobile Offshore Structures*, Elsevier, London, 125-155.

Bransby, M. F. and O'Neill, M. P. 1999. Drag anchor fluke-soil interaction in clays. *Proc. Int. Symp. on Numerical Models in Geomechanics (NUMOG VII)*, Graz, Austria, 489-494.

Bransby, M.F. and Randolph, M.F. 1999. The effect of embedment depth on the undrained response of skirted foundations to combined loading. *Soils and Foundations,* 39(4), 19-33.

Bransby, M.F. and Randolph, M.F. 1998. Combined loading of skirted foundations. *Géotechnique* 48(5), 637-655.

Brinch Hansen, J. 1961. A general formula for bearing capacity. *Danish Geotechnical Institute Bulletin*, 11, 38-46.

Brinch Hansen, J. 1970. A revised and extended formula for bearing capacity. *The Danish Geotechnical Institute*, Copenhagen, 98, 5-11.

Brown, J.D. and Meyerhof, G.G. 1969. Experimental study of bearing capacity in layered clays. *Proc. 7th ICSMFE*, 2, 45-51.

Brucy, F., Meunier, K. and Nauroy, J.F. 1991. Behaviour of pile plug in sandy soils during and after driving. *Proc. Annual Offshore Technology Conf.*, Houston, Paper OTC 6514.

Bustamente,M. and Gianeselli, L. 1982. Pile bearing capacity prediction by means of static penetrometer CPT. *Proc. ESOPT II*, Amsterdam, 2, 492-500.

Butterfield, R. and Ticof, J. 1979. Design parameters for granular soils (discussion contribution). *Proc. 7th ECSMFE*, Brighton, 4, 259-261.

Butterfield, R., Houlsby, G.T. and Gottardi, G. 1997. Standardized sign conventions and notation for generally loaded foundations. *Géotechnique* 47(5), 1051-1054.

Bye, A., Erbrich, C., Rognlien, B. and Tjelta, T.I. 1995. Geotechnical design of bucket foundations. *Proc. Annual Offshore Technology Conf.,* Houston, PaperOTC 7793.

Byrne, B.W. 2000. *Investigations of Suction Caissons in Dense Sand*, DPhil Thesis, The University of Oxford.

Byrne, B. and Cassidy, M.J. 2002. Investigating the response of offshore foundations in soft clay soils. *Proc. 21th Int. Conf. on Offshore Mech. & Arctic Eng.* (*OMAE*)., Oslo, OMAE2002-28057.

Byrne, B.W. and Houlsby, G.T. 2001. Observations of footing behaviour on loose carbonate sands, *Géotechnique* 51(5), pp463-466.

Caltrans 1997. *California Foundation Manual, State of California*, Dept of Transportation. Office of Structure Construction, Los Angeles.

Carter, J.P., Davies, P.J. and Krasnostein, P. 1999. The future of offshore site investigation – robotic drilling on the sea-bed. *Australian Geomechanics*, 34(3), 77-84.

Cassidy, M.J. 1999. *Non-Linear Analysis of Jack-Up Structures Subjected to Random Waves*, D.Phil Thesis, University of Oxford.

Cassidy, M.J. 2003. Centrifuge experiments investigating the reinstallation of spudcans close to existing footprints. *Geo:03296*, COFS, The University of Western Australia, Perth.

Cassidy, M.J. and Bienen, B. 2002. Three-dimensional numerical analysis of jack-up structures on sand. *Proc. 12th Int. Offshore and Polar Engng Conf.*, Kitakyushu, Japan, 2, 807-814.

Cassidy, M.J., Byrne, B.W., Houlsby, G.T. 2002[a]. Modelling the behaviour of circular footings under combined loading on loose carbonate sand. *Géotechnique*, 52(10), 705-712.

Cassidy, M.J., Byrne, B.W. and Randolph, M.F. 2004a. A comparison of the combined load behaviour of spudcan and caisson foundations on soft normally consolidated clay. *Géotechnique*, 54(2), 91-106.

Cassidy, M.J., Eatock Taylor, R. and Houlsby, G.T. 2001. Analysis of jack-up units using a Constrained NewWave methodology. *Applied Ocean Research*, 23, 221-234.

Cassidy, M.J. and Houlsby, G.T. 1999. On the modelling of foundations for jack-up units on sand, *Proc. 31st Offshore Technology Conf.,* Houston, Paper OTC 10995.

Cassidy, M.J. and Houlsby, G.T. 2002. Vertical bearing capacity factors for conical footings on sand. *Géotechnique*, 52(9), 687-692

Cassidy, M.J., Houlsby, G.T., Hoyle, M., Marcom, M. 2002b. Determining appropriate stiffness levels for spudcan foundations using jack-up case records. *Proc. 21th Int. Conf. on Offshore Mech. & Arctic Eng.* (OMAE), Oslo, Norway, OMAE2002-28085.

Cassidy, M.J., Martin, C.M., Houlsby, G.T. 2004b. Development and application of force resultant models describing jack-up foundation behaviour. *Marine Structures*, 17(3-4), 165-193.

Cassidy, M.J., Taylor, P.H., Eatock Taylor, R., Houlsby, G.T. 2002c. Evaluation of long-term extreme response statistics of jack-up platforms. *Ocean Engineering*, 29(13), 1603-1631.

Cerato, A.B. and Lutenegger, A.J. 2004. Disturbance effects of field vane tests in a varied clay. *Proc. 2nd Int. Conf. on Site Characterisation*, Porto.

Chandler, R.J. 1988. The in-situ measurement of the undrained shear strength of clays using the field vane. *Vane Shear Strength Testing of Soils: Field and Laboratory Studies*, ASTM STP 1014, 13-45.

Chen, W. and Randolph, M.F. 2005. Axial capacity and stress changes around suction caissons. submitted to *Géotechnique*.

Chiba, S., Onuki, T. and Sao, K. 1986. Static and dynamic measurement of bottom fixity. *The Jack-up Drilling Platform Design and Operation*, Collins, London, 307-327.

Chow, F.C. 1996. *Investigations into the Behaviour of Displacement Piles for Offshore Foundations*. PhD thesis, Imperial College, University of London.

Christophersen, H.P. 1993. The non-piled foundation systems of the Snorre field. *Offshore Site Investigation and Foundation Behaviour,* Soc. for Underwater Technology, 28, 433-447.

Chung, S.F. and Randolph, M.F. 2004. Penetration resistance in soft clay for different shaped penetrometers. *Proc. 2nd Int. Conf. on Site Characterisation*, Porto, 1, 671-678.

Clausen, C.J.F. 1976. The Condeep story. *Proc. Offshore Soil Mechanics,* Cambridge University. Ed.George. P. and Wood, D., 256-270.

Clausen, C.J.F., Dibiagio, E., Duncan, J.M. and Andersen, K.H. 1975. Observed behaviour of the Ekofisk oil storage tank foundation. *Proc. Annual Offshore Technology Conf.,* Houston, OTC 2373.

Clukey E.C., Morrison, M.J., Garnier, J. and Corté, J.F. 1995. The response of suction caissons in normally consolidated clays to cyclic TLP loading conditions, *Proc. Annual Offshore Technology Conf.,* Houston, Paper OTC 7796.

Clunie-Ross, B. 1999. *Reinstallation of Spudcan Footings in Clay*. Honours Thesis, Dept. of Civil and Resource Engineering, The University of Western Australia, Perth

Colliat, J-L. and Dendani, H. 2002. Girassol: geotechnical design analyses and installation of the suction anchors. *Proc. Int. Conf. on Offshore Site Investigation and Geotechnics,* Society for Underwater Technology, London.

Cox, A.D, Eason, G., and Hopkins, H.G. 1961. Axially symmetric plastic deformation in soils. *Proc. Royal Soc. London*, Ser. A, 254,1-45.

Craig, W.H. and Chua, K. 1990. Deep penetration of spudcan foundation on sand and clay. *Géotechnique*, 40(4), 551-563.

Cremer, C., Pecker, A., Davenne, L. (2001). Cyclic macro-element for soil-structure interaction: material and geometrical non-linearities. *Int. J. Num. & Analytical Methods in Geomech.*, 25, 1257-1284.

Davis, E.H. and Booker, J.R. 1973. The effect of increasing strength with depth on the bearing capacity of clays. *Géotechnique* 23(4), 551-563.

Dean, E.T.R., and Serra, H. 2004. Concepts for mitigation of spudcan-footprint interaction in normally consolidated clay, *Proc. 14th Int. Offshore and Polar Engineering Conf.* (*ISOPE*), Toulon, France.

DeJong, J.T. and Frost, J.D. 2002. A multi-friction sleeve attachment for the cone penetrometer. *ASTM Geotechnical Testing Journal* 25(2),111-127.

DeJong, J.T., Yafrate, N.J., DeGroot, D.J. and Jakubowski, J. 2004. Evaluation of the undrained shear strength profile in soft layered clay using full-flow probes. *Proc. 2nd Int. Conf. on Site Characterisation*, Porto, 1, 679-686.

DeMello, J.R.C., Amarai, C.D.S., Maia da Costa, A., Rosas, M.M., Decnop Coelho, P.S. and Porto, E.C. 1989. Closed-ended pipe piles: testing and piling in calcareous sand. *Proc. Annual Offshore Technology Conf.*, Houston, Paper OTC 6000.

Dendani, H. and Colliat, J-L. 2002. Girassol: design analyses and installation of the suction anchors. *Proc. Annual Offshore Technology Conf.*, Houston, Paper OTC 14209.

De Nicola A. and Randolph M.F. 1993. Tensile and compressive shaft capacity of piles in sand. *J. Geot. Eng. Div., ASCE*, 119(12), 1952-1973.

DNV. 1992. *Classification Notes No. 30.4, Foundations*, Det Norske Veritas, Oslo

Digre, K.A., Kipp, R.M., Hunt, R.J., Hanna, S.Y., Chan, J.H. and van der Voort, C. 1999. URSA TLP: tendon, foundation design, fabrication, transportation and TLP installation. *Proc. Annual Offshore Tech. Conf.*, Houston, Paper OTC 10756.

Doherty, J.P. and Deeks, A.J. 2003. Elastic response of circular footings embedded in a non-homogeneous half-space, *Géotechnique* 53(8), 703-714.

Dolwin, J. Khorshid, M.S. and van Goudoever, P. 1988. Evaluation of driven pile capacity – methods and results. *Proc. Int. Conf. on Engineering for Calcareous Sediments*, Peth, 2, 409-428.

Dove, P., Treu, H. and Wilde, B. 1998. Suction embedded plate anchor (SEPLA): a new anchoring solution for ultra-deepwater mooring. *Proc. DOT Conf.*, New Orleans.

Doyle, E.H., Dean, E.T.R., Sharma, J. S., Bolton, M. D., Valsangkar, A.J. and Newlin, J.A. 2004. Centrifuge model tests on anchor piles for tension leg platforms. *Proc. Annual Offshore Technology Conf.,* Houston, Paper OTC 16845.

Dyson G.J. and Randolph M.F. 2001. Monotonic lateral loading of piles in calcareous sediments. *J. Geotech Eng. Div, ASCE*, 127(4), 346-352.

Dyvik, R., Andersen, K.H., Hansen, S.B. and Christophersen, H.P. (1993). Field tests of anchors in clay. I: Description. *J. Geot. Eng. Div., ASCE*, 119(10), 1515-1531.

Ehlers, C.J., Young, A.G. and Chen, J.H. 2004. Technology assessment of deepwater anchors. *Proc. Annual Offshore Technology Conf.*, Houston, Paper OTC 16840.

Einav, I. and Randolph, M.F. 2005. Combining upper bound and strain path methods for evaluating penetration resistance. *Int. J. Num. Methods in Eng.*, in press.

Erbrich C.T. 1994 Modelling of a novel foundation for offshore structures, *proc. UK ABAQUS Users' Conf., Oxford, September 1994*

Erbrich, C.T. 2004. A new method for the design of laterally loaded anchor piles in soft rock. *Proc. Annual Offshore Technology Conf.,* Houston, Paper OTC 16441.

Erbrich C.T. 2005. Australian frontiers – spudcans on the edge. *Proc. Int. Symp. on Frontiers in Offshore Geotechnics (ISFOG),* Perth.

Erbrich, C. and Hefer, P. 2002. Installation of the Laminaria suction piles – a case history. *Proc. Annual Offshore Technology Conf*, Houston. Paper OTC 14240.

Erbrich, C.T. and Neubecker S.R. 1999. Geotechnical design of a grillage and berm anchor. *Proc. Annual Offshore Technology Conf.,* Houston, Paper OTC 10993.

Erbrich, C.T. and Tjelta, T.I. 1999. Installation of bucket foundations and suction caissons in sand – Geotechnical performance. *Proc. Annual Offshore Technology Conf., Houston*, Paper OTC 10990.

Erickson, H.L. and Drescher, A. 2002. Bearing capacity of circular footings. *J. Geotech. Geoenviron. Eng.*, ASCE, 128(1), 38-43.

Eurocode 7. 1997. *Calcul Geotechnique*. AFNOR, XP ENV 1997-1, 1996.

Fahey, M. and Jewell, R.J. .1988. Model pile tests in calcarenite. *Proc. Conf. on Engineering for Calcareous Sediments*, Perth, 2, 555-564.

Fahey, M., Jewell, R.J., Khorshid, M.S. and Randolph, M.F. 1992. Parameter selection for pile design in calcareous sediments. *Proc. Wroth Memorial Symposium*, Thomas Telford, London, 261-278.

Finnie, I. 1993. *Performance of Shallow foundations in Calcareous Soil*. PhD Thesis, The University of Western Australia, Perth.

Fleming, W.G.K. 1992. A new method for single pile settlement prediction and analysis. *Géotechnique*, 42(3), 411-425.

Foo, K.S., Quah, M.C.K., Wildberger, P. and Vazquez, J.H. 2003[a]. Rack phase difference (RPD). *Proc. 9th Int. Conf. Jack-Up Platform Design, Construction and Operation*, City University, London, UK.

Foo, K.S., Quah, M.C.K., Wildberger, P. and Vazquez, J.H. 2003[b]. Spudcan footing interaction and rack phase difference. *Proc. 9th Int. Conf. Jack-Up Platform Design, Construction and Operation*, City University, London, UK.

Frieze, P.A., Bucknell, J., Birkenshaw, M., Smith, D. and Dixon, A.T. 1995. Fixed and jack-up platforms: basis for reliability assessment. *Proc. 5th Int. Conf. on Jack-Up Platform Design, Construction and Operation*, City University, London.

Frydman, S. and Burd, H.J. 1997. Numerical studies of bearing-capacity factor N_γ *J. Geotech. Geoenviron. Eng.*, ASCE, 123(1), 20-29.

Fugro 2004. Axial pile capacity design method for offshore driven piles in sand. *Report to American Petroleum Institute, Contract No. 2003-100825*, Fugro Report No. P1003.

Garside, R., Bowen, K.G., Stevens, J.W., Doyle, E.H., Henry, D.M. and Romijn, E. 1997. Mars TLP – integration and installation. *Proc. Annual Offshore Tech. Conf.*, Houston, Paper OTC 8373.

Geer, D.A., Douglas Devoy, S, Rapoport, V. 2000. Effects of soil information on economics of jackup installation. *Proc. 32nd Offshore Technology Conf.*, Houston, Paper OTC 12080.

Geise, J.M., Hoope, J. and May, R. 1988. Design and offshore experience with an in situ vane. *Vane Shear Strength Testing of Soils: Field and Laboratory Studies*, ASTM STP 1014, 318-338.

Gemeinhardt, J.P. and Focht, J.A., Jr 1970. Theoretical and observed performance of mobile rig footings on clay. *Proc. 2nd Offshore Technology Conf.,* Houston, Vol. 1, pp. 549-558.

Georgiadis, M. 1985. Load-path dependent stability of shallow footings, *Soils and Foundations* 25(1), 84-88.

Gottardi, G. and Butterfield, R. 1993. On the bearing capacity of surface footings on sand under general planar loads, *Soils and Foundations* 33(3), 68-79.

Gottardi, G. and Butterfield, R. 1995. The displacement of a model rigid surface footing on dense sand under general planar loading, *Soils and Foundations* 35(3), 71-82.

Gottardi, G., Houlsby, G.T. and Butterfield, R. 1999. The plastic response of circular footings on sand under general planar loading, *Géotechnique* 49(4), 453-470.

Gourvenec, S. 2003. Alternative design approach for skirted footings under general combined loading. *Proc. BGA International Conf. on Foundations (ICOF),* Dundee, Scotland.

Gourvenec, S. 2004. Bearing capacity under combined loading – a study of the effect of shear strength heterogeneity. *Proc. 9th Australia New Zealand Conf. on Geomechanics,* Auckland, New Zealand.

Gourvenec, S. and Randolph, M.R. 2003a. Failure of shallow foundations under combined loading. *Proc. 13th ECSMGE,* Prague, Czech Republic, 583-588.

Gourvenec, S. and Randolph, M.R. 2003b. Effect of strength non-homogeneity on the shape and failure envelopes for combined loading of strip and circular foundations on clay. *Géotechnique* 53(6), 575-586.

Graham, J. and Stewart, J.B. 1984. Scale and boundary effects in foundation analysis. *J. of the Soil Mechanics and Foundation Division, ASCE*, 97(SM11), 1533-1548.

Green, A.P. 1954. The plastic yielding of metal junctions due to combined shear and pressure. *J Mech. Phys. Solids* 2(3), 197-211.

Grenda, K.G. 1986. Wave dynamics of jackup rigs. *Proc.Annual Offshore Technology Conf.*, Houston, Paper OTC 5304.

Hanna, A.M. and Meyerhof, G.G. 1980. Design carts for ultimate bearing capacity of foundations on sand overlaying soft clay. *Canadian Geotechnical Journal*, 1, 300-303.

Hansen, B., Nowacki, F., Skomedal, E. and Hermstad, J. 1992. Foundation design, Troll Platform. *Proc. Int. Conf. on Behaviour of Offshore Structures, BOSS'92,* London. 921-936.

Hattori, Y., Ishihama, T., Matsumoto, K., Arima, K., Sakata, N. and Ando, A. 1982. Full-scale Measurement of natural frequency and damping ratio of jackup rigs and some theoretical considerations. *Proc. 14th Offshore Technology Conf.*, Houston, Paper OTC 4287.

Hawkins, R.A. and Markus, A. 1998. New developments in offshore geotechnical investigations. *Proc Int. Conf. Offshore Site Investigations and Foundation Behaviour*, SUT, London. 259-276.

Heerema, E.P. 1980. Predicting pile driveability: Heather as an illustration of the "friction fatigue" theory. *Ground Engineering*, 13, 15-37.

Hefer, P.A and Neubecker, S.R. 1999. A recent development in offshore site investigation tools: the T-bar. *Proc. Australasian Oil and Gas Conf.*, Perth.

Hefer, P.P. 2004. Personal communication.

Higham, M.D. 1984. *Models of Jack-Up Rig Foundations*. M.Sc Thesis, University of Manchester.

Hight D. & Potts D. 1988. Finite element analysis of a deep skirted gravity base, *Proc. BOSS 1988*. Trondheim.

Hossain, M.K. and Briaud, J.L. 1993. Improved Soil Characterisation for Piles in Sand in API RP-2A. *Proc. Annual Offshore Tech. Conf.*, Houston, Paper OTC 7193.

Hossain, M.S. 2004. *Investigation of Soil Failure Mechanisms During Spudcan Foundation Installation*. Master of Engineering Thesis, Curtin University of Technology, Perth.

Hossain, M.S., Hu, Y. and Randolph, M.F. 2003. Spudcan foundation penetration into uniform clay. *Proc. 13th Int. Offshore and Polar Engineering Conf.* (*ISOPE*), Hawaii, USA, 647-652.

Hossain, M.S., Hu, Y. and Randolph, M.F. 2004. Bearing behaviour of spudcan foundation on uniform clay during deep penetration. *Proc. 23rd Int. Conf. on Offshore Mech. and Arctic Eng.* (OMAE)., Vancouver, Canada, OMAE2004-51153.

Hossain, M.S., Hu, Y., Randolph, M.F. and White, D.J. 2005. Punch-through of spudcan foundations in two-layer clay. *Proc. Int. Sym. on Frontiers in Offshore Geotechnics (ISFOG)*, Perth, Australia.

Houlsby, G.T. 2003. Modelling of shallow foundations for offshore structures. *Proc. Int. Conf. on Foundations*, Dundee, Thomas Telford, 11-26

Houlsby, G.T. and Cassidy, M.J. 2002. A plasticity model for the behaviour of footings on sand under combined loading. *Géotechnique*, 52(2), 117-129.

Houlsby, G.T. and Martin, C.M. 1992. Modelling of the behaviour of foundations of jack-up units on clay. *Proc. Wroth Memorial Symp. "Predictive Soil Mechanics"*, Oxford, 339-358.

Houlsby, G.T. and Martin, C.M. 2003. Undrained bearing capacity factors for conical footings on clay, *Géotechnique*, 53(5), 513-520

Houlsby, G.T. and Puzrin, A.M. 1999. The bearing capacity of a strip footing on clay under combined loading. *Proc. Royal Soc. Lond., Ser. A*. 455, 893-916.

House, A.R., Oliveira, J.R.M.S. and Randolph, M.F. 2001. Evaluating the coefficient of consolidation using penetration tests, *Int. J. of Physical Modelling in Geotechnics*, 1(3), 17-25.

Hu, Y. and Randolph, M.F. 2002. Bearing capacity of caisson foundations on normally consolidated clay. *Soils and Foundations*, 42(5), 71-77.

Hu, Y., Randolph, M.F. and Watson, P.G. 1999. Bearing response of skirted foundations on non-homogeneous soil. *J. Geotech. Engng. Div. ASCE*, 125(11), 924-935.

Humpheson, C. 1998. Foundation design of Wandoo B concrete gravity structure. *Offshore Site Investigation and Foundation Behaviour,* Soc. For Underwater Technology, 353-367.

Hunt, R.J. and Marsh, P.D. 2004. Opportunities to improve the operational and technical management of jack-up deployments. *Marine Structures*, 17(3-4), 261-273

Hyden, A.M., Hulett, J.M., Murff, J.D. and Abbs, A.F. 1988. Design practice for grouted piles in Bass Strait calcareous soils. *Proc. Int. Conf. on Calcareous Sediments,* Perth, Balkema, 1,`297-304.

ISO 2000. *Petroleum and natural gas industries: Offshore structures: Part 4: Geotechnical and foundation design considerations*. ISO/DIS 19901-4, International Standards Office, British Standards Institute, London.

ISO 2004. *Draft international standard for the design of fixed steel offshore platforms*. ISO/DIS 19902, International Standards Office, British Standards Institute, London.

ISSMGE 1999. International reference test procedure for the cone penetration test (CPT) and the cone penetration test with pore pressure (CPTU). Report of ISSMGE TC16 on Ground Property Characterisation from In-situ Testing, *Proc. 12th Eur. Conf. on Soil Mech. and Geot. Eng.,* Amsterdam, 3, 2195-2222. Balkema.

James, R.G. and Tanaka, H. 1984. An investigation of the bearing capacity of footings under eccentric and inclined loading in sand in a geotechnical centrifuge. *Proc. Symp. Recent Advances in Geotechnical Centrifuge Modelling*, University of California, Davis, 88-115.

Jardine, R. J., Lehane, B. M. and Everton, S. J. 1992. Friction coefficients for piles in sands and silts. *Proc. Int. Conf. on offshore site investigation and foundation behaviour*, Soc. of Underwater Tech., London, 661-680.

Jardine, R.J. and Chow, F.C. 1996. *New Design Methods for Offshore Piles*, MTD Publication 96/103.

Jardine, R.J., Kovecevic, N., Hoyle, M.J.R., Sidhu, H.K. and Letty, A. 2001. A study of eccentric jack-up penetration into infilled footprint craters, *Proc. 8th Int. Conf. The Jackup Platform*, City University, London.

Jardine, R.J. and Saldivar, E. 1999. An alternative interpretation of the West Delta 58a tension-pile research results. *Proc. Annual Offshore Technology Conf.*, Houston, Paper OTC 10827.

Janbu N., Grande L. and Eggereide K. 1976. Effective Stress Stability Analysis for Gravity Structures. *Proc BOSS 1976,* Trondheim, 1.

Jewell, R.J. and Khorshid, M.S. 1988. *Engineering of Calcareous Sediments*, Volume 2, Balkema, Rotterdam.

Joer, H.A and Randolph, M.F. 1994. Modelling of the shaft capacity of grouted driven piles in calcareous soil. *Proc. Int. Conf. on Design and Construction of Deep Found.*, FHWA, Orlando, 2, 873-887.

Johnson, G.W., Hamilton, T.W., Ebelhar, R.J., Mueller, J.L. and Pelletier, J.H. 1988. Comparison of in situ vane, cone penetrometer and laboratory test results for Gulf of Mexico deepwater clays. *Vane Shear Strength Testing of Soils: Field and Laboratory Studies*, ASTM STP 1014, 293-305.

Kassimali, A. 1983. Large deformation analysis of elasto-plastic frames. *Journal of Structural Engineering, ASCE.* 109(8), 1869-1886.

Kimura, T., Kusakabe, O. and Saitoh, K. 1985. Geotechnical model tests of bearing capacity problems in centrifuge, *Géotechnique*, 35(1), 33-45.

Kolk, H.J., Hooper, J. and Imms, B.W. 1988. Evaluation of offshore in situ vane test results. *Vane Shear Strength Testing of Soils: Field and Laboratory Studies*, ASTM STP 1014, 339-353.

Kolk, H.J. and van der Velde, E. 1996. A reliable method to determine friction capacity of piles driven into clays. *Proc. Annual Offshore Technology Conf*., Houston, Paper OTC 7993.

Lee, K.L. and Focht, J.A. 1975. Liquefaction potential at Ekofisk tank in North Sea. *J. Geotech. Div*. , *ASCE*, 100(GT1), 1018.

Leffler, W.L., Pattarozzi. R. and Sterling, G. 2003. *Deepwater Petroleum Exploration and Production.* PenWell

Lehane, B.M. and Jardine, R.J. 1994. Displacement-pile behaviour in a soft marine clay. *Canadian Geotechnical Journal*, 31(2), 181-191.

Lehane, B.M., Jardine, R.J., Bond, A.J. and Frank, R. 1993. Mechanisms of shaft friction in sand from instrumented pile tests. *J. Geot. Eng. Div., ASCE*, 119(1), 19-35.

Lehane, B.M. and Randolph, M.F. 2002. Evaluation of a minimum base resistance for driven pipe piles in siliceous san*d. J. Geotech. and Geoenv. Eng. Div, ASCE,* 128(3), 198-205.

Levy, N.H., Einav, I. and Randolph, M.F. 2005. Modelling combined loading of piles with local interacting yield surfaces. *Proc. Int. Symp. on Frontiers in Offshore Geotechnics (ISFOG),* Perth.

Lieng, J.T., Hove, F. and Tjelta, T.I. 1999. Deep Penetrating Anchor: Subseabed deepwater anchor concept for floaters and other installations. *Proc. 9th Int. Offshore and Polar Eng. Conf*., Brest, 613-619.

Lieng, J.T., Kavli, A., Hove, F. and Tjelta, T.I. 2000. Deep Penetrating Anchor: Further development, optimization and capacity clarification. *Proc. 10th Int. Offshore & Polar Eng. Conf*., Seattle, 410-416.

Lo Presti, D.C.F., Jamiolkowski, M. and Favazzi M. 1991. Maximum shear modulus measurements using bender elements during oedometer test. *Experimental Characterization and Modelling of Soils and Soft Rocks,* University of Naples, 99-112.

Lloyd's. 1999. *Rules and regulations for the classification of a floating offshore installation at a fixed location – Part 3*. Lloyd's Register of Shipping, London.

Lu, Q., Randolph, M.F., Hu, Y. and Bugarski, I.C. 2004. A numerical study of cone penetration in clay. *Géotechnique*, 54(4), 257-267.

Lunne, T. 2001. In situ testing in offshore geotechnical investigations. *Proc. Int. Conf. on In Situ Measurement of Soil Properties and Case Histories*, Bali, 61-81.

Lunne T, Berre T. and Strandvik S. 1997b. Sample disturbance effects in soft low plastic norwegian clay. *Proc. Conf. on Recent Developments in Soil and Pavement Mechanics*, Rio de Janeiro, 81-102.

Lunne, T., Berre, T., Strandvik, S., Andersen, K.H. and Tjelta, T.I. 2001. Deepwater sample disturbance due to stress relief. *Proc. OTRC Int. Conf. on Geotechnical, Geological and Geophysical Properties of Deepwater Sediments,* OTRC, Austin, 64-85.

Lunne, T., Christoffersen, H.P. and Tjelta, T.I. 1985. Engineering use of piezocone data in North Sea clays. *Proc. 11th Int. Conf. on Soil Mech. and Found. Eng*., San Francisco, 2, 907-912.

Lunne, T., Robertson, P.K. and Powell, J.J.M. 1997a. *Cone Penetration Testing in Geotechnical Engineering*, Blackie Academic and Professional, London.

Martin, C.M. 1994. *Physical and numerical modelling of offshore foundations under combined loads*. DPhil Thesis, University of Oxford.

Martin, C.M. 2001. Vertical bearing capacity of skirted circular foundations on Tresca soil. *Proc. 15th ICSMGE*, Istanbul, 1, 743-746.

Martin, C.M. 2003. New software for rigorous bearing capacity calculations. *Proc. Int. Conf. on Foundations*, Dundee, UK, 581-592.

Martin, C.M. 2004. Calculations using Martin's ABC program (Martin, 2003) and published in Randolph et al., 2004.

Martin, C.M. and Houlsby, G.T. 1999. Jackup units on clay: structural analysis with realistic modelling of spudcan behaviour. *Proc. Annual Offshore Technology Conf.,* Houston, Paper OTC 10996.

Martin, C.M. and Houlsby, G.T. 2000. Combined loading of spudcan foundations on clay: laboratory tests, *Géotechnique* 50(4), 325-338.

Martin, C.M. and Houlsby, G.T. 2001. Combined loading of spudcan foundations on clay: numerical modelling, *Géotechnique* 51(8), 687-700.

Martin, C.M. and Randolph, M.F. 2001. Applications of the lower and upper bound theorems of plasticity to collapse of circular foundations. *Proc. 10th Int. Conf. on Computer Methods and Advances in Geomechanics*, Tucson, 2, 1417-1428.

Matlock, H. 1970. Correlations for design of laterally loaded piles in soft clay. *Proc. Annual Offshore Technology Conf*., Houston, Paper OTC 1204.

McCarron, W.O. and Sukumaran, B. 2000. Ultimate capacities of suction caissons and pile elements for deepwater applications. *Proc. 10th Int. Conf. On Offshore and Polar Engng*, Seattle, 2, 466-469.

Medeiros, C.J. 2001. Torpedo anchor for deep water. *Proc. Deepwater Offshore Technology Conf*., Rio de Janeiro.

Medeiros, C.J. 2002. Low cost anchor system for flexible risers in deep waters. *Proc. Annual Offshore Technology Conf*., Houston, Paper OTC 14151.

Merifield, R.S., Lyamin, A., Sloan, S.W. and Yu, H.S. 2003. Three-dimensional lower bound solutions for stability of plate anchors in clay. *J. of Geotechnical and Geoenviromental Engineering*, ASCE, 129(3), 243-253.

Meyerhof, G.G. 1951. The ultimate bearing capacity of foundations. *Géotechnique*, 2(4), 301-332.

Meyerhof, G.G. 1953. The bearing capacity of foundations under eccentric and inclined loads. *Proc. 3rd ICSMFE*, Zurich, 1, 440-445.

Meyerhof, G.G. and Hanna, A.M. 1978. Ultimate bearing capacity of foundations of layered soils under inclined loads. *Can. Geotech. J.* 15, 565-572.

Morandi, A.C., Frieze, P.A., Birkinshaw, M., Smith, D. and Dixon, A.T. 1997. Reliability of fixed and jack-up structures: a comparative study. *Proc. of BOSS'97 Behaviour of Offshore Structures,* 3, Delft University of Technology, 111-126.

Murff, J.D. 1994. Limit analysis of multi-footing foundation systems, *Proc. 8th Int. Conf. on Computer Methods and Advances in Geomechanic*s, Morgantown, 1, 223-244.

Murff, J.D. and Hamilton, J.M. 1993. P-ultimate for undrained analysis of laterally loaded piles. *J. Geot. Eng. Div., ASCE*, 119(1), 91-107.

Murff, J.D., Prins, M.D., Dean, E.T.R., James, R.G. and Schofield, A.N. 1992. Jackup rig foundation modelling. *Proc. Annual Offshore Technology Conf.,* Houston, Paper OTC 6807.

Murff, J.D., Randolph, M.F., Elkhatib, S., Kolk, H.J., Ruinen, R., Strom, P.J. and Thorne, C. 2005. Vertically loaded plate anchors for deepwater applications. *Proc. Int. Symp. on Frontiers in Offshore Geotechnics (ISFOG)*, Perth, Australia.

NCEL. 1987. *Drag Embedment Anchors for Navy Moorings*. Naval Civil Engineering Laboratory, Port Hueneme, California, Techdata Sheet 83-08R.

Nelson, K., Smith, P., Hoyle, M., Stoner, R. and Versavel, T. 2000. Jack-up response measurements and the underprediction of spud-can fixity by SNAME 5-5A. *Proc. Annual Offshore Technology Conf.*, Houston, Paper OTC 12074.

Neubecker, S.R. and Erbrich, C.T. 2004. Bayu-Udan substructure foundations: Geotechnical design and analysis. *Proc. Annual Offshore Technology Conf.*, Houston, Paper OTC 16157.

Neubecker, S.R. and Randolph, M.F. 1995. Profile and frictional capacity of embedded anchor chain, *J. Geotechnical Eng. Div., ASCE*, 121(11), 787-803.

Neubecker, S.R. and Randolph, M.F. 1996. The performance of drag anchor and chain systems in cohesive soil. *Marine Georesources and Geotechnology*, 14, 77-96.

Neubecker S.R., O' Neill M.P. and Erbrich C.T. 2005. Preloading of Drag Anchors in Carbonate Sediments, *Proc. International Symposium on Frontiers in Offshore Geotechnics (ISFOG)*, Perth, Western Australia, Balkema: Rotterdam

Newlin, J.A. 2003. Suction anchor piles for the Na Kika FDS mooring system. Part 2: Installation performance. *Deepwater Mooring Systems: Concepts, Design, Analysis, and Materials*, ASCE, Houston, USA, 55-57.

NGI. 2000. Windows Program HVMCap. Version 2.0: Theory, user manual and certification. Norwegian Geotechnical Institute Report 524096-7, Rev. 1 (Confidential).

Ngo-Tran, C.L. 1996. *The Analysis of Offshore Foundations Subjected to Combined Loading*. D.Phil. Thesis, University of Oxford.

Nguyen-Sy, L. and Houlsby, G.T. 2005. The theoretical modelling of suction caisson foundation using hyperplasticity theory. *Proc. International Symposium on Frontiers in Offshore Geotechnics (ISFOG),* Perth, Australia.

Norris, V.A. and Aldridge, T.R. 1992. Recent analytical advances in the study of the influence of spudcan fixity on jack-up unit operations. *Recent Developments in Jack-Up Platforms*, Elsevier, London, 424-450.

Nova, R. and Montrasio, L. 1991. Settlements of shallow foundations on sand. *Géotechnique*, 41(2), 243-256.

Novello, E. 1999. From static to cyclic p-y data in calcareous sediments. *Proc. 2nd Int. Conf. on Engineering for Calcareous Sediments*, Bahrain, 1, 17-27.

O'Loughlin, C.D, Randolph, M.F. and Richardson, M. 2004. Experimental and theoretical studies of deep penetrating anchors. *Proc. Annual Offshore Tech. Conf.,* Houston, Paper OTC 16841.

O'Neill, M.P., Bransby, M.F., and Randolph, M.F. 2003. Drag anchor fluke-soil interaction in clays, *Canadian Geotechnical Journal*, 40(1), 78-94.

O'Neill, M.W. and Murchison, J.M. 1983. An evaluation of p-y relationships in sands. *Report PRAC 82-41-1* to American Petroleum Institute, University of Houston, Houston.

O'Reilly, M.P. and Brown, S.F. 1991. *Cyclic loading of soils*. Blackie.

Osborne, J.J., Trickey, J.C., Houlsby, G.T. and James, R.G. 1991. Findings from a joint industry study on foundation fixity of jackup units. *Proc. Annual Offshore Technology Conf.*, Houston, OTC 6615.

Paik, K.H., Salgado, R., Lee, J. and Kim, B. 2003. Behaviour of open and closed-ended piles driven into sand. *J. Geotech. and Geoenv. Eng. Div, ASCE*, 129(4), 296-306.

Pelipenko, S. and Frigaard, I.A. (2005). Visco-plastic fluid displacements in near-vertical narrow eccentric annuli: prediction of travelling wave solutions and interfacial instability. *J. Fluid Mechanics* (submitted).

Peuchen, J. 2000. Deepwater cone penetration tests. *Proc. Annual Offshore Technology Conf.*, Houston, Paper OTC 12094.

Poulos, H.G. 1988. *Marine Geotechnics*. Unwin Hyman.

Prandtl, L. 1921. Eindringungsfestigkeit und festigkeit von schneiden. Angew. *Math. U. Mech* 1(15).

Prasad,Y.V.S.N. and Chari, T.R. 1999. Lateral capacity of model rigid piles in cohesionless soils, *Soils and Foundations*, 39(2), 21-29.

Quirós, G.W. and Little, R.L. 2003. Deepwater soil properties and their impact on the geotechnical program, *Proc. Annual Offshore Technology Conf.*, Houston, Paper OTC 15262.

Quirós, G.W. and Young, A.G. 1988. Comparison of field vane, CPT and laboratory strength data at Santa Barbara Channel site. *Vane Shear Strength Testing of Soils: Field and Laboratory Studies*, ASTM STP 1014, 306-317.

Randolph, M.F. 2003. 43rd Rankine Lecture: Science and empiricism in pile foundation design. *Géotechnique*, 53(10), 847-875.

Randolph, M.F. 2004 Characterisation of soft sediments for offshore applications, Keynote Lecture, *Proc. 2nd Int. Conf. on Site Characterisation*, Porto, 1, 209-231.

Randolph, M.F., Dolwin, J. and Beck, R.D. 1994. Design of driven piles in sand. *Géotechnique*, 44(3), 427-448.

Randolph, M.F and Erbrich, C.T. 2000. Design of shallow foundations for calcareous sediments. *Proc. Engineering for Calcareous Sediments.* Ed. Al-Shafei, Balkema, 2, 361-378.

Randolph, M.F., Hefer, P.A., Geise, J.M. and Watson, P.G. 1998a. Improved seabed strength profiling using T-bar penetrometer. *Proc Int. Conf. Offshore Site Investigation and Foundation Behaviour - "New Frontiers"*, Society for Underwater Technology, London, 221-235.

Randolph, M.F. and Houlsby, G.T. 1984. The limiting pressure on a circular pile loaded laterally in cohesive soil. *Géotechnique*, 34(4), 613-623.

Randolph M.F. and House A.R. 2002. Analysis of suction caisson capacity in clay. *Proc. Annual Offshore Technology Conf.*, Houston, Paper OTC 14236

Randolph, M.F., Jamiolkowski, M.B. and Zdravkovi, L. 2004. Load carrying capacity of foundations. *Proc. Skempton Memorial Conf., London*, 1, 207-240.

Randolph M.F., Joer H.A., Khorshid M.S. and Hyden A.M. 1996. Field and laboratory data from pile load tests in calcareous soil. *Proc. Annual Offshore Tech. Conf.*, Houston, Paper OTC 7992.

Randolph, M.F., Leong, E.C. and Houlsby, G.T. 1991. One dimensional analysis of soil plugs in pipe piles. *Géotechnique*, 41(4), 587-598.

Randolph, M.F., Martin, C.M. and Hu, Y. 2000. Limiting resistance of a spherical penetrometer in cohesive material. *Géotechnique*, 50(5), 573-582.

Randolph, M.F. and Murphy, B.S. 1985. Shaft capacity of driven piles in clay, *Proc.Annual Offshore Tech. Conf.*, Houston, OTC 4883.

Randolph, M.F., O'Neill, M.P., Stewart, D.P. and Erbrich, C. 1998b. Performance of suction anchors in fine-grained calcareous soils. *Proc. Annual Offshore Technology Conf.*, Houston, OTC 8831.

Reardon, M.J. 1986. Review of the geotechnical aspects of jack-up unit operations. *Ground Engineering*, 19(7), 21-26.

Rickman, J.P. and Barthelemy, H.C. 1988. Offshore construction of grouted driven pile foundations. *Proc. of Int. Conf. on Calcareous Sediments*, Perth, Balkema, 1, 313-319.

Rowe, R.K. and Davis, E.H. 1982. The behaviour of anchor plates in clay. *Géotechnique*, 32(1), 9-23.

Roy, M., Tremblay, M., Tavenas, F. and La Rochelle, P. 1982. Development of pore pressure in quasi-static penetration tests in sensitive clay, *Canadian Geotechnical Journal*, 19, 124-138.

Salençon, J. and Matar, M. 1982. Capacité portante des fondations superficielles circulaires. *Journal de Mécanique théorique et appliquée* 1(2), 237-267.

Santa Maria, P.E.L. de 1988. *Behaviour of Footings for Offshore Structures Under Combined Loading*. DPhil Thesis, Univ. of Oxford.

Schotman, G.J.M. 1989. The effects of displacements on the stability of jackup spudcan foundations, *Proc. Annual Offshore Technology Conf., Houston*, Paper OTC 6026.

Schotman, G.J.M. and Hospers, B. 1992. An improved calculation method for conductor setting depths in sand. *Proc. Conf. on Behaviour of Offshore Structures, BOSS 1992*.

Senders, M. and Kay, S. 2002. Geotechnical suction pile anchor design in deep water soft clays. *Proc. Conf. on Deepwater Risers, Mooring and Anchorings*, London.

Senpere D. and Auvergne GA. 1982. Suction Anchor Piles – A Proven Alternative to Driving or Drilling, *Proc. Annual Offshore Technology Conf., Houston*, Paper OTC 4206.

Sharples, B.P.M., Bennett Jr, W.T. and Trickey, J.C. 1989. Risk analysis of jack-up rigs. *Proc. of 2nd Int. Conf. on the Jack-Up Drilling Platform*, City University, London, 101-123.

Sims, M.A., Smith, B.J.A and Reed, T. 2004. Bayu-Udan substructure foundations: Conception, design and installation aspects. *Proc. Annual Offshore Technology Conf.*, Houston, Paper OTC 16158.

Skempton, A. W. 1951. The bearing capacity of clays. *Proc. Building and Research Congress*, London 1, 180-189.

SNAME 1997. Guidelines for site specific assessment of mobile jack-up units. Society of Naval Architects and Marine Engineers, Technical and Research Bulletin 5-5A Rev. 1, New Jersey.

Springman, S.M. and Schofield, A.N. 1998. Monotonic lateral load transfer from a jack-up platform lattice leg to a soft clay deposit. *Proc. Conf. Centrifuge 98*, Tokyo, Balkema, 563-568.

Stewart, D.P. and Finnie, I.M.S. 2001. Spudcan-footprint interaction during jack-up workovers, *Proc. 11th Int. Offshore and Polar Engineering Conf.* (*ISOPE*), Stavanger, Norway.

Stewart, D.P. and Randolph, M.F. 1991. A new site investigation tool for the centrifuge. *Proc. Int. Conf. On Centrifuge Modelling – Centrifuge 91*, Boulder, Colorado, 531-538.

Stewart, D.P. and Randolph, M.F. 1994. T-bar penetration testing in soft clay. *J. Geot. Eng. Div., ASCE*, 120(12), 2230-2235.

Stewart, D.P., Boyle, R.S. and Randolph, M.F. 1998. Experience with a new drum centrifuge. *Proc. Int. Conf. Centrifuge '98*, Tokyo, Japan, 1, 35-40.

Stiff, J.J., Sharples, B.P.M. and Bowie, R.D. 1997. Jack-ups: classification past, present, and future. *Proc. 6th Int. Conf. Jack-Up Platform Design, Construction and Operation*, City University, London.

Stoner, R.W.P, Hoyle, M.J.R., Nelson, K., Smith, N.P. and Hunt, R.P. 2004. Recovery of an elevated jack-up with leg bracing member damage. *Marine Structures*, 17(3-4), 325-351.

Stφve, O.J., Bysveen, S. and Christophersen, H.P. 1992. New foundation systems for the Snorre development. *Proc. Annual Offshore Technology Conf.*, Houston, Paper OTC 6882.

Sukumaran, B., McCarron, W.O., Jeanjean, P. and Abouseeda, H. 1999. Efficient finite element techniques for limit analysis of suction caissons under lateral loads. *Computers & Geotechnics*, 24(2), 89-107.

Sumrow, M. 2002. Industry funded project investigates jack up rig, spudcan footprint interactions, *Oil and Gas Journal*, Tulsa, Oct 28, 100(44), 56-57.

Supachawarote, C., Randolph, M.F. and Gourvenec, S. 2004. Inclined pull-out capacity of suction caissons, *ISOPE*, Toulon, 2, 500-506.

Supachawarote, C., Randolph, M.F. and Gourvenec, S. 2005. The effect of crack formation on the inclined pull-out capacity of suction caissons. *IACMAG-05*, Torino.

Svano G. 1981. *Undrained Effective Stress Analysis*. Dr. Thesis, Norwegian Institute of Technology, Trondheim.

Taiebat, H.A. and Carter, J.P. 2002a. Bearing capacity of strip and circular foundations on undrained clay subjected to eccentric loads. *Géotechnique* 52(1), 61-64.

Taiebat, H.A. and Carter, J. P. 2002b. A Failure Surface for the Bearing Capacity of Circular Footings on Saturated Clays, *Proc.VIII Int. Symp. Numerical Models in Geomechanics, NUMOG VIII,* Pande and Pietruszczak (Eds), Rome, Italy, 457-462.

Tan, F.S.C. 1990. *Centrifuge and Theoretical Modelling of Conical Footings on Sand*. PhD. Thesis, University of Cambridge.

Teh, C.I. and Houlsby, G.T. 1991. An analytical study of the cone penetration test in clay. *Géotechnique*, 41(1), 17-34.

Temperton, I., Stoner, R.W.P. and Springett, C.N. 1997. Measured jack-up fixity: analysis of instrumentation data from three North Sea jack-up units and correlation to site assessment procedures. *Proc. of 6th Int. Conf. Jack-Up Platform Design, Construction and Operation*, City University, London.

Terzaghi, K. 1943. *Theoretical soil mechanics* Wiley, New York.

Tetlow, J.H., Ellis, N., Mitra, J.K. 1983. The Hutton tension leg platform. *Design in Offshore Structures*, Thomas Telford, London, 137-150.

Thorne, C.P. 1998. Penetration and load capacity of marine drag anchors in soft clay. *J. of Geotechnical and Geoenvironmental Engineering, ASCE*, 124(10), 945-953.

Tjelta, T.I. 1993. Foundation behaviour of Gullfaks C *Offshore Site Investigation and Foundation Behaviour,* Soc. for Underwater Technology, 28, 451-467.

Tjelta, T.I. 1995. Geotechnical experience from the installation of the Europipe jacket with bucket foundations. *Proc. Annual Offshore Technology Conf., Houston*, Paper OTC 7795.

Tjelta, T.I. 1998. Foundation design for deepwater gravity base structure with long skirts on soft soil. *Proc. Int. Conf. on Behaviour of Offshore Structures, BOSS'98*, The Hague, 173-192.

Tjelta, T.I., Aas, P.M., Hermstad, J. and Andenaes, E. 1990. The skirt piled Gullfaks C platform installation. *Proc. Annual Offshore Technology Conf., Houston*, Paper OTC 6473.

Tjelta, T.I. Guttormsen, T.R and Hernstad, J. 1986. Large scale penetration test at a deepwater site. *Proc. Annual Offshore Technology Conf., Houston*, Paper OTC 5103.

Tjelta, T.I. and Haaland, G. 1993. Novel foundation concept for a jacket finding its place. *Offshore Site Investigation and Foundation Behaviour,* Soc. for Underwater Technology, 28, 717-728.

Tomlinson, M.J. 1957. The adhesion of piles driven in clay soils. *Proc. 4th Int. Conf. on Soil Mech. and Found. Eng.*, 2, 66-71.

Treacy, G. 2003, *Reinstallation of Spudcan Footings next to Existing Footprints*, Honours Thesis, University of Western Australia.

Tromans P.S., Anaturk A.R., Hagemeijer, P. 1991. A new model for the kinematics of large ocean waves - applications as a design wave. *Proc. 1st Int. Offshore & Polar Engng Conf.*, Edinburgh, 3, 64-71.

Uesugi, M. and Kishida, H. 1986. Influential factors of friction between steel and dry sands. *Soils and Foundations*, 26(2), 29-42.

Ukritchon, B. Whittle, A.J. and Sloan, S.W. 1998. Undrained limit analysis for combined loading of strip footings on clay. *J. Geot. and Geoenv. Eng., ASCE* 124(3), 265-276.

Veldman, H. and Lagers, G. 1997. 50 years offshore. *Foundation for Offshore Studies*, Delft, The Netherlands.

Vesic, A.S. 1970. Tests on instrumented piles, Ogeechee River site. *J. of the Soil Mech. and Found. Div., ASCE*, 96(SM2), 561-584.

Vesic, A.S. 1975. Bearing capacity of shallow foundations. *In Foundation Engineering Handbook* (*ed. Winterkorn, H.F. and Fang, H.Y.*), Van Nostrand, New York, 121-147.

Vijayvergiya, V.N. and Focht, J.A. 1972. A new way to predict capacity of piles in clay. *Proc. Annual Offshore Technology Conf.*, Houston, Paper OTC 1718.

Vivatrat, V., Valent, P.J. and Ponterio, A. 1982. The influence of chain friction on anchor pile design. *Proc. Annual Offshore Technology Conf.*, Houston, Paper OTC 4178.

Vlahos, G. 2004. *Physical and Numerical Modelling of a Three-Legged Jack-Up Structure on Clay Soil*, PhD Thesis, The University of Western Australia.

Vryhof. 2000. *Anchor Manual 2000*. Vryhof Anchors, Krimpen ad YJssel, The Netherlands.

Wang, C.X. and Carter, J.P. 2002. Deep penetration of strip and circular footings into layered clays. *Int. J. Geomech.* 2(2), 205-232.

Watson, P.G. 1999. *Performance of Skirted Foundations for Offshore Structures*. PhD Thesis, The University of Western Australia.

Watson. P.G. & Humpheson, C. 2005. Geotechnical interpretation for the Yolla A Platform. *Proc. International Symposium on Frontiers in Offshore Geotechnics (ISFOG),* Perth, Australia.

Watson, P.G., Newson, T.A. and Randolph, M.F. 1998. Strength profiling in soft offshore soils. *Proc. 1st Int. Conf. On Site Characterisation - ISC '98*, Atlanta, 2, 1389-1394.

Wesselink, B.D., Murff, J.D., Randolph, M.F., Nunez, I.L., and Hyden, A.M. 1988. Analysis of centrifuge model test data from laterally loaded piles in calcareous sand. *Proc. Int. Conf. Calcareous Sediments*, Balkema, 1, 261-270.

White, D.J. 2005. A general framework for shaft resistance on displacement piles in sand. *Proc. International Symposium on Frontiers in Offshore Geotechnics (ISFOG),* Perth, Australia.

White D.J. and Bolton M.D. 2004. Displacement and strain paths during plane strain model pile installation in sand. *Géotechnique*. 54(6), 375-398.

White, D.J. and Lehane, B.M. 2005. Friction fatigue on displacement piles in sand. *Géotechnique*, 55, in press.

White D.J., Take W.A. and Bolton M.D. 2003 Soil deformation measurement using particle image velocimetry (PIV) and photogrammetry. *Géotechnique*, 53(7), 619-631.

White, D.J., Take, W.A, Bolton, M.D. and Munachen, S.E. 2001a. A deformation measuring system for geotechnical testing based on digital imaging, close-range photogrammetry, and PIV image analysis. *Proc. 15th ICSMGE,* Istanbul. Balkema 1, 539-542.

White, D.J., Take, W.A. and Bolton M.D. 2001b. Measuring soil deformation in geotechnical models using digital images and PIV analysis. *Proc. 10th Int. Conf. on Computer Methods and Advances in Geomechanics*. Tucson, Arizona. Balkema, 997-1002.

Whittle, A.J. 1992. Assessment of an effective stress analysis for predicting the performance of driven piles in clays. *Proc. Conf. on Offshore Site Investigation and Foundation Behaviour*, Society for Underwater Technology, Kluwer, 28, 607-643.

Wilde, B., Treu, H. and Fulton, T. 2001. Field testing of suction embedded plate anchors. *Proc. 11th Int. Offshore and Polar Eng. Conf.*, Stavanger, 2, 544-551.

Williams, A.F., Dunnavant, T.W., Anderson, S., Equid, D.W. and Hyden, A.M. 1988. The performance and analysis of lateral load tests on 356 mm dia piles in reconstituted calcareous sand. *Proc. Int. Conf. Calcareous Sediments*, Balkema, 1, 271-280.

Williams M.S., Thompson R.S.G. and Houlsby G.T. 1998. Non-linear dynamic analysis of offshore jack-up units. *Computers and Structures*, 69(2), 171-180.

Wiltsie, E.A., Hulett, J.M., Murff, J.D. Hyden, A.M. and Abbs, A.F. 1988. Foundation design for external strut strengthening system for Bass Strait first generation platforms. *Proc. Conf. on Engineering for Calcareous Sediments*, Perth, Balkema, 2, 321-330.

Young, A.G. and Focht, J.A. 1981. Subsurface hazards affect mobile jack-up rig operations. *Sounding*, McClelland Engineers Inc., Houston, 3(2),4-9.

Young, A.G., Honganen, C.D., Silva, A.J. and Bryant, W.R. 2000. Comparison of geotechnical properties from large diameter long cores and borings in deep water Gulf of Mexico. *Proc. Annual Offshore Technology Conf.*, Houston, Paper OTC 12089.

Young, A.G., Kraft, L.M. and Focht, J.A. 1975. Geotechnical considerations in foundation design of offshore gravity structures. *Proc. Annual Offshore Technology Conf.*, Houston, Paper OTC 2371.

Young, A.G., McClelland, B. and Quirós, G.W. 1988. In situ vane testing at sea. *Vane Shear Strength Testing of Soils: Field and Laboratory Studies*, ASTM STP 1014, 46-67.

Young, A.G., Remmes, B.D. and Meyer, B.J. 1984. Foundation performance of offshore jack-up drilling rigs. *J. Geotech Engng Div., ASCE*, 110(7), 841-859.

Zhang, J. 2001. *Geotechnical Stability of Offshore Pipelines in Calcareous Sand*. PhD Thesis, The University of Western Australia.

Zuidberg, H.M.and Vergobbi, P. 1996. Euripides: Load tests on large driven piles in dense silica sands. *Proc. Annual Offshore Tech. Conf.,* Houston, Paper OTC 7977.